Generation and Functional Characterization of a Transgenic Mouse Line Expressing a Ca^{2+} Biosensor in Cone Photoreceptors

Dissertation

der Mathematisch-Naturwissenschaftlichen Fakultät

der Eberhard Karls Universität Tübingen

zur Erlangung des Grades eines

Doktors der Naturwissenschaften

(Dr. rer. nat.)

vorgelegt von

Tao Wei

aus LIAONING, CHINA

Tübingen

2011

Tag der mündlichen Qualifikation:	25. 01. 2012
Dekan:	Prof. Dr. Wolfgang Rosenstiel
1. Berichterstatter:	Prof. Dr. Thomas Euler
2. Berichterstatter:	Prof. Dr. Hanspeter A. Mallot

Acknowledgement

I thank **Prof. Dr. Eberhart Zrenner** and **Prof. Dr. Theo van Veen** very much for introducing me to the very fascinating research field and their constant support.

I thank **Prof. Dr. Hanspeter A. Mallot** for kindly evaluating my thesis as a second advisor.

I would like to thank **Prof. Dr. Peter Ruth** and **Prof. Dr. Konrad Kohler** for kindly being members of my examination board and the evaluation of my Disputation.

I especially thank **Prof. Dr. Thomas Euler** and **Prof. Dr. Bernd Wissinger** for their constant support, their advice and sharing their vast knowledge.

Prof. Dr. Thomas Euler as my first supervisor provides the excellent working environment to perform physiological study and supports me with his excellent expertise.

Prof. Dr. Bernd Wissinger as my co-supervisor in molecular genetics laboratory shares his vast expertise and knowledge in this research field.

I thank **Dr. Francois Paquet-Durand** and **Dr. Thomas Ladewig** for sharing their knowledge in photoreceptor degeneration and Ca^{2+} measurements as well as their advice and suggestions.

I thank **Dr. Timm Schubert** for improving my practical skills, discussing all the technical problems with me during the project and reviewing the written thesis.

I thank **Dr. Daniel Rathbun** very much for kindly proofreading the thesis.

I thank **Dr. Katja Köppen** for helping me to get started in the molecular genetics laboratory.

I thank **Wadood Haq, Peggy Reuter** and **Joachim Täger** for their help, suggestions and discussion during my work.

I thank **Le Chang** for introducing me to the imaging setup and constant help and **Dr. Tobias Breuninger** for his cordial help and necessary discussion about my project.

I thank **Dr. Tom Baden** for helpful comments on my project.

I thank **Gordon Eske** for his technical assistance.

I thank **Norman Rieger** and **Britta Baumann** for their technical assistance in molecular genetics lab and animal-breeding.

Many thanks also go to all my past and current colleagues in
1) Centre for Integrative Neuroscience, University of Tübingen,
2) Institute for Ophthalmic Research, Centre for Ophthalmology, University of Tübingen,
3) Molecular Genetics Laboratory, Centre for Ophthalmology, University of Tübingen, Germany.

I want to especially thank my sweetheart **Gao Yongsheng** for her constant support during the PhD study.

Last but not least, I thank my beloved father **Wei Yuliang** and mother **Lin Xueying** especially for being always by my side to support and encourage me.

This study was supported by the DFG (EXC 307, FOR 701, KFO 134), the BMBF (BCCN, Bernstein Center for Computational Neuroscience, Tübingen, FKZ:01GQ1002) and the Tistou und Charlotte Kerstan Stiftung.

TABLE OF CONTENTS

1. Abbreviations:

8-pCPT-cGMP:	8-(4-Chlorophenylthio) guanosine-3',5'-cyclic monophosphate
ACSF:	artificial cerebral spinal fluid
BSA:	bovine serum albumin
Ca^{2+}:	calcium ion
$[Ca^{2+}]$:	calcium ion concentration
CICR:	calcium-induced calcium release
cGMP:	3',5'-cyclic guanosine monophosphate
[cGMP]:	3',5'-cyclic guanosine monophosphate concentration
CLSM:	confocal laser scanning microscope
CMV:	cytomegalovirus promoter
CNG channels:	cyclic nucleotide-gated channels
CNS:	central nervous system
cpfl1:	cone photoreceptor function loss 1
DMSO:	dimethyl sulfoxide
DNA:	deoxyribonucleic acid
dNTP:	deoxynucleoside triphosphate
ECFP:	enhanced cyan fluorescent protein
ER:	endoplasmic reticulum
ERG:	electroretinogram
FRET:	fluorescence/Förster resonance energy transfer
GC:	guanylate cyclase
GCAP:	guanylate cyclase activating protein
GCL:	ganglion cell layer
GECI:	genetically encoded calcium indicator
GFP:	green fluorescent protein
GTP:	guanosine triphosphate
IP3:	inositol 1,4,5-triphosphate
IPL:	inner plexiform layer
IS:	inner segment
IVM:	*in vitro* mutagenesis
kb:	kilobase pair
KCl:	potassium chloride
K^{+}:	potassium ion
LB:	*lysogeny* broth

LED:	light-emitting diode
M-(opsin/cone):	medium wavelength (opsin/cone)
Na^+:	sodium ion
NADPH:	β-Nicotinamide adenine dinucleotide phosphate
NBT:	Nitro Blue Tetrazolium
NCKX:	sodium/calcium-potassium exchanger
NCX:	sodium/calcium exchanger
NFL:	nerve fiber layer
NGS:	normal goat serum
NO:	nitric oxide
NOS:	nitric oxide synthase
NO-sGC pathway:	nitric oxide-soluble guanylate cyclase pathway
ODQ:	1H-[1,2,4]Oxadiazolo[4,3-a]quinoxalin-1-one
ONL:	outer nuclear layer
OPL:	outer plexiform layer
OS:	outer segment
PCR:	polymerase chain reaction
PBS:	phosphate buffered saline
PBS-T:	phosphate buffered saline with Trixon-100
PDE:	phosphodiesterase
PFA:	paraformaldehyde
PKG:	protein kinase G
PMCA:	plasma membrane calcium ATPase
q-PCR:	quantitative polymerase chain reaction
rd1:	retina degeneration 1
ROI:	region of interest
RPE:	retinal pigment epithelium
rpm:	revolutions per minute
RyR:	ryanodine receptor
SAP:	shrimp alkaline phosphatase
SCCI:	synthetic chemical calcium indicator
sGC:	soluble guanylate cyclase
SNAP:	S-Nitroso-N-acetyl-DL-penicillamine
S-(opsin/cone):	short wavelength (opsin/cone)
TRPC:	transient receptor potential channel
VGCC:	voltage-gated calcium channel

2. Abstract:

Calcium (Ca^{2+}) is a universal and ubiquitous signaling messenger that controls a large variety of cellular processes under physiological conditions. Deviations from the normal range of spatial and temporal Ca^{2+} dynamics can result in cell death (Choi, 1992; Eimerl and Schramm, 1994; Nicotera and Orrenius, 1998; Berliocchi et al., 2005).

Cone photoreceptors are responsible for photopic vision and convert light signals into electric signals (Pugh and Lamb, 1993; Muller and Kaupp, 1998; Arshavsky et al., 2002; Fu and Yau, 2007; Mustafi et al., 2009). Calcium plays multiple roles in cone photoreceptors of the vertebrate retina including modulating phototransduction in the outer segment, metabolic processes in the inner segment and mediating transmitter release at the synaptic terminal. Furthermore, studies on retinal degeneration strongly imply the involvement of an aberrant Ca^{2+} homeostasis in cone photoreceptor cell death, e.g. apoptosis in hereditary retinal dystrophies. Therefore, to monitor the subcellular Ca^{2+} dynamics in cones is crucial not only for understanding cone function but also to gain important insights into the pathophysiological processes that occur in cones before and during degeneration. To this end, a transgenic mouse line (HR2.1:TN-XL) was generated in which cone photoreceptors selectively express the genetically encoded ratiometric Ca^{2+} biosensor TN-XL. With immunohistochemistry and ERG recordings we confirmed that TN-XL is expressed in both types of mouse cones and that the biosensor's presence does not affect photoreceptor function. Light-evoked Ca^{2+} responses from single cone terminals were characterized via two-photon imaging – demonstrating that cone Ca^{2+} dynamics can be easily studied through the pharmacological modulation of different components/steps of the phototransduction cascade. Using this approach, we tested the hypothesis that nitric oxide (NO) modulates the Ca^{2+} dynamics in cone terminals via the "classical" soluble guanylate cyclase (sGC) dependent pathway (NO-sGC pathway). While it was confirmed that Ca^{2+} resting levels in mouse cones can be modulated by NO, no evidence was found that supports an involvement of the NO-sGC pathway. In conclusion, the HR2.1:TN-XL mouse line offers a great opportunity to elucidate the light-driven Ca^{2+} dynamics and its regulation in mouse cone photoreceptors under physiological and pathophysiological conditions.

3. Zusammenfassung:

Kalzium (Ca^{2+}) ist ein ubiquitärer und universeller „Botenstoff“, der auf der einen Seite eine Vielzahl von zellulären Prozessen unter physiologischen Bedingungen reguliert. Andererseits kann das Überschreiten der normalen räumlichen und zeitlichen Grenzen der Ca^{2+} Dynamik zum Zelltod führen (Choi, 1992; Eimerl and Schramm, 1994; Nicotera and Orrenius, 1998; Berliocchi et al., 2005).

Zapfen-Photorezeptoren sind für das photopische Sehen verantwortlich und wandeln Lichtsignale in elektrische Signale um (Pugh and Lamb, 1993 1505; Muller and Kaupp, 1998 1496; Arshavsky et al., 2002 1508; Fu and Yau, 2007 1494; Mustafi et al., 2009 464). Kalzium spielt mehrere wichtige Rollen in Zapfen-Photorezeptoren der Retina: Es moduliert die Phototransduktion im Außensegment sowie Stoffwechselvorgänge im Innensegment, und vermittelt die Transmitterfreisetzung an der synaptischen Endigung (Terminalien). Darüber hinaus implizieren Studien über Netzhautdegeneration, dass eine stark abweichende Ca^{2+}-Homöostase am Zelltod von Zapfen-Photorezeptoren, z.B. bei Apoptose in hereditären Netzhautdystrophien, beteiligt ist. Daher ist die Untersuchung der subzellulären Ca^{2+}-Dynamik in Zapfen-Photorezeptoren nicht nur entscheidend, um die Funktion von Zapfen-Photorezeptoren zu verstehen, sondern auch um wichtige Einblicke in die pathophysiologischen Vorgänge zu gewinnen, die in Zapfen-Photorezeptoren vor bzw. während ihrer Degeneration ablaufen. Zu diesem Zweck wurde eine transgene Mauslinie (HR2.1:TN-XL) generiert, in der Zapfen-Photorezeptoren selektiv den genetisch-kodierten ratiometrischen Ca^{2}-Biosensor TN-XL exprimieren. Mittels immunohistochemischer Färbungen und ERG-Ableitungen konnten wir zeigen, dass TN-XL in beiden Typen von Zapfen-Photorezeptoren der Maus exprimiert wird und dass die Gegenwart des Biosensors die Funktion dieser Zellen nicht beeinträchtigt. Mittels Zweiphotonenmikroskopie wurden licht-induzierte Ca^{2}-Antworten von einzelnen Zapfen-Photorezeptor-Terminalen gemessen und charakterisiert. Dabei konnte gezeigt werden, dass sich mit dieser Methode die Ca^{2}-Dynamik von Zapfen-Photorezeptoren besonders effizient untersuchen lässt, beispielsweise indem gleichzeitig verschiedene Komponenten bzw. Reaktionschritte der Phototransduktionskaskade pharmakologisch moduliert werden. Mit diesem Ansatz testeten wir die Hypothese, dass Stickstoffmonoxid (NO) die Ca^{2}-Dynamik in den Terminalien von Zapfen-Photorezeptoren über einen Signalweg moduliert, der eine lösliche Guanylatzyklase (sGC) involviert (NO-sGC Signalweg). Wir konnten bestätigen, dass das Ca^{2}-Niveau in Zapfen-Photorezeptoren unter Ruhebedingungen durch NO moduliert werden kann. Allerdings fanden wir keinen Beleg für eine

Beteiligung des vorgeschlagenen NO-sGC Signalwegs. Zusammenfassend kann man sagen, dass die hier erzeugte HR2.1:TN-XL Mauslinie ein wichtiges „Werkzeug“ darstellt, um die Licht-induzierte Ca^2-Dynamik und deren Regulation in den Zapfen-Photorezeptoren der Maus unter physiologischen und pathophysiologischen Bedingungen aufzuklären.

4. Introduction:

4.1. The structure of the retina:

The vertebrate retina senses as well as processes visual information from the outside world: it transforms light into electric signals, extracts salient features from the visual scene and transmits these via the optic nerve to the visual centers of the brain. The vertebrate retina is a part of central nervous system (CNS) and due to its highly organized structure and accessibility it offers an excellent opportunity to study CNS function. The retina is composed of a diversity of cell classes including neurons (such as photoreceptors, horizontal cells, bipolar cells, amacrine cells and retinal ganglion cells, (Ramón y Cajal et al., 1972); translation of the author's La rétine des vertébrés published in 1892) and glial cells (such as Müller cells, astroglia cells and microglia cells, (Boycott and Hopkins, 1981)) that are derived from multipotent progenitor cells and differentiated in a highly chronological order (Cepko, 1993; Livesey and Cepko, 2001).

The structure of the mature retina is layered and well organized (see Fig. 1). The following layers can be distinguished (Kolb, 2003): 1) the retinal pigment epithelium layer (RPE), 2) the layer containing outer and inner segments (OS+IS) of cone and rod photoreceptors in contact with RPE, 3) the outer nuclear layer (ONL), which is composed of cone and rod photoreceptor somata, 4) the outer plexiform layer (OPL), which is formed by synapses of photoreceptors, bipolar cells and horizontal cells, 5) the inner nuclear layer (INL), which includes bipolar cell, horizontal cell and amacrine cell somata, 6) the inner plexiform layer (IPL), which is formed by processes and synapses of bipolar cells, amacrine cells and ganglion cells, 7) the ganglion cell layer (GCL) with the ganglion cell somata and 8) the optic nerve fiber layer (NFL) that is formed by ganglion cell axons.

Incoming light is projected by the eye optics onto the light-sensitive OS of the photoreceptors. Because the vertebrate retina has an inverted structure, on the way to the photoreceptors the light has to pass all the neural retinal layers, which are nearly transparent. Light stimuli are converted by photoreceptors into electrochemical signals, which are then further processed by the retinal neurons including bipolar cells, horizontal cells, amacrine cells and ganglion cells (Boycott and Wassle, 1999; Masland, 2001; Wassle, 2004). Finally, the processed and integrated information is sent to the brain as spike trains via the ganglion cell axons which compose the optic nerve. The signals transmitted contain, for example, information about the

segregation of local and background motion (Olveczky et al., 2003), direction of moving objects (Taylor et al., 2000; Euler et al., 2002; Fried et al., 2002), chromatic properties (for review see (Dacey and Packer, 2003)) and contrast (Brown and Masland, 2001; Baccus and Meister, 2004).

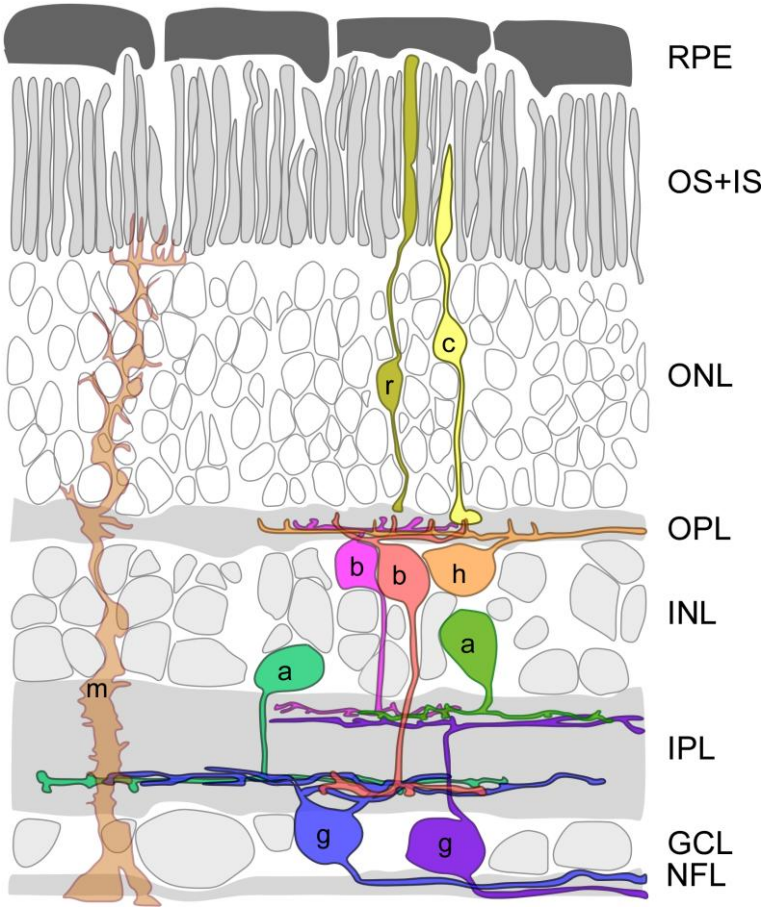

Fig. 1: Schematic structural organization of the vertebrate retina.

The vertebrate retina is a layered structure and composed of: retinal pigment epithelium (RPE), outer and inner segments (OS and IS) of cone and rod photoreceptors, outer nuclear layer (ONL), outer plexiform layer (OPL), inner nuclear layer (INL), ganglion cell layer (GCL) and nerve fiber layer (NFL).

(cones, c; rods, r; horizontal cells, h; bipolar cells, b; amacrine cells, a; ganglion cells, g; Müller cells, m)

Figure modified from (Euler et al., 2009).

4.2. Photoreceptors (rods and cones):

Photoreceptor cells represent the machinery to convert light signals into electric signals (Pugh and Lamb, 1993; Muller and Kaupp, 1998; Arshavsky et al., 2002; Fu and Yau, 2007; Mustafi et al., 2009). There are two types of photoreceptors in the

vertebrate retina: rods are responsible for vision at low light levels (scotopic condition), whereas cones are responsible for vision in daylight (photopic condition). At mesopic condition both rods and cones contribute to vision.

Most mammalian species possess two types of cones and are therefore dichromatic, while old-world primates including humans feature trichromatic color vision based on three types of cone photoreceptors (Jacobs, 1993). Tetrachromacy is among most of birds and several species of fish, amphibians and reptiles. In the mouse retina, rods are dominating in number, with cones constituting less than 3% of the photoreceptor population (Jeon et al., 1998). Mice have dichromatic vision based on short (S) and medium (M) wavelength-sensitive cones with approximate absorption maxima at 360 and 510 nm, respectively (Jacobs et al., 1991).

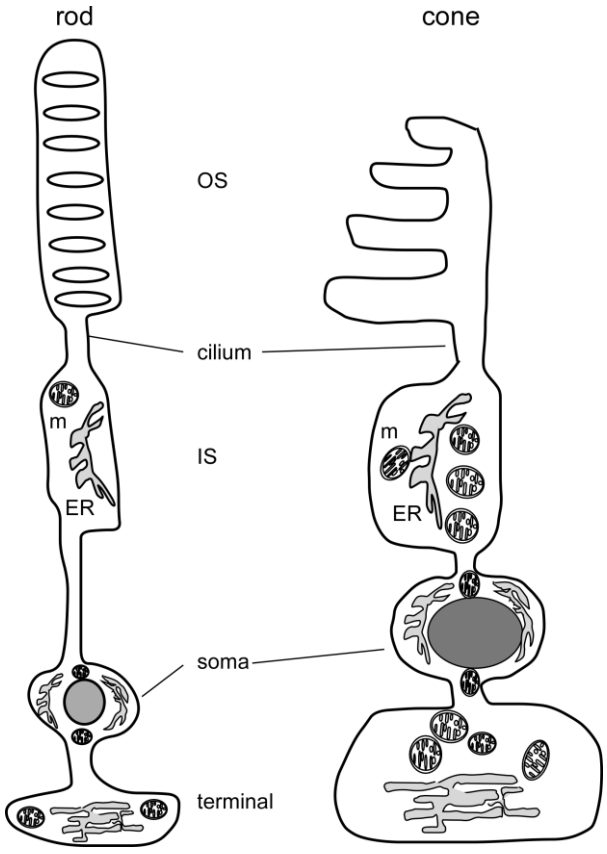

Fig.2: Rod and cone photoreceptor cells.
Schematic drawing of rod and cone photoreceptor cells.
(outer segment, OS; inner segment, IS; mitochondria, m; endoplasmic reticulum, ER).

Rods and cones have similar primary structures (Fig. 2) including OS, IS, soma and synaptic terminal (Kaneko, 1979; Muller and Kaupp, 1998; Mustafi et al., 2009). The OS of photoreceptors is filled densely with disks: in rods these disks are pinched off from the cell membrane, while cones possess open disks formed by invaginations of

cell membrane. These disks in the OS contain visual pigment molecules, rhodopsin in rods and opsin in cones. The OS is linked to the IS by a thin intracellular bridge, the so-called connecting cilium arising from the basal body in the IS. The IS hosts the metabolic machinery, whereas the cell body contains the nucleus and focuses on gene expression. The synaptic terminal contains the machinery responsible for the release of transmitter (glutamate) onto postsynaptic neurons including bipolar cells and horizontal cells.

In contrast to most "conventional" neurons, the vertebrate photoreceptors are considered non-spiking cells that maintain sustained depolarization and tonic transmitter release from the synaptic terminal in darkness. Light evokes intensity-dependent graded hyperpolarizing responses that decrease transmitter release from photoreceptor terminals. Rods are highly light-sensitive and capable of detecting and signaling single-photon events but display responses with slower kinetics, while cones are less light-sensitive but display much faster response kinetics (Korenbrot and Rebrik, 2002). These distinct response properties of rods and cones are attributable to differences in the phototransduction cascade (Tachibanaki et al., 2001; Kefalov et al., 2003; Rebrik and Korenbrot, 2004). Moreover, the kinetics of synaptic transmission is also faster in cones than in rods. The factors determining this difference include the properties of synaptic Ca^{2+} channels, differences in the diffusion distance from Ca^{2+} channels to transmitter release sites as well as vesicle replenishment and glutamate removal mechanisms (Schnapf and Copenhagen, 1982; Copenhagen et al., 1983; Thoreson, 2007).

4.3. Phototransduction in photoreceptors:

Phototransduction occurs in rod and cone photoreceptor OS based on an enzymatic cascade triggered by light-evoked activation of visual pigments (Pugh and Lamb, 1993; Muller and Kaupp, 1998; Burns and Baylor, 2001; Arshavsky et al., 2002; Fu and Yau, 2007; Mustafi et al., 2009). The visual pigment in vertebrate photoreceptors is generally composed of a chromophore (11-cis-retinal) and a transmembrane protein (opsin). Among vertebrate species, opsins can be further subdivided into cone opsins and rod-specific rhodopsins. They have very similar amino acid sequences but with specific differences that alter the peak wavelength sensitivity (for review see (Stenkamp et al., 2002)).

In darkness, high [cGMP] in the OS keeps cyclic nucleotide-gated cation (CNG) channels open leading to membrane depolarization. This depolarization opens voltage-gated Ca^{2+} channels (VGCCs), which allow Ca^{2+} influx into the synaptic terminal, leading to sustained transmitter release. Light initiates the phototransduction cascade (see Fig. 3; phototransduction in rod OS as an example) with the absorption of photons by 11-cis retinal within opsin proteins (rod rhodopsin or cone opsin). The retinal is photoisomerized to all-trans retinal, thereby inducing a conformational change in the opsin protein, which in turn binds to the G-protein transducin. Binding of opsin to transducin exchanges the GDP with GTP, which activates the α-subunit of transducin to dissociate from transducin complex, with GTP bound to the transducin α-subunit. The α-subunit-GTP complex activates membrane associated phosphodiesterase (PDE). Activated PDE hydrolyzes cGMP to 5'-GMP resulting in decrease of the intracellular [cGMP]. Drop of intracellular [cGMP] causes closure of CNG channels, leading to hyperpolarization of the membrane potential and closure of VGCCs at the terminals. Efficient pumps and exchangers at the terminals (for details see section 4.4) quickly lower intracellular [Ca^{2+}] and thereby decrease release of glutamate at the synaptic terminals.

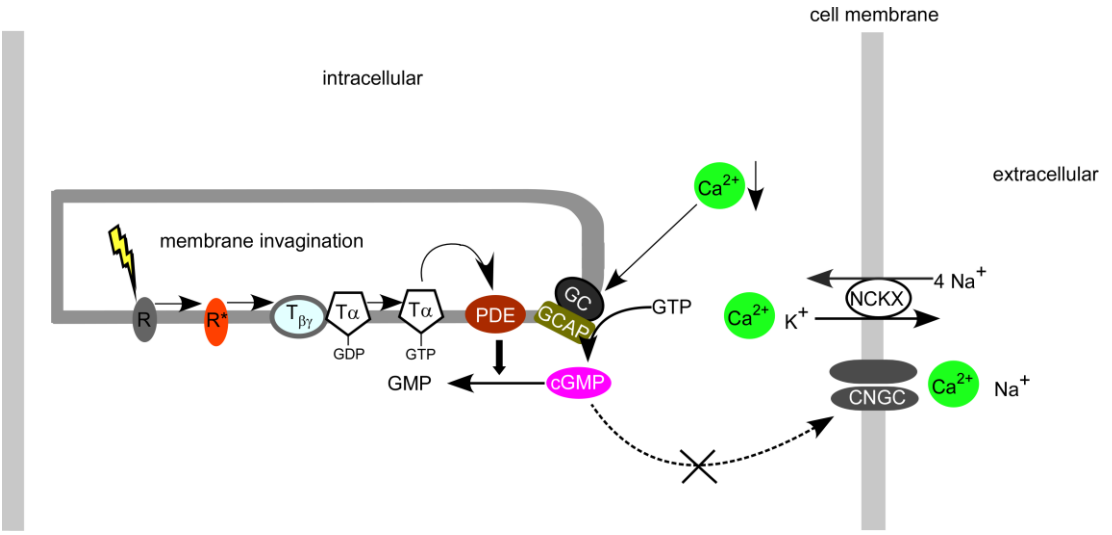

Fig.3: Schematic drawing of phototransduction cascade in photoreceptor OS.
Schematic diagram illustrates biochemical cascade of phototransduction in vertebrate photoreceptor OS.
(rhodopsin, R; activated rhodopsin, R*; transducin, T; phosphodiesterase, PDE; guanylate cyclase, GC; guanosine triphosphate, GTP; GC activating proteins, GCAP; sodium/calcium-potassium exchanger, NCKX; cyclic nucleotide-gated channel, CNGC).

Recovery of the light response requires restoration of the [cGMP] to the dark level. The [cGMP] is determined by PDE mediated hydrolysis and guanylate cyclase (GC)-mediated synthesis (Koch, 1991; Venkataraman et al., 2003). Guanylate cyclase activity is regulated by the GC activating proteins (GCAPs, (Subbaraya et al., 1994; Olshevskaya et al., 1997)) in a Ca^{2+} dependent manner. In darkness, the relatively high [Ca^{2+}] promotes the formation of the Ca^{2+}-bound form of GCAPs, which inhibits GC. When the [Ca^{2+}] declines during the light response, the dissociation of Ca^{2+} allows GCAPs to activate GC, thereby restoring the basal [cGMP].

4.4. Calcium regulation in photoreceptors:

Calcium is a universal and ubiquitous signaling messenger to control a large variety of cellular processes (Carafoli et al., 2001; Berridge et al., 2003) including fertilization, proliferation, development, learning and memory, contraction and secretion (Berridge et al., 2000). The signaling potential of Ca^{2+} is based on the steep concentration gradient between cytosol (with basal [Ca^{2+}] typically ~50 nM) and extracellular space (with [Ca^{2+}] ~1.5 mM) (Krizaj and Copenhagen, 2002). Because of the [Ca^{2+}] gradient between the cytosol and the extracellular space, Ca^{2+} influx across the plasma membrane and/or Ca^{2+} release from intracellular stores can produce significant changes of free cytosolic [Ca^{2+}] (Berridge et al., 2000).

In photoreceptors, Ca^{2+} regulates intracellular processes in a highly compartmentalized manner. Changes in intracellular [Ca^{2+}] modulate phototransduction cascade in OS (see section 4.3), energy metabolism in IS, gene expression in soma and transmitter release at terminal (Korenbrot, 1995; Koutalos and Yau, 1996; Fain et al., 2001; Krizaj and Copenhagen, 2002; Johnson et al., 2007).

To elucidate the compartmentalized Ca^{2+} functions in photoreceptors, it is essential to identify the spatial distribution of the Ca^{2+} regulating “toolkits” such as Ca^{2+} buffers, channels, transporters and intracellular stores (see Fig. 4). Calcium regulation is similar in rod and cone photoreceptors, however, Ca^{2+} dynamics in rods and cones differs in kinetics and capacities (Krizaj and Copenhagen, 2002; Johnson et al., 2007; Kramer et al., 2007).

Calcium dynamics in the OS, where phototransduction cascade takes place, is regulated by CNG channels and sodium/calcium-potassium exchangers (NCKXs, (Korenbrot, 1995; Krizaj and Copenhagen, 1998)). CNG channels are transmembrane proteins that open a cation-permeable pore across the membrane in response to the direct binding of intracellular cGMP (for review see (Kaupp and

Seifert, 2002; Matulef and Zagotta, 2003)). The opening of CNG channels results in Ca^{2+} and Na^{+} influx into the OS. The K^{+}-dependent NCKX is thought to be the main mechanism for transporting Ca^{2+} out of the photoreceptor OS. Nevertheless, accumulated evidence suggests that there are very likely other yet unknown pathways to regulate Ca^{2+} in the OS. For instance, loss of the cone specific NCKX2 (Prinsen et al., 2000; Schnetkamp, 2004) did not show any obvious cone dysfunction (Li et al., 2006), suggesting that other Ca^{2+} extruding pathways can compensate for the lack of NCKX2 in cones. Evidences for other pathways that are not yet well characterized include the type 1 inositol 1,4,5-triphosphate (IP3) receptor (Wang et al., 1999) and ryanodine receptors (RyRs, (Shoshan-Barmatz et al., 2007)) based on their localization in photoreceptor OS revealed by immunohistochemistry. Another result that implies the presence of further Ca^{2+} regulating pathways in the OS is that the disks were shown to take up Ca^{2+} in an ATP-dependent manner, leading to the suggestion of an ATPase pump residing on disk membrane propound being involved in the Ca^{2+} regulation (Carretta and Cavaggioni, 1976; Sack and Harris, 1977; Puckett et al., 1985; Panfoli et al., 1994).

The photoreceptor IS contains mitochondria and endoplasmic reticulum (ER), both of which are generally considered to serve as Ca^{2+} stores (Gunter et al., 2000; Verkhratsky, 2005; Szabadkai and Duchen, 2008; Berridge, 2009; Puzianowska-Kuznicka and Kuznicki, 2009). An anatomical study on the distribution of mitochondria and ER in photoreceptors revealed that both organelles are present at high densities in the IS (Johnson et al., 2007). The ER is the most important Ca^{2+} store and controls cytosolic Ca^{2+} dynamics in concert with mitochondria and cell membrane-bound Ca^{2+} regulating components (for Ca^{2+} regulation by ER see review (Puzianowska-Kuznicka and Kuznicki, 2009)). Mitochondria can participate in Ca^{2+} regulation, especially under pathological conditions (Toescu and Verkhratsky, 2003; Toescu, 2004). However, it remains to be elucidated how Ca^{2+} is regulated in this region.

In the photoreceptor soma, Ca^{2+} regulates gene expression, but it is unclear how Ca^{2+} dynamics is regulated in this compartment. An immunohistochemical study revealed that the transient receptor potential channel 6 (TRPC6) is expressed in photoreceptor somata (Krizaj, 2005) suggesting a potential involvement in somatic Ca^{2+} regulation in photoreceptors. However, its exact role in Ca^{2+} regulation remains unknown.

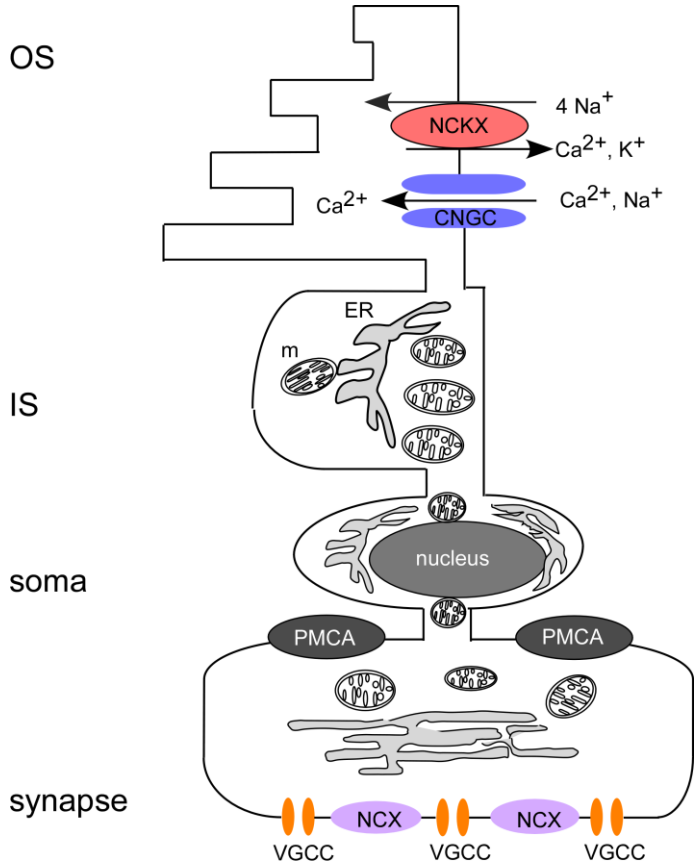

Fig. 4: Schematic diagram of calcium regulating machineries in mouse cone photoreceptor.
The drawing shows distribution of Ca^{2+} regulating channels, transporters as well as intracellular Ca^{2+} stores including mitochondria and ER.
(outer segment, OS; inner segment, IS; cyclic nucleotide-gated channel, CNGC; sodium/calcium-potassium exchanger, NCKX; mitochondria, m; endoplasmic reticulum, ER; voltage-gated Ca^{2+} channels, VGCC; plasma membrane Ca^{2+} ATPase, PMCA; sodium/calcium exchanger, NCX).
Schematic drawing is based on (Johnson et al., 2007).

In photoreceptor synaptic terminals, the main role of Ca^{2+} is to regulate release of the transmitter glutamate. In darkness, rod terminals maintain lower [Ca^{2+}] than cone terminals do, resulting in a lower exocytosis rate in rods, whereas cone terminals are able to reduce the higher intra-terminal [Ca^{2+}] to achieve a greater degree in graded hyperpolarization during light adaptation (Johnson et al., 2007; Sheng et al., 2007). L-type voltage-gated Ca^{2+} channels (VGCCs) sensitive to membrane potential are the main mode for Ca^{2+} entry into photoreceptor terminals (Nachman-Clewner et al., 1999; Krizaj and Copenhagen, 2002; Szikra and Krizaj, 2006; Johnson et al., 2007). Extrusion of Ca^{2+} from the terminal is implemented by the plasma membrane Ca^{2+} ATPase (PMCA) and the sodium/calcium exchanger (NCX, (Krizaj et al., 2002; Johnson et al., 2007)). The photoreceptor PMCA has a higher Ca^{2+} affinity and

removes Ca^{2+} in an ATP-dependent manner with a relatively low turnover rate, whereas NCX has a higher capacity for Ca^{2+} extrusion and is especially well suited for recovery from a massive [Ca^{2+}] increase. Their respective properties suggest that at high [Ca^{2+}], NCX lowers [Ca^{2+}] rapidly to its K_d value and that PMCA is crucial for the fine tuning of [Ca^{2+}] (Zylinska and Soszynski, 2000).

There is evidence that in amphibian (Krizaj et al., 1999; Cadetti et al., 2006; Suryanarayanan and Slaughter, 2006) and mammalian rod terminals (Babai et al., 2010) Ca^{2+} influx induces Ca^{2+} release from internal stores (Ca^{2+}-induced Ca^{2+} release, CICR) to amplify synaptic transmitter release. Such a role of CICR for Ca^{2+} amplification has been described in details for controlling myocyte contraction (Endo et al., 1970; Fabiato and Fabiato, 1975; Fabiato, 1983). Whether or not ER-mediated CICR serves a similar role in (mammalian) cone terminals is not known. Furthermore, novel pathways for Ca^{2+} regulation that involve internal Ca^{2+} stores in (amphibian) photoreceptor terminals have been proposed, such as for example contribution of store-operated Ca^{2+} entry (Szikra et al., 2009).

Taken together, the Ca^{2+} regulation in photoreceptors is highly compartmentalized and involves a number of different Ca^{2+} entry, uptake and extrusion mechanisms, which are not yet completely understood.

4.5. Potential role of calcium imbalance in photoreceptor disorders:

Unsurprisingly, due to its versatility in cellular processes, Ca^{2+} dynamics plays a crucial role not only in physiological but also in pathophysiological processes (for review see (Cheng et al., 2006)). Imbalance in Ca^{2+} homeostasis leads to pathological processes: depletion of cytosolic Ca^{2+} leads to rapid and inevitable cell death (Verkhratsky and Toescu, 2003; Paschen and Mengesdorf, 2005) as well as overload of cytosolic Ca^{2+} is highly toxic and represents a general mechanism of cell demise (Choi, 1992; Eimerl and Schramm, 1994; Nicotera and Orrenius, 1998; Berliocchi et al., 2005).

Also in photoreceptors, abnormalities in Ca^{2+} dynamics are tightly connected to pathophysiological processes such as degeneration (Chang et al., 1993; Fox et al., 1999; Sancho-Pelluz et al., 2008). Calcium overload was proposed to trigger photoreceptor cell death (Fox et al., 1999). Activation of calpain-type proteases in degenerating rod and cone photoreceptors was observed by using *in situ* biochemical assay (Paquet-Durand et al., 2006; Trifunovic et al., 2010). Because

calpain is a Ca^{2+}-dependent protease, this finding suggested that intracellular [Ca^{2+}] is, in fact, elevated during the neurodegenerative process.

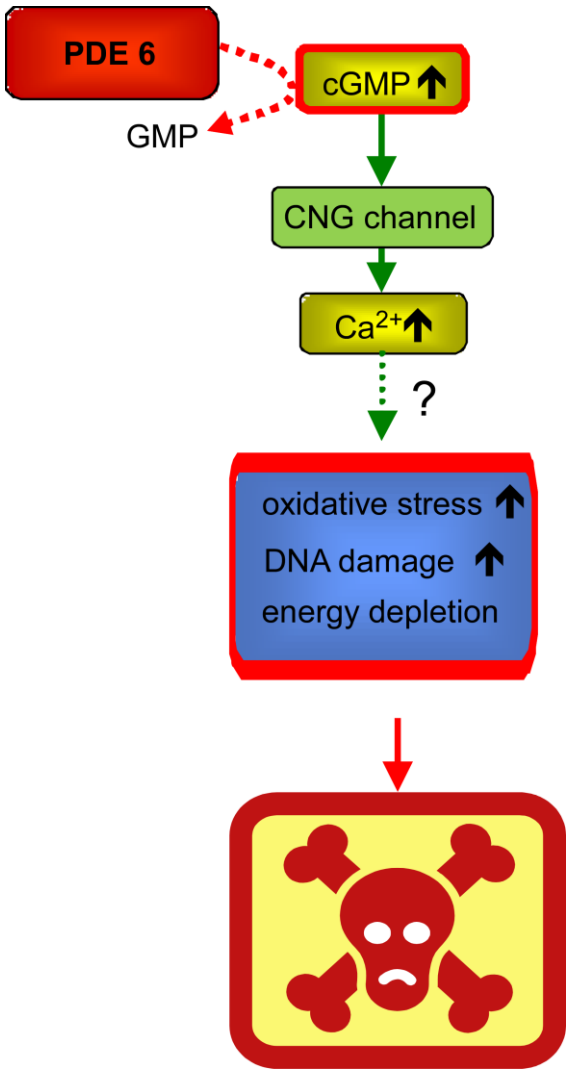

Fig. 5: Molecular pathways during retinal photoreceptor degeneration.
PDE6 mutation-induced deregulation of cGMP results in accumulation of cGMP, thereby causes Ca^{2+} influx through CNG cation-channels resulting in Ca^{2+} overload in OS. Elevated [Ca^{2+}] causes oxidative DNA damage, energy depletion and cell death, eventually.
Figure modified from (Sancho-Pelluz et al., 2008).

In retina degeneration 1 (*rd1)* retina, accumulation of cGMP leads to rod cell death due to a mutation in the rod specific *Pde6b* (Bowes et al., 1990). Binding of cGMP to CNG channels in the OS increases the open possibility of these channels and increased Ca^{2+} influx through CNG channels leads to Ca^{2+} accumulation, and eventually rod degeneration ((Sancho-Pelluz et al., 2008); see Fig. 5). Recently, it was reported that in *rd1* mice that lack functional CNG channels photoreceptor degeneration was postponed significantly (Paquet-Durand et al., 2011). Lack of

functional CNG channels should result in decreased Ca^{2+} influx, which will in principle compensate Ca^{2+} overload as caused by *Pde6b* mutation. Therefore, this *Cngb1*$^{-/-}$ x *rd1* line confirmed that Ca^{2+} is crucial for the progress of retinal degeneration in *rd1*.

In cone photoreceptor function loss 1 (*cpfl1)* retina (Chang et al., 2009), loss of functional cone-specific PDE6 (mutation in *Pde6c*) leads to cone degeneration (Trifunovic et al., 2010). The underlying degeneration mechanism has been suggested to be similar to that in *rd1* retina: Elevated [cGMP] leads to opening of CNG channels, which in turn was proposed to cause Ca^{2+} overload in *cpfl1* cones (Trifunovic et al., 2010).

While all the aforementioned reports support the hypothesis that Ca^{2+} is elevated before and/or during retinal degeneration, these data consist of indirect evidence. Yet to really understand the role of Ca^{2+} dynamics in these degenerative processes it is important to be able to monitor intracellular Ca^{2+} dynamics directly in living photoreceptors.

4.6. Optical calcium recording:

Calcium imaging makes use of synthetic or genetically encoded fluorophors that change their fluorescence properties (e.g. spectral distribution, fluorescence lifetime) as a function of intracellular [Ca^{2+}]. Therefore, these indicator dyes are of immense importance for studying cellular Ca^{2+} signaling (Knot et al., 2005), which is, as discussed above, involved in controlling a plethora of cellular processes under physiological as well as pathophysiological conditions. While Ca^{2+} imaging provides extremely useful spatially and temporally resolved information about intracellular Ca^{2+} dynamics, one has also to keep in mind, that different processes contribute to the measured intracellular [Ca^{2+}] and that therefore an increase in [Ca^{2+}], for instance, does not necessarily represent depolarization. Calcium levels are affected by 1) Ca^{2+} entry through VGCC and/or ligand-mediated receptors from the extracellular space, 2) Ca^{2+} release from intracellular stores (i.e. ER and mitochondria), 3) Ca^{2+} extrusion from the cytosol mediated by pumps and exchangers and 4) Ca^{2+} uptake into intracellular stores (for review see (Berridge et al., 2000)). Therefore, the recorded Ca^{2+} signal requires careful interpretation and further dissection, e.g. with pharmacological means. Still, in many cases Ca^{2+} activity approximates neuronal activity and therefore Ca^{2+} imaging allows for comprehensive functional studies of microcircuits in neuronal networks. Often, Ca^{2+} imaging can be used to indirectly monitor action potential trains, because action potential trains cause brief Ca^{2+} influx

through VGCCs in neuronal membranes (Gobel and Helmchen, 2007). This method of “imaging spiking activity” has become very important in neuroscience and generated significant insights into the operation of the CNS (Voitenko et al., 1999; Mao et al., 2001; Ghozland et al., 2002; Cossart et al., 2003).

Calcium indicators can be categorized into two groups, synthetic chemical Ca^{2+} indicators (SCCI), which are typically small fluorescent molecules capable of chelating Ca^{2+} ions, and genetically encoded Ca^{2+} indicators (GECI, synonym: Ca^{2+} biosensor), which are basically a combination of one or more fluorescent proteins and a Ca^{2+} binding protein. These two groups of Ca^{2+} indicators have distinct advantages and disadvantages.

Synthetic Ca^{2+} indicators possess typically a greater dynamic range (fractional change in intensity or ratio) and faster kinetics compared to GECIs (Palmer and Tsien, 2006; Paredes et al., 2008). In the AM ester form, SCCIs provide an easy loading method for introducing these dyes into living cells (Tsien, 1989, 1992). The major disadvantages of such AM-forms are that 1) they can be compartmentalized into cellular organelles (instead of remaining in the cytosol, where one typically wants to monitor Ca^{2+}), 2) they can leak out of the cells and make chronic imaging over long time periods impossible and 3) they cannot be targeted to specific cell populations or cellular compartments (Palmer and Tsien, 2006; Mank and Griesbeck, 2008; Paredes et al., 2008).

Calcium biosensors or GECIs possess several advantages over conventional SCCIs: 1) They can be expressed in a cell type-specific manner and therefore allow monitoring Ca^{2+} dynamics in defined cell types, 2) they can be targeted to specific subcellular compartments, 3) their continuous expression over extended time periods allows chronic time-lapse imaging. Their main disadvantages include that 1) in general they possess a smaller dynamic range of their fluorescence intensity/ratio compared to SCCIs, 2) by FRET-based GECIs the baseline ratio cannot be always adjusted to zero even in the absence of FRET, which makes it very difficult to detect small changes in low [Ca^{2+}] range (for review see (Takahashi et al., 1999)), 3) it requires more sophisticated methods to introduce GECIs into cells such as electroporation, lipofection and viral transduction (McCombs and Palmer, 2008).

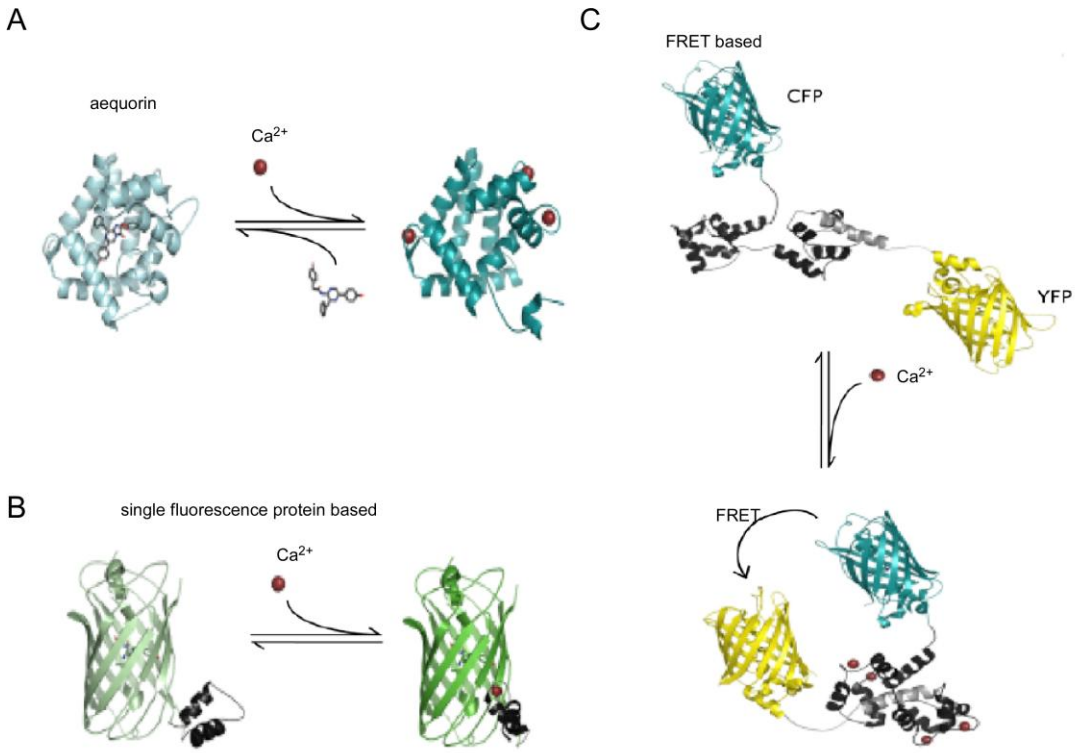

Fig. 6: Three classes of genetically encoded calcium indicators that have been developed with different strategies.

(**A**): The aequorin in complex with coelenterazine. Upon binding of Ca^{2+}, aequorin undergoes a conformational change, releasing coelenteramide and emitting light.

(**B**): Single fluorescent protein-based sensor. Binding of Ca^{2+} causes a change in protein conformation and a shift in the protonation state of the chromophore.

(**C**): FRET-based sensor containing a Ca^{2+} binding domain between two fluorescent proteins. By Ca^{2+} binding, distance between the two fluorescent proteins is shortened thereby increasing the efficiency of FRET.

Figure modified from (McCombs and Palmer, 2008).

So far, three main classes of Ca^{2+} biosensors (see Fig. 6) have been developed with different strategies (McCombs and Palmer, 2008): 1) GECIs can be based on aequorin, a photoprotein from the bioluminescent jellyfish aequorea, which upon Ca^{2+} binding emits fluorescence due to a chemical reaction that requires reconstitution of the indicator with a cofactor, 2) GECIs can consist of a single fluorescent protein, into which Ca^{2+} sensitive elements are inserted and alter the spectral properties of the protein upon binding/unbinding of Ca^{2+}, 3) GECIs utilize FRET; here the Ca^{2+} sensitive moiety is typically flanked by two fluorescent proteins and alters the efficiency of FRET between them. In the latter two cases, the fluorescent proteins are in most cases the green fluorescent protein (GFP) or its derivatives.

The criterion how to choose an appropriate Ca^{2+} indicator depends on the purpose and setup in the researcher's projects.

4.7. TN-XL calcium biosensor and HR2.1 promoter:

In the present study, the Ca^{2+} biosensor TN-XL (Mank et al., 2006) was used to detect Ca^{2+} dynamics in mouse cones.

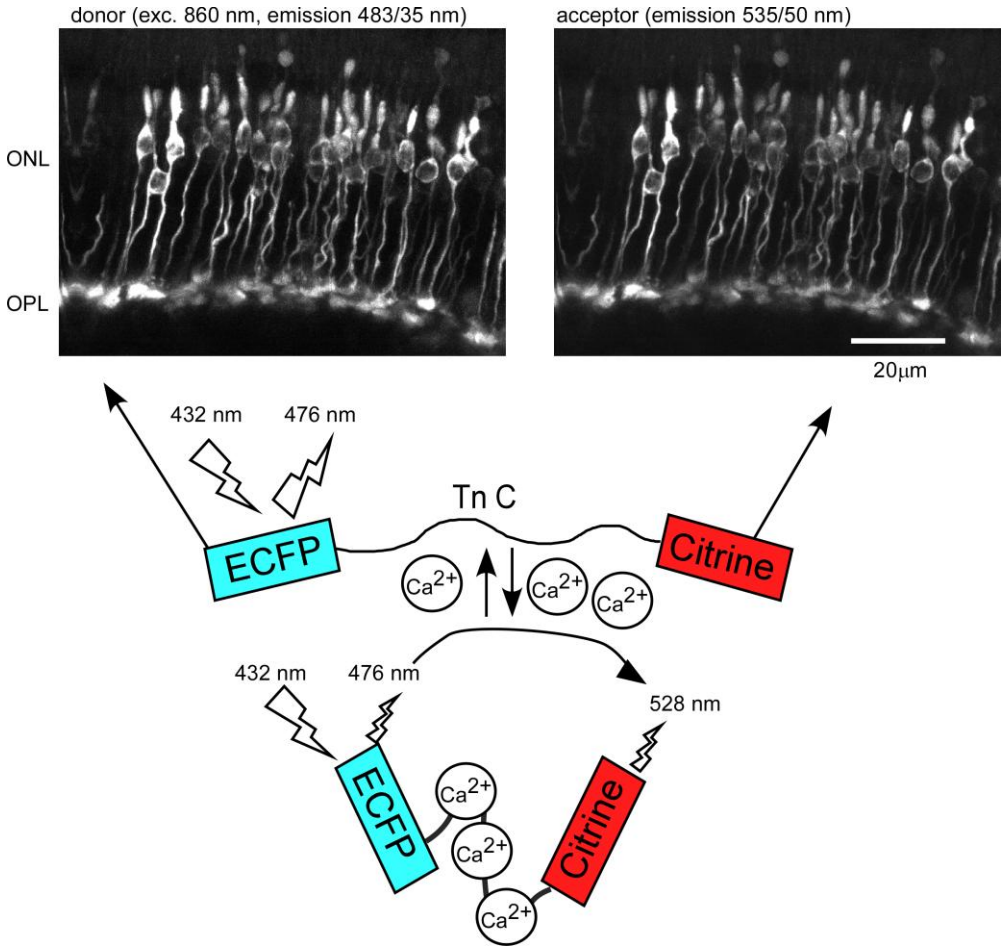

Fig. 7: Schematic drawing of FRET-based TN-XL with exemplary calcium imaging by two-photon microscopy.

Calcium ions bind to Troponin C (TnC) of the TN-XL Ca^{2+} biosensor leading to a conformational change in TN-XL, thereby enhancing FRET from the donor (ECFP) to the acceptor moiety (Citrine). The illumination wavelength is chosen so as to excite only the donor, the ensuing donor and acceptor emissions are monitored separately at their respective wavelengths (upper example for Ca^{2+} imaging by two-photon microscopy).

TN-XL is a FRET-based Ca^{2+} indicator that uses mutated chicken skeletal Troponin C as Ca^{2+} binding moiety. The mutated form of Troponin C displays a much increased affinity to Ca^{2+} (Mank et al., 2006; Mank and Griesbeck, 2008). Troponin C is flanked by ECFP and circular permuted Citrine acting as fluorescence donor and

acceptor, respectively, in the FRET process (see Fig. 7). TN-XL displays a large fractional fluorescence change in its emission ratio over a large [Ca^{2+}] range. *In vivo* Ca^{2+} imaging demonstrated that TN-XL exhibits stable fluorescence signals in the presynaptic motor neuron terminals of transgenic fruit flies (Mank et al., 2006). TN-XL possesses a faster decay time-constant compared to other GECIs (Garaschuk et al., 2007; Hendel et al., 2008). Its Ca^{2+} affinity *in vitro* was reported to be relatively low (K_d = 2.20 µM), however, *in vivo* it appears to be somewhat higher (K_d ~0.77 µM, (Hendel et al., 2008)) depending on the local environment of different cell types. The relatively low Ca^{2+} affinity of TN-XL could limit its application, i.e. when very small Ca^{2+} fluctuation needs to be detected. On the other hand, due to this property TN-XL is expected to have minimal effect on intrinsic Ca^{2+} buffering capacity (Takahashi et al., 1999).

To drive TN-XL expression specifically in mouse cones, we used the HR2.1 promoter, which is a 2.1 kb fragment of the upstream sequence of human red opsin gene. This sequence contains a 1.6 kb BamHI–StuI fragment joined to a proximal promoter of 495 base pairs of the human red pigment gene (Wang et al., 1992; Li et al., 2008). The version of human red opsin promoter has been shown to be sufficient to drive cone photoreceptor-specific expression of reporter genes in mouse (Wang et al., 1992), rat and guinea pig (Li et al., 2008) retinas. Using this promoter, in rat the reporter expressing was M-cone selective (Li et al., 2008), whereas in mouse both cone types, M- and S-cones, expressed the transgene (Wang et al., 1992). The reason for this species-related difference could be ascribed to the species difference (Li et al., 2008).

4.8. Physiological role of nitric oxide in retinal functions:

Nitric oxide (NO) was proposed to modulate Ca^{2+} dynamics in amphibian photoreceptor terminals via a NO-sGC pathway (Kurenny et al., 1994; Savchenko et al., 1997; Blom et al., 2009). By using the established HR2.1:TN-XL mouse line, we investigated whether NO modulates Ca^{2+} dynamics in mouse cone terminals through such a pathway.

Nitric oxide is a well known to exert a variety of functions on cell physiology (Rosselli et al., 1998; Doutheil et al., 2000; Guix et al., 2005; Gotoh and Mori, 2006; Garthwaite, 2008). It is produced by NO synthase (NOS) from the amino acid L-arginine (see Fig. 8) and is a membrane permeable signaling molecule with a short half-life (Knowles and Moncada, 1992; Feldman et al., 1993; Hakim et al., 1996). Thus, it exerts its actions either within the source cell or diffuses from the source cell to affect adjacent cells (Lubos et al., 2008).

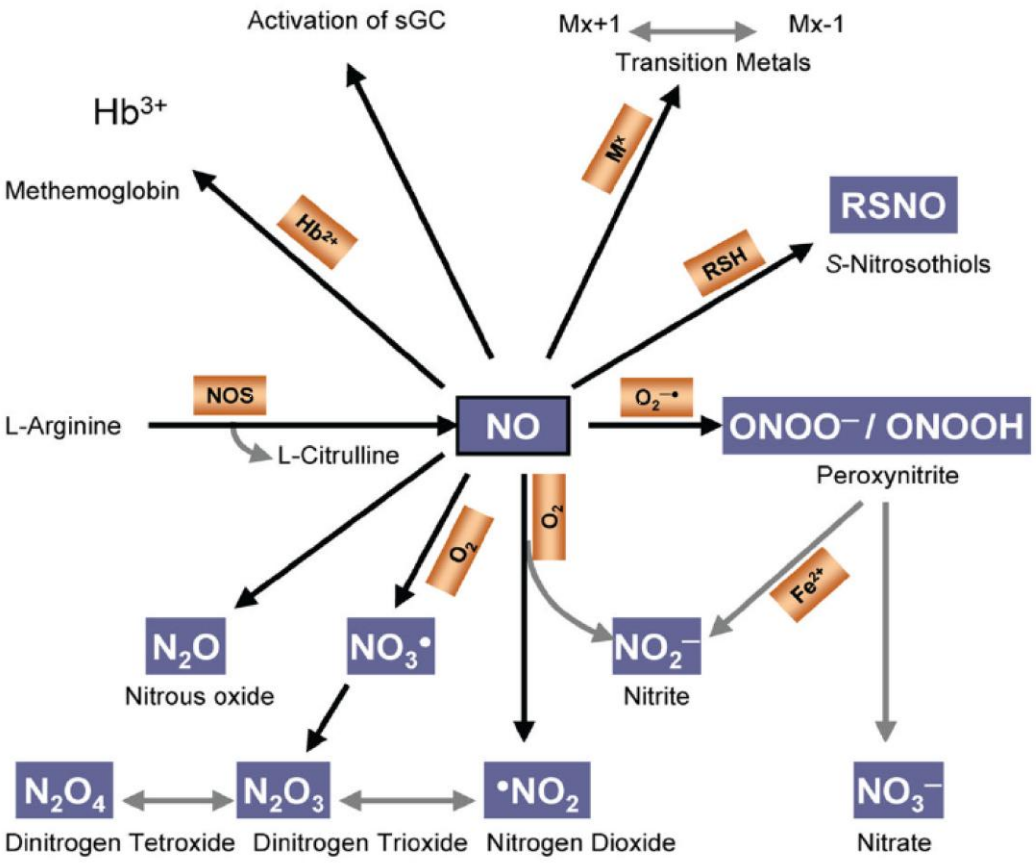

Fig. 8: Biochemical reactions of nitric oxide and its derivates.
Nitric oxide (NO) is synthesized by nitric oxide synthase (NOS) using L-arginine and reacts with a variety of targets. It reacts with soluble guanylate cyclase (sGC) to produce cGMP, with transition metals (M), with thiol groups (RSH) to produce *S*-nitrosothiols (RSNO) and with superoxide anion ($O_2^{-\bullet}$) to form peroxynitrite (ONOO−/ONOOH). Nitric oxide can be reduced to nitrous oxide (N_2O) or oxidized to nitrite (NO_2^-).
Figure modified from (Lubos et al., 2008).

One well described function of NO is to activate soluble guanylate cyclase (sGC) through the “classical” NO-sGC pathway (see Fig. 9) in a number of physiological processes (Denninger and Marletta, 1999). The hemoprotein sGC is activated by NO

(with an estimated half-maximal effective concentration EC_{50} of ~1 nM, (Wykes and Garthwaite, 2004)) and converts GTP into cGMP, resulting in a rise of cytosolic [cGMP], which transmits the NO signal to the subsequent target of cGMP, such as cGMP-dependent protein kinases and CNG channels (for review see (Calabrese et al., 2007)).

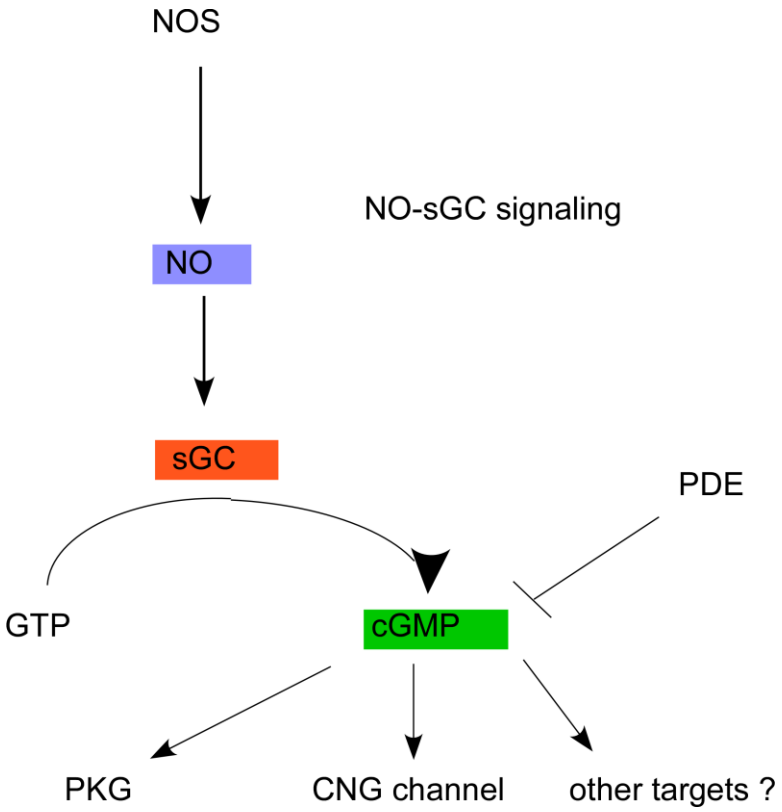

Fig.9: NO-sGC pathway.
Soluble guanylate cyclase (sGC) is activated by the binding of NO to transform GTP into cGMP, resulting in increase of intracellular [cGMP]. Intracellular cGMP has several downstream effectors including protein kinase G (PKG) and the CNG channels. Phosphodiesterase (PDE) hydrolyzes cGMP and therefore acts to counteract excessive production of cGMP.

As an oxidizing agent NO can also react with a large variety of potential targets, depending on its local concentration and environment (see Fig. 8). Nitric oxide can react with thiol groups (RSH) to produce *S*-nitrosothiols (RSNO). Nitric oxide reacts with superoxide anion ($O_2^{-\bullet}$) to produce peroxynitrite ($ONOO^-$), which is a powerful oxidant, and therefore cytotoxic. Furthermore, NO can be reduced to nitrous oxide (N_2O) or oxidized to nitrite (NO_2^-). In summary, NO exerts its functions either through direct NO interactions with its targets or indirectly through its metabolites. Important cellular effects of NO include: protein posttranslational modification nitration and S-nitrosylation to alter activities of target proteins (Lipton et al., 1996; Broillet, 1999;

Cassina et al., 2000; Doutheil et al., 2000; Amici et al., 2003), inhibition of cytochrome C oxidase in mitochondria (Brown and Cooper, 1994; Cleeter et al., 1994; Brown, 1999) and suppression of protein synthesis in ER (Doutheil et al., 2000). Excessive NO causes cytotoxic effects including genetic mutations (Nguyen et al., 1992; Routledge et al., 1994; Juedes and Wogan, 1996), inhibition of DNA repair enzymes (Kwon et al., 1991; Lepoivre et al., 1991) as well as ER stress (Doutheil et al., 2000; Li et al., 2000; Gotoh and Mori, 2006).

Nitric oxide has been shown to be involved in retinal functions and was suggested to be a contributor to the pathology underlying (some) retinal diseases (Goldstein et al., 1996; Kelly and Barnes, 1997; Gotzes et al., 1998; Muller and Koch, 1998; Djamgoz et al., 2000). It is well established that NO modulates the functions of ganglion cells and amacrine cells in inner retina (Ahmad et al., 1994; Mills and Massey, 1995; Wang et al., 2003; Hoffpauir et al., 2006). Nitric oxide was also reported to regulate gap junction permeability and modulate glutamate receptors in horizontal cells (Devries and Schwartz, 1992; McMahon and Ponomareva, 1996) as well as activate sGC in bipolar cells (Shiells and Falk, 1992; Snellman and Nawy, 2004).

Several studies also demonstrated NO effects on photoreceptors (Schmidt et al., 1992; Rieke and Schwartz, 1994; Levy et al., 2004) and it was proposed that NO modulates Ca^{2+} dynamics in amphibian photoreceptor terminals via a NO-sGC pathway (Kurenny et al., 1994; Savchenko et al., 1997; Blom et al., 2009). Based on electroretinogram (ERG) recordings, NO was reported to also affect rodent photoreceptor function (Sato and Ohtsuka, 2010; Vielma et al., 2010), but it is still unclear whether or not the effects in amphibian and mammals are based on the same pathway.

4.9. Aim and contributions:

4.9.1. Aim of this study:

Due to the importance of Ca^{2+} in regulating intracellular processes under physiological and pathophysiological conditions, it is crucial to be able to monitor Ca^{2+} dynamics in such processes *in vivo*. Moreover, monitoring Ca^{2+} activity in cones provides the possibility for comprehensive functional studies of microcircuits in early visual processing. However, this direct approach of assessing Ca^{2+} dynamics has so far been hampered by different factors, including the relatively low number of cone photoreceptors in the mouse retina and the lack of cell-specific labeling techniques with Ca^{2+} indicators.

The aim of the present study was to investigate Ca^{2+} dynamics specifically in mouse cones using the genetically encoded Ca^{2+} indicator TN-XL. To achieve the goal, the tasks in the project include:

(A) to design a construct on which expression of the Ca^{2+} biosensor (here TN-XL) is driven by using a specific promoter (the human red opsin promoter HR2.1);

(B) to generate a transgenic mouse line carrying the construct that stably expresses TN-XL in cones specifically;

(C) to characterize the generated mouse line using immunohistochemistry and ERG;

(D) to evaluate pharmacologically modulated Ca^{2+} signal in different compartments;

(E) to evaluate light-evoked Ca^{2+} responses in subcellular resolution;

(F) to modulate light-evoked Ca^{2+} responses pharmacologically;

(G) to investigate specific hypothesis (here Ca^{2+} modulation by NO through NO-sGC pathway in cone terminals) by using the HR2.1:TN-XL mouse line.

4.9.2. Contributions:

I performed following experimental procedures and methods:

- ✓ Creation of the HR2.1:TN-XL construct
- ✓ Screening of the transgenic founder mice by using single-photon confocal laser scanning microscope
- ✓ Immunohistochemical study on retinal whole mounts and vertical sections
- ✓ Tissue preparation for physiological measurements
- ✓ Ca^{2+} imaging with pharmacology using single-photon confocal laser scanning microscope
- ✓ Ca^{2+} imaging by using two-photon microscope and light-evoked Ca^{2+} response experiments
- ✓ Pharmacological manipulation of light-evoked Ca^{2+} response
- ✓ Analysis of Ca^{2+} imaging data obtained with single- and two-photon microscopes

The following experimental procedures and methods were carried out by Norman Rieger and Britta Baumann (Molecular Genetics Laboratory, Centre for Ophthalmology, University Clinics Tübingen):

- ✓ Screening of the transgenic founder mice by PCR and quantitative PCR

The following experimental procedures and methods were carried out by the group of Thomas Ott (Transgenic Animals Core Facility, University Medical School, Tübingen):

- ✓ Microinjection of HR2.1:TN-XL construct into pronuclei of fertilized ova and manipulation of fertilized ova into foster mice

The following experimental procedures and methods were carried out by Naoyuki Tanimoto (Division of Ocular Neurodegeneration, Centre for Ophthalmology, Institute for Ophthalmic Research, University of Tübingen):

- ✓ Electroretinogram examination on one month old HR2.1:TN-XL mice

The following experimental procedures and methods were carried out by Gorden Eske (Centre for Integrative Neuroscience (CIN)/Institute for Ophthalmic Research, Centre for Ophthalmology, University of Tübingen):

- ✓ Preparation of retinal sections for immunochemical staining

The following experimental procedure was carried out by Francois Paquet-Durand (Institute for Ophthalmic Research, Centre for Ophthalmology, University of Tübingen):

- ✓ NOS diaphorase assay

5. Materials and methods:

5.1. Equipments and materials:

5.1.1. Setups and microscopes:

Two-photon microscopy system

Newport Spectra-Physics, **Darmstadt, Germany**	Ti/sapphire laser (MaiTai-HP DeepSee) calibrated photometer (Model 842-PE, 200-1100 nm)
Sutter Instruments, **Novato, CA, USA**	movable objective microscope, custom-modified in lab of AG Euler
Olympus, **Tokyo, Japan**	XLUMPlanFL 20x/0.95w objective
AHF, Tübingen, Germany	HC 483/32 optic filter D 535/50 optic filter

Light stimulator

AHF, Tübingen, Germany	UV: 360 BP 10 green: 520 BP 10 beamsplitter: 400 DCLP
Arduino **http://www.arduino.cc**	open source microprocessor board

CLSM system

Nikon, Tokyo, Japan	Eclipse FN1 microscope Fluor, 40x/0.80w objective
AHF, Tübingen, Germany	HC 469/35 optic filter ET 535/30 optic filter
Coherent, Dieburg, Germany	Radius 405-25 diode laser system
ALA Scientific Instrument, **Westbury, NY, USA**	$VC^3$4 System focal perfusion system 100 µm-diameter tip manifold

Equipments for immunohistochemistry

Leica Microsystems GmbH, Wetzlar, Germany	JUNG CM3000 cryotome
Zeiss, Oberkochen, Germany	Zeiss Imager Z1 Apotome Plan-APOCHROMAT 5x/0.16, 20x/0.8 EC Plan-NEOFLUAR 40x/1.3 oil filter sets 38 for Alexa 488, excitation 470/40 nm, emission 525/50 nm filter sets 50 for Alexa 660, excitation 640/30 nm, emission 690/50 nm

Molecular genetics equipments

Applied Biosystems, Foster City, USA	GeneAmp PCR System 2400 GeneAmp PCR System 9600 GeneAmp PCR System 9700
Biorad, Richmond, USA	agarose gel electrophoresis chamber
Eppendorf, Hamburg, Germany	Thermomixer comfort
GFL, Burgwedel, Germany	water bath shaker
Hereaus, Osterode, Germany	Biofuge Fresco Biofuge 15 incubator
Thermo Fisher Scientific Inc. Wilmington, US	NanoDrop-ND-1000-Spectrophotometer

5.1.2. Chemical list:

Baxter, Unterschleißheim, Germany	Isoflurane
BioLog, Bremen, Germany	8-pCPT-cGMP

Biozym Biotech Trading GmbH, Wien, Austria	LE agarose
Carl Roth GmbH+Co., Karlsruhe, Germany	ampicillin powder milk
Calbiochem, Darmstadt, Germany	proteases inhibitor cocktail
GE Healthcare, Munich, Germany	bromophenol blue
Merck, Damstadt, Germany	ethanol 70% glucose KCl
Serva Feinbiochemica GmbH, Heidelberg, Germany	ethidium bromide
Sigma-Aldrich, Steinheim, Germany	BSA caffeine DMSO $MgCl_2$ NaCl NADPH NGS NBT ODQ PFA SNAP Triton X-100 zaprinast
USB Amersham, Cleveland, USA	dNTPs

5.1.3. Consumbles and reagent kits:

Applied Biosystems, Foster City, USA	BigDye® Terminator V3.1 sequencing kit

Dow Corning, Midland, USA	high vacuum grease
Electron Microscopy Sciences, Hatfield, PA, USA	plastic cover slips for acute retinal slices
Eppendorf, Hamburg, Germany	Fast Plasmid Mini Kit
MARTOR KG, Solingen, Germany	blades for tissue chopper
MBI Fermentas, Vilnius, Lithuania	GeneJET Plasmid Miniprep Kit
Millipore, Cork, Ireland	0.8 µm pore filter membrane
Qiagen, Hilden, Germany	QIAquick Gel Extraction Kit
Vector, Burlingame, CA, USA	vectashield mounting medium

5.1.4. Buffers and media:

ACSF	125 mM NaCl 26 mM $NaHCO_3$ 1.25 mM NaH_2PO4 2.5 KCl 1 mM $MaCl_2$ 2 mM $CaCl_2$ 20 mM glucose 0.5 mM L-glutamine
dNTP-solution	5 mM dATP 5 mM dCTP 5 mM dGTP 5 mM dTTP 5 mM Tris (pH 7.5)
microinjection buffer	0.1 mM EDTA 10 mM Tris-HC (pH 7.5)

PBS	20 NaH_2PO_4, 80 Na_2HPO_4, 154 NaCl (pH 7.4)
50 x TAE buffer	2 M Tris base 5.71% (v/v) acetic acid 50 mM EDTA pH 8.0
TE buffer	1 mM EDTA 10 mM Tris (pH 7.5)

5.1.5. Antibodies:

Abcam, Cambridge, UK	rabbit anti-sGC (#AB50238)
Chemicon International, **Hofheim, Germany**	rabbit anti-blue opsin (#AB5407) rabbit anti-red/green opsin (#AB5405)
Novus Biologicals, **Littleton, CO, USA**	mouse anti-GFP (#NB600-597)
Invitrogen, Molecular Probes, **Eugene, OR, USA**	secondary antibodies Alexa Fluor 488 and 660

5.1.6. Enzymes for molecular genetics:

New England Biolabs, **Beverly, USA**	restriction enzymes AscI BamHI BglII NheI
Perkin Elmer, Foster City, USA	Taq polymerase
Stratagene, La Jolla, USA	Pfu Turbo DNA polymerase
USB Amersham, Cleveland, USA	SAP

5.1.7. Primer list:

*** Feo 164:**	CCT GAG GGT CAC GGC GCT TTA T
*** Feo 203:**	CCA GCA AAT CCC TCT GAG CC
*** Feo 207:**	TTA GGA GTA GTC GCA TTA GAG A
*** Feo 208:**	CAG AGG AGG AGT GGG GTG TC
*** HR 2.1-fwA:**	AGT GAG ATC TGC TAG CCC TAC AGC AGC CAG GGT GAG
*** HR 2.1 revA:**	CTG GCA GAT CTG GCT ATG GAA AGC CCT GTC C
MM-OPA1_QF:	CCT CTG CGT TTA TTT GAA GAA TG
MM-OPA1_QR:	AAA AGG GTA GAA CGG GAG GA
*** RGCP-30FW:**	AAC GTG ACT CGA CCC AGT AA
*** RGCP-20RV:**	GGC CAG GGT GGA AGA TTA GAT G
TN-XXL-fw:	CAA CAT CGA GGA CGG CAG
*** TNX1-rev:**	GCC CTG AGA ATC TCA CC
TNXL Seq R1:	TGC ACG CCC CAG GTC AG

(5’ -> 3’; * for DNA sequencing)

5.2. Molecular genetics:

5.2.1. Overview of the cloning strategy and procedure:

The TN-XL plasmid construct (Mank et al., 2006) was kindly provided by Oliver Griesbeck (Max-Planck-Institute for Neurobiology, München-Martinsried, Germany) and the Human red opsin promoter (HR2.1) containing plasmid (Wang et al., 1992) was kindly provided by Jeremy Nathans (Howard Hughes Medical Institute, Baltimore, MD, USA). A strategy was devised to combine parts of both plasmids to generate the new construct HR2.1:TN-XL, in which the TN-XL is under the control of the HR2.1 promoter, which has been shown to drive specific expression in mouse cone photoreceptors (S- and M-cones, (Wang et al., 1992)). The cloning strategy and procedure are presented as an overview (Fig. 10) followed:

1. HR2.1 was amplified by PCR. Subsequently, the PCR product was digested by BglII and the fragment was gel purified.
2. Into the TN-XL plasmid an AscI restriction site was introduced downstream of the TN-XL sequence by *in vitro* mutagenesis for later linearization of the final construct.
3. The TN-XL ($AscI^+$) plasmid was digested by BamHI and BglII, then the large DNA fragment was gel purified.
4. The purified DNA fragments (from steps 1. and 3.) were ligated and the ligation products were transformed into *E. coli* cells.
5. Correct clones were identified by colony PCR and isolated plasmid DNA was verified by DNA sequencing, subsequently.
6. Eventually, the final construct HR2.1:TN-XL ($AscI^+$) was linearized by restriction enzyme digestion and purified for later microinjection.

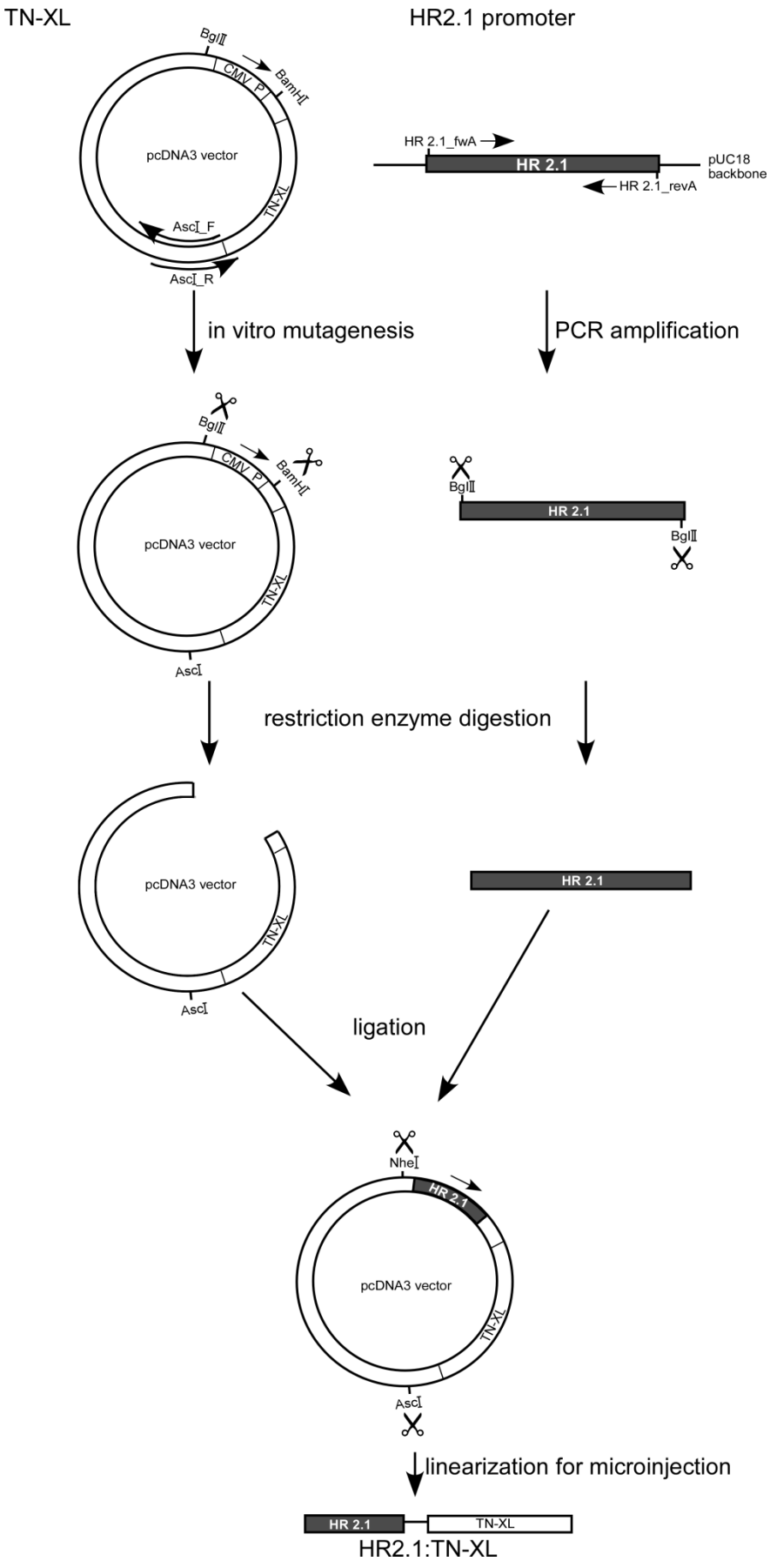
TN-XL
HR2.1 promoter
BglII
CMV P
BamHI
pcDNA3 vector
TN-XL
AscI_F
AscI_R
HR 2.1_fwA
HR 2.1
HR 2.1_revA
pUC18
backbone
in vitro mutagenesis
PCR amplification
BglII
CMV P
BamHI
pcDNA3 vector
TN-XL
AscI
BglII
HR 2.1
BglII
restriction enzyme digestion
pcDNA3 vector
TN-XL
AscI
HR 2.1
ligation
NheI
HR 2.1
pcDNA3 vector
TN-XL
AscI
linearization for microinjection
HR 2.1
TN-XL
HR2.1:TN-XL

Fig. 10 Flow chart for design of HR2.1:TN-XL.

Strategy and procedures for design of HR2.1:TN-XL are presented as flow chart. HR2.1 and TN-XL were combined, so that TN-XL is under the control of HR2.1. For microinjection of the construct, HR2.1:TN-XL was linearized from vector by restriction digestion.

5.2.2. PCR amplification:

The HR2.1 promoter fragment was amplified by PCR using the HR2.1 plasmid as template; the selective amplification of DNA sequence was performed with appropriate sense and antisense primers.

PCR reaction setup:

0.5 µl HR2.1-plasmid (100 ng)

0.9 µl primer HR2.1-fwA (100 ng)

1.1 µl primer HR2.1- revA (100 ng)

4 µl 10x PfuTurbo buffer

2 µl dNTPs

30.5 µl H_2O

1 µl PfuTurbo DNA polymerase (2.5 U/µl)

PCR Cycling conditions:

	cycles	temperature	duration
1. denaturation	1	94°C	1 min
2. denaturation annealing elongation	30	94°C	1 min
		58°C	1 min
		72°C	3 min
3. final elongation	1	72°C	10 min

After the thermal cycling, the reaction was cooled down to 8°C and the PCR product was stored at 4°C until use.

5.2.3. *In vitro* mutagenesis by PCR:

The excision of the DNA fragment for later microinjection (devoid of most vector backbone sequences) requires unique restriction sites to be present on the HR2.1:TN-XL plasmid with one located upstream and one located downstream of the promoter/TN-XL sequence. Here, a unique downstream restriction site was created on the original TN-XL plasmid by site-directed mutagenesis. At base positions 3312-3319 (ggc ttt cc) of the TN-XL plasmid the -ttt- sequence was replaced by the

sequence -gcg-, thereby generating the restriction site AscI at this site. Primer sequences for *in vitro* mutagenesis were as follows:

Primer (5' -> 3'):

AscI_F: CCA CGT TCG CCG GCG CGC CCC GTC AAG CTC

AscI_R: GAG CTT GAC GGG GCG CGC CGG CGA AAC GTG G

(nucleotides exchanged with respect to the template DNA in red) Tm = 80,57

Reaction Setup:

5 µl 10 x Pfu buffer

20 ng Plasmid DNA

125 ng AscI_F primer

125 ng AscI_R primer

2 µl dNTP (5 mM each dNTP)

1µl PfuTurbo DNA polymerase (2.5 U/µl)

H_2O added to 50 µl

PCR Cycling conditions:

	cycles	temperature	duration
1. denaturation	1	95°C	30 s
2. denaturation annealing elongation	18	95°C	30 s
		55°C	1 min
		68°C	8 min
3. final elongation	1	68°C	8 min

An elongation time of 1 minute per kilobase pairs (kb) of plasmid length was recommended, therefore, elongation for the TN-XL plasmid was applied for 8 minutes with an approximate size of 8 kb. After the thermal cycling, the reaction was cooled down to 8°C.

5.2.4. Restriction enzyme digestion of plasmid DNA or PCR-products:

The TN-XL ($AscI^+$) plasmid contains the cytomegalovirus (CMV) promoter upstream of the TN-XL gene. To replace the CMV promoter with the HR2.1 promoter, the CMV promoter was excised by restriction enzyme digestion. For this purpose TN-XL ($AscI^+$) plasmid DNA was digested with BamHI and BglII.

Reaction Setup:

2.45 µl TN-XL ($AscI^+$) DNA (408.5 ng/µl)

2 µl 10 x NEB 3 buffer

2 µl BSA (1mg/ml)

12.55 µl H_2O

0.5 µl BamHI (10 U/µl)

0.5 µl BglII (10 U/µl)

The digestion mix was incubated for 1 hour at 37°C. Subsequently, dephosphorylation (which is required to prevent re-circularization of the linearized plasmid in the later ligation step) was performed by adding 2U shrimp alkaline phosphatase (SAP) for 1 hour at 37°C. The reaction was stopped by heating the sample to 65°C for 15 minutes, which completely inactivates SAP activity.

The PCR product of the HR2.1 promoter fragment was digested with BglII as follows:

25 µl PCR product (196.5 ng/µl)

4 µl 10 x NEB 3 buffer

10 µl H_2O

1 µl BglII (10 U/µl)

The digestion reaction was incubated for 1 hour at 37°C.

5.2.5. Gel electrophoresis purification and DNA extraction:

For separation and purification of the DNA fragments used for the later ligation reaction, both restriction enzyme digestions were electrophoresed on a 1% (m/v) agarose gel in 1x TAE buffer. The QIAquick Gel Extraction Kit (Qiagen, Hilden, Germany) was used for the purification of DNA from gel slices. The agarose gel was stained with ethidium bromide (1/1000 vol. of 100µg/ml ethidium bromide in gel) and the desired fragments were excised from the gels and collected into an Eppendorf cup. The gel slices were mixed with three volumes of buffer QG and dissolved by incubation for 10 minutes at 50°C. After the addition of one gel volume of isopropanol, the samples were applied to QIAquick column and centrifuged for 1 minute at 12,000 rpm. The spin columns were washed once with 500 µl QG and once with 500 µl PE and then were placed into clean 1.5 ml centrifuge tubes. The bound DNA was eluted from the column with 50 µl EB buffer applying centrifugal force (1 minute – 12,000 rpm). DNA concentrations were quantified with a NanoDrop-ND-1000-Spectrophotometer (Thermo Fisher Scientific Inc. Wilmington, DE, USA) according to manufacturer's instruction.

5.2.6. Ligation of TN-XL ($AscI^+$) and HR2.1 fragments:

Ligation of the gel-purified DNA fragments of TN-XL ($AscI^+$) and HR2.1 (molar ratio of insert to vector = 5:1) was performed by applying T4 DNA Ligase.

Ligation Reaction Setup:
1.8 µl TN-XL ($AscI^+$) fragment (20 ng)
15.5 µl HR2.1 promoter fragment (100 ng)
2 µl 10 x T4 ligase buffer
1 µl T4 DNA ligase (4 U/µl)

The ligation reaction mix was incubated at 16°C over night.

5.2.7. Transformation of chemically competent *E. coli* cells:

Transformation of chemical competent *E. coli* cells with the ligation product HR2.1: TN-XL ($AscI^+$) was performed according to the manufacturer's recommendations (Invitrogen BV, Groning, NL).

30 µl competent cells (*DH5α*) were thawed on ice. 2 µl of the ligation reaction were added to the cells and the suspension was incubated on ice for 20 minutes. A heat shock was applied to the cells by incubating in a 42°C water bath for 20 seconds. Afterwards the cells were put back on ice for another 2 minutes. 300 µl SOC medium were added to the transformation mix and then the cell suspension was incubated for 1 hour at 37°C while shaking at 225 rpm. To obtain single colonies, the transformation suspensions were plated on selective LB-agar plates (with ampicillin as an antibiotic).

5.2.8. Colony PCR:

In order to identify bacterial colonies that contain the plasmid with desired construct and confirm that HR2.1 ($AscI^+$) and TN-XL are in correct orientation, colony PCR was performed, which is a quick and simple method to screen for plasmid inserts, directly from *E. coli* colonies. Single colonies were picked from the LB-agar plates and resuspended in 40 µl H_2O with some rest of each colony spread onto backup LB-agar plates. Colony suspensions were mixed with 10 µl of a PCR reaction mix composed of:

2 µl dNTP-mix (5 mM)
5 µl ATI buffer

1 µl forward-primer FEO 203 (10 pmol/µl)

1 µl reverse-primer TNX 1(10 pmol/µl)

0.8 µl H_2O

0.2 ml Taq polymerase (5 U/µl)

PCR Cycling Conditions:

	cycles	temperature	duration
1. Pre-PCR	1	60°C	20 min
2. denaturation	1	94°C	4 min
3. denaturation	25	94°C	30 s
annealing		53°C	30 s
elongation		72°C	3 min
4. final elongation	1	72°C	5 min

After termination of the reaction the temperature was set at 8°C.

5.2.9. Isolation of plasmid DNA:

For small-scale plasmid isolation, 5 ml LB-medium supplemented with 5 µl ampicillin (final concentration = 100µg/ml) were inoculated with a single bacterial colony (screened positive by colony PCR) and incubated for 12-16 hours at 37°C while shaking at 200-250 rpm. Before plasmid isolation 500 µl of the culture were mixed with 500 µl 50% glycerol and stored at -80°C as frozen stock.

The plasmid isolation was performed according to the GeneJET Plasmid Miniprep Kit (MBI Fermentas, Vilnius, LT) user manual. Harvested plasmid DNA was resuspended in TE buffer and quantified by Nanodrop measurement.

5.2.10. DNA sequencing:

The integrity and correctness of the new construct was validated by DNA sequencing. Sequencing of the purified plasmid DNA was performed by Cycle Sequencing using BigDye® Terminator V3.1 chemistry (Applied Biosystems, Foster City, USA) with the primers that cover the entire length of HR2.1:TN-XL fragment (see primer list).

Reaction Setup:

1.5 µl DNA (500ng)

4 µl BigDye sequencing buffer 5x

2 µl BigDye v3.1

11.5 µl H_2O

1 µl primer (5pmol/µl)

Cycling conditions:

	cycles	temperature	duration
1. denaturation	1	96°C	2 min
2. denaturation annealing elongation	25	96°C	15 s
		53°C	15 s
		60°C	4 min
3. final elongation	1	8°C	∞

After termination the reaction was cooled down to 8°C.

5.2.11. Preparation of linearized construct for microinjection:

For the microinjection into fertilized eggs, the HR2.1:TN-XL core fragment was excised from the vector backbone by restriction enzyme digestion with NheI and AscI.

Digestion reaction setup:
1 µl DNA (2.32 µg)
4 µl 10 x Tango buffer
2 µl NheI (10U/µl)
2 µl AscI (10U/µl)
31 µl H_2O

The reaction was incubated at 37°C for 3 hours, then the enzymes were heat inactivated by incubation for 20 minutes at 65°C. Digested DNA fragments were stored at -20°C before purification by gel electrophoresis. Separation of the digestion products was performed by gel electrophoresis on a 0.8% TAE/Seakem agarose gel. The HR2.1:TN-XL core fragment was excised from the gel and purified using the QIAquick Gel Extraction Kit (Qiagen, Hilden, Germany) as described above. Purified DNA was dissolved in microinjection buffer containing 0.1 mM EDTA and 10 mM Tris-HCl (pH 7.5). DNA quantity was determined by Nanodrop analysis. In addition an aliquot of the DNA was subjected to electrophoresis on a 1.5% agarose along with a series of a DNA standard (2, 5, 10, 20, 50 and 100 ng of λHindIII/EcoRI standard). The DNA samples were stored at 4°C.

Following the same strategy and procedure, two further constructs were created by Britta Baumann (Molecular Genetics Laboratory, Centre for Ophthalmology, University Clinics Tübingen). One construct was designed to

express TN-XL under the HR2.1 promoter – similar to the construct described above (HR2.1:TN-XL), but then supplemented with human CNGB3 gene of the CNG channel at the 3' end. This was done to direct localization of TN-XL specifically in cone OS. The second construct was designed to express TN-XL under the control of the mouse Nrl promoter (Akimoto et al., 2006) to target specific expression of TN-XL in mouse rods. The linearized constructs were also prepared for microinjection for generating transgenic mouse lines.

5.3. Generation of the transgenic mouse line expressing TN-XL in photoreceptors:

In order to achieve stable expression of TN-XL in photoreceptors, the mouse line HR2.1:TN-XL was generated by standard transgene technologies (Gordon and Ruddle, 1981).

5.3.1. Microinjection of HR2.1:TN-XL construct into the pronuclei of fertilized ova:

All procedures including isolation of oocytes, microinjection of the DNA fragment and re-implantation of embryos into foster mothers were performed by lab members of Dr. Thomas Ott (Transgenic Animals Core Facility, University Medical School, Tübingen).

All procedures were performed in accordance with the law of animal experimentation issued by the German Federal Government (Tierschutzgesetz) and approved by the State's legal body (Regierungspräsidium Tübingen) for the evaluation animal experimentation. Transgenic mice were generated by direct microinjection of the HR2.1:TN-XL core DNA fragment into the pronuclei of fertilized ova (Gordon and Ruddle, 1981). The manipulated fertilized ova were transferred into the oviducts of foster mice, which had a heterogenic genetic background that was known to yield superior injection results.

5.3.2. Selection of transgenic mice by PCR and quantitative PCR:

All procedures of the identification of transgenic founder mice by PCR, the determination of the transgene copy numbers by q-PCR as well as animal cross-breeding were carried out by Norman Rieger and Britta Baumann (Molecular Genetics Laboratory, Centre for Ophthalmology, University Clinics Tübingen).

Newborn mice from the microinjection experiment were analyzed by PCR for the presence of the transgene HR2.1:TN-XL. For that DNA was extracted from ear punches and subjected to PCR amplification with primers FEO203 and TNXLSeqR1 that cover a junction fragment between HR2.1 and TN-XL.

Quantitative PCR (q-PCR) was performed to estimate the copy numbers of the integrated transgene fragment and to assess its stability in subsequent breeding. For quantification the ΔΔCt method (Livak and Schmittgen, 2001; Schmittgen and Livak, 2008) was applied by comparing the amplification of a transgene fragment with that of a genomic locus (Opa1). Quantitative PCRs were carried out with probes of the Universal Probe Library (Roche, Mannheim, Germany) and performed on a Lightcycler 480 instrument (Roche). For calibration of genomic copy numbers the serial dilutions of the HR2.1:TN-XL plasmid spiked into mouse genomic DNA were used.

5.3.3. Selection of transgenic mice by using single-photon confocal laser scanning microscopy (CLSM):

These founder mice positive for transgene integration were crossed with C57Bl6 wild-type mice and the obtained F1 offspring of the founder mice were screened for TN-XL expression. For that purpose unfixed retinal whole mounts and sections (for procedure of tissue preparation see 5.4.2) were analyzed by CLSM (for procedure of microscopy see methods 5.7.1).

5.3.4. Generation of the purebred mouse line HR2.1:TN-XL:

The offspring of founder mice were analyzed for TN-XL expression in photoreceptors using fluorescence microscopy (see 5.5.3). Only the offspring of one founder animal (HR2.1:TN-XL) with an estimated copy number of ~15 yielded stable and strong expression of TN-XL. To establish a purebred mouse line that carries the transgene insertion on both chromosomes (and therefore supersedes genotyping of newborn mice), transgene-positive animals were cross-bred and identified with a doubling in the copy numbers (and thus most likely homozygous for the transgene insertion) by q-PCR for subsequent breeding. This line referred to HR2.1:TN-XL was used for all subsequent histological and physiological experiments.

5.4. Animals and tissue preparation:

Animals were housed under a standard white cycling lighting (12 hours). For retina dissection the animals were anesthetized with isoflurane (Baxter, Unterschleißheim,

Germany) inhalation and killed by cervical dislocation. All procedures were performed in accordance with the law of animal experimentation issued by the German Federal Government (Tierschutzgesetz) and approved by the State's legal body (Regierungspräsidium Tübingen) for the evaluation animal experimentation.

5.4.1.Retinal whole-mounts and sections for immunohistochemistry:

Retinal sectioning for immunohistochemistry was carried out by Gorden Eske (Centre for Integrative Neuroscience (CIN)/Institute for Ophthalmic Research, Centre for Ophthalmology, University of Tübingen).

For immunohistochemistry retinal whole mounts and vertical sections were prepared from eight weeks old HR2.1:TN-XL animals (purebred line). After the mice were sacrificed, the eyes were marked at the nasal side to be able to maintain the retinal orientation and quickly enucleated. The retinas were dissected out and fixed in 4% paraformaldehyde (PFA) diluted in PBS containing (in mM) 20 NaH_2PO_4, 80 Na_2HPO_4, 154 NaCl (pH 7.4) for 45 minutes at 4°C. Then the retinas were washed with PBS and cryoprotected in increasing concentrations of sucrose (10, 20 and 30%). For vertical sections, completely fixed eyes were embedded in tissue freezing medium, frozen in liquid N_2 and sectioned into 12 µm using a cryotome (JUNG CM3000, Leica Microsystems GmbH, Wetzlar, Germany). The sections were collected on glass slides and stored at -20°C for later use.

5.4.2. Acute retinal slices for calcium imaging:

For Ca^{2+} imaging, acute retinal slices were prepared from 4-7 weeks old HR2.1:TN-XL mice. For those experiments that involved light stimulation (two-photon imaging) the animals were dark adapted for at least 2 hours before the dissection. After the mice were sacrificed, the eyes were quickly enucleated and hemisected in carboxygenated (95% O_2, 5% CO_2) ACSF solution containing (in mM) 125 NaCl, 2.5 KCl, 2 $CaCl_2$, 1 $MgCl_2$, 1.25 NaH_2PO_4, 26 $NaHCO_3$ and 20 glucose (pH 7.4). Remaining vitreous was carefully removed using forceps, before the retina was dissected from the eyecup. The retinas were cut in half, flattened by cutting off their edges and put onto filter paper (0.8 µm pore size, Millipore, Ireland) with the photoreceptor layer facing up. Approximately 200 µm thin vertical slices were cut by using a custom-made tissue chopper (Werblin, 1978) with razor blades (MARTOR KG, Solingen, Germany). Slices with the filter paper attached were then stabilized using high vacuum grease (Dow Corning, Midland, USA) on plastic cover slips (Electron Microscopy Sciences, Hatfield, PA, USA). This way the slices could be

stored in a holding chamber with carboxygenated ACSF at room temperature before they were placed in the recording chambers under the microscopes. In the respective recording chambers of the two microscope systems (see 5.7), the slices were perfused constantly with warmed (~36°C) carboxygenated ACSF.

5.5. Anatomy:

5.5.1. Immunohistochemistry:

Retinal sections on slides stored at -20 C were desiccated at 37 C and subsequently rehydrated in PBS. The slices were then incubated for 1 hour at room temperature in blocking solution containing 0.3% PBS-T, 1% BSA and 5-10% corresponding normal serum from the host animal (goat or rabbit) in which the respective secondary antibodies were raised. Primary antibodies including rabbit anti-blue opsin (1:200), rabbit anti-red/green opsin (1:200), mouse anti-GFP (1:200) and rabbit anti-sGC (1:200) were diluted in blocking solution and applied to the sections. After over-night incubation at 4°C with the primary antibodies, the sections were washed four times for 5 minutes in PBS and then incubated for 1 hour at room temperature with secondary antibodies (Alexa Fluor 488 and 660, Invitrogen, Molecular Probes, Eugene, OR, USA) diluted 1:500 in PBS. After washing six times in PBS, the sections were covered with coverslips by using vectashield mounting medium (Vector, Burlingame, CA, USA).

5.5.2. NOS activity assay:

The NOS diaphorase assay was carried out by Francois Paquet-Durand (Institute for Ophthalmic Research, Centre for Ophthalmology, University of Tübingen).

The NOS diaphorase assay (Hope et al., 1991) was performed by incubating rehydrated retinal tissue sections for 4 hours at 37°C in 0.3% PBS-T, 0.7 mM NADPH, 0.25 mM Nitro Blue Tetrazolium (NBT; both from Sigma-Aldrich, Steinheim, Germany). After washing three times in PBS the sections were mounted using vectashield.

5.5.3. Standard fluorescence microscopy:

Standard fluorescence microscopy was performed on a Zeiss Imager Z1 Apotome Microscope (Zeiss, Oberkochen, Germany), equipped with a Zeiss Axiocam digital camera, Zeiss objectives (Plan-APOCHROMAT 5x/0.16, 20x/0.8 and EC Plan-NEOFLUAR 40x/1.3 oil) and Zeiss filter sets (filter set #38 for Alexa 488, excitation

470/40 nm, emission 525/50 nm; filter set #50 for Alexa 660, excitation 640/30 nm, emission 690/50 nm). Images were acquired with Zeiss Axiovision® 4.8 software and processed using Canvas (ACD Systems International Inc., Saanichton, BC, Canada).

5.6. Electroretinograms (ERGs):

ERGs were performed by Naoyuki Tanimoto (Division of Ocular Neurodegeneration, Centre for Ophthalmology, Institute for Ophthalmic Research, University of Tübingen).

To determine whether the expression of TN-XL in cones alters visual function of the mouse line, binocular ERGs were recorded on HR2.1:TN-XL mice at the age of 4 weeks, as described previously (Seeliger et al., 2001; Tanimoto et al., 2009). The ERG equipment consisted of a Ganzfeld bowl, a direct current amplifier, and a PC-based control and recording unit (Multiliner Vision; VIASYS Healthcare GmbH, Hoechberg, Germany). First, mice were anaesthetized using Ketamine (66.7 mg/kg body weight) and Xylazine (11.7 mg/kg body weight). Then their pupils were dilated and single flash ERG responses were obtained under dark-adapted (after overnight dark adaptation) and light-adapted (with a background illumination of 30 cd/m^2 starting 10 minutes before recording) conditions. Single white-flash stimuli ranged from -4 to 1.5 log cd*s/m^2 under dark-adapted and from -2 to 1.5 log cd*s/m^2 under light-adapted conditions. Ten responses were averaged with inter-stimulus intervals of 5 seconds (for -4 to -0.5 log cd*s/m^2) or 17 seconds (for 0 to 1.5 log cd*s/m^2). Responses to trains of flashes (flicker) for a fixed intensity (0.5 log cd*s/m^2; the *International Society for Clinical Electrophysiology of Vision* standard flash [ISCEV SF] intensity; (Marmor et al., 2004a)) at 18 and 20 Hz were obtained under dark-adapted conditions. Flicker responses were averaged 30 times. Band-pass filter cut-off frequencies were 0.3 and 300 Hz for all ERG recordings. The Mann-Whitney rank sum test was used to test for statistical significance of differences in a-wave and b-wave ERG amplitudes in HR2.1:TN-XL (n=6) and wt (littermates, n=6) mice.

5.7. Calcium imaging:

5.7.1. Single-photon confocal laser scanning microscopy (CLSM):

The microscope used for recording drug-evoked Ca^{2+} responses in the TN-XL expressing cones was an Eclipse FN1 microscope (Nikon, Tokyo, Japan) equipped with a diode laser (Radius 405-25, Radius Laser System, Coherent, Dieburg, Germany) that allowed exciting the fluorescence donor (ECFP) of the TN-XL indicator at 405 nm. A 40x water immersion objective (Fluor, 40x/0.80w, Nikon,

Tokyo, Japan) was used to acquire images (256x256 pixels, for time-lapsed recordings every 5 seconds) at the emission wavelengths of ECFP (HC 469 BP 35 filter, AHF, Tübingen, Germany) and Citrine, the fluorescence acceptor (ET 535 BP 30, AHF). Control images were recorded for at least 2 minutes before drug application (see 5.9.1.), for which a focal perfusion system was used ($VC^3$4 System, manifold with tip diameter of 100 µm; ALA Scientific Instrument, Westbury, NY, USA).

5.7.2. Two-photon microscopy:

A custom-built two-photon microscope (Denk et al., 1990) was used as described earlier (Euler et al., 2009; Breuninger et al., 2011). In brief, the system was equipped with a mode-locked Ti/sapphire laser (MaiTai-HP DeepSee, Newport Spectra-Physics, Darmstadt, Germany) tuned to ~860 nm, two detection channels for fluorescence imaging of ECFP (483 BP 35, AHF) and Citrine (D 535 BP 50, AHF) and a 20x water-immersion objective (XLUMPlanFL 20× water-immersion, 0.95 NA, Olympus). Retinal slices were placed in recording chamber at 36°C - 36.5°C perfused with carbogenated ACSF. Image acquisition was performed using customized software (CfNT, by Michael Müller, MPImF) and by taking 128x8 pixel images (at 62.5 Hz frame rate) restricted to the row of cone pedicles in the OPL (see Fig. 11). This way, bleaching of the light-sensitive cone OS by the scanning laser could be largely avoided.

5.8. Light stimulation:

A custom-designed dichromatic light stimulator (Breuninger et al., 2011) was mounted below the recording chamber and consisted of two band pass-filtered (UV: 360 BP 10, green: 520 BP 10; AHF) LEDs. Their light was combined by a beam-splitter (400 DCLP, AHF), focused by an achromatic air condenser lens (0.8 NA,H DIC, Zeiss) and projected through the glass bottom of the recording chamber. The LEDs were driven by an open-source microprocessor board (http://arduino.cc). Because the UV LED evoked weak but detectable fluorescence in the tissue, the LED was synchronized on-time with the two-photon microscope's scanner retrace and thereby prevented stimulation artifacts during data acquisition time fraction of a scan line (when the laser scanned the cone pedicles). A combination of dichroic mirrors in front of the photomultipliers and in the detection path prevented light from the stimulation LEDs interfering with the fluorescence detection directly (for details see (Euler et al., 2009). Stimulator intensity was measured at the level of the recording chamber using a calibrated photometer (Model 842-PE, 200-1100 nm, Newport, Darmstadt, Germany) set to the respective center wavelengths of the LED

filters (see above). Cone photo-isomerization rates were calculated using the relative sensitivities of the mouse cone opsins at the LED filter wavelengths via an opsin-template (Stockman and Sharpe, 2000) fitted to the peak sensitivities (360 and 511 nm, (Jacobs et al., 1991)) and assuming a cone's light collection area of 0.2 µm² (Nikonov et al., 2006). The stimuli always covered the whole retinal slice (full field, see Fig.11).

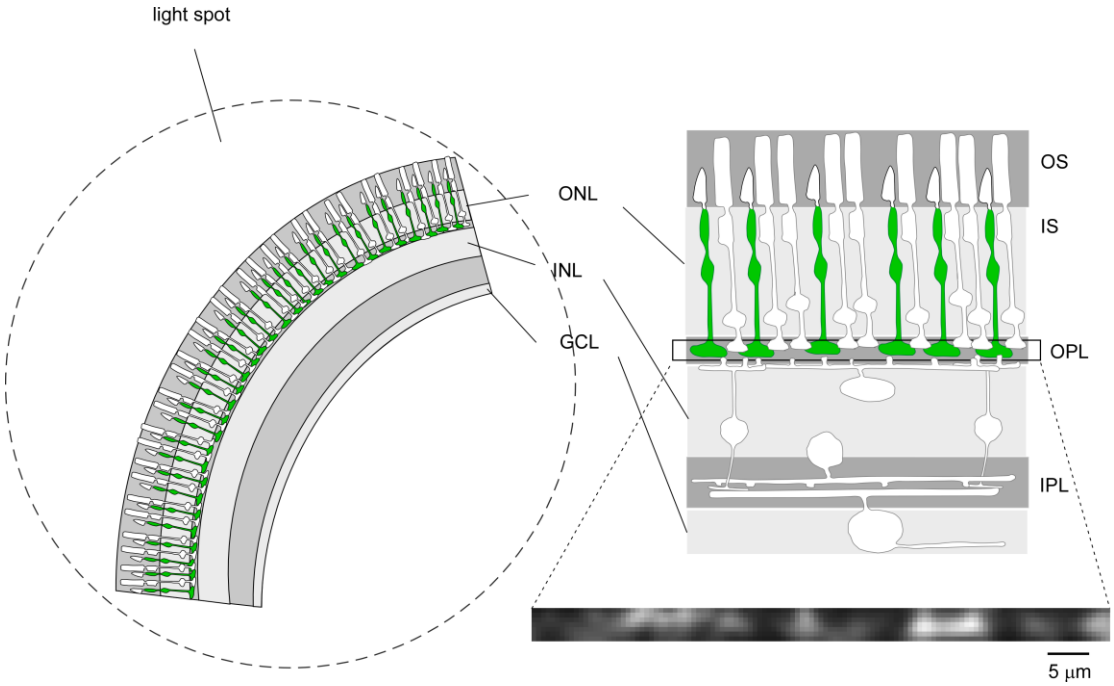

Fig. 11: Schematic drawing of light stimulation experiment on cones.
Retinal slice was stimulated by the full field light stimulation (indicated by dotted circle covering the entire retinal slice, left). Only the cone terminals were scanned for avoiding strong stimulation of OS (rectangle). Green highlight indicates localization of TN-XL expression.

Two light stimulation protocols were used: in the first protocol, bright 1-second flashes were presented every 5 seconds and repeated 7-10 times. During the flashes, the intensity (as photo-isomerization rate, $10^3 \cdot P^* s^{-1} cone^{-1}$) was stepped from background level to 13.0 and 12.8 for M- and S-opsins, respectively. Here, the background level meant that the stimulator LEDs were off but the excitation laser was scanning. Since the laser light scattered in the tissue, this provided a low basal illumination (see laser effect in Fig. 17), to which the cone photoreceptors adapted within tens of seconds. In the second protocol, bright and dark flashes (1 second duration, every 5 seconds, 7 repeats) were presented by stepping the intensity (in $10^3 \cdot P^* s^{-1} cone^{-1}$) from a medium level of 6.3 (for both opsins) to 8.85 and 11.4 ("bright") and 1.26 and 3.79 ("dark") for both M- and S-opsins. For both protocols, the

slices were kept at the background (protocol 1) or the medium (protocol 2) intensity level for 1 minute after the laser-scanning started before flashes were presented. This was necessary to allow the cone photoreceptors to adapt to scatter excitation laser light.

5.9. Pharmacology:

For stock solutions, all drugs were dissolved in H_2O or DMSO, according to the vendor's instructions. Before each experiment, drugs were freshly prepared from stock solutions in carboxygenated ACSF.

5.9.1. Drug-evoked calcium responses:

In the CSLM experiments, the drug solutions included 100 mM KCl, 50 mM Caffeine and 500 µM 8-pCPT-cGMP (BioLog, Bremen, Germany; the others from Sigma-Aldrich, Steinheim, Germany) and were puffed using a focal perfusion system (see 5.7.1).

5.9.2. Pharmacological modulation of light-evoked calcium responses:

In the two-photon experiments, the final concentrations of the drug solutions were: 200 µM zaprinast, 200 µM SNAP, 100 µM ODQ and 50 µM 8-pCPT-cGMP (BioLog, Bremen, Germany; the others from Sigma-Aldrich). The drugs were applied with the bath solution. Drug effects were analyzed statistically for wash-in (from application start) and wash-out (from end of drug application) durations of at least 20 minutes (see also 5.10).

5.10. Data analysis:

For analysis of the drug-evoked Ca^{2+} response data acquired with the CSLM, the commercial EZ C1 confocal imaging software (Nikon) of the microscope system was used. For analyzing light-evoked Ca^{2+} response data, the public domain software ImageJ (http://rsb.info.nih.gov/ij/) and custom-written scripts for the commercial IgorPro software (Wavemetrics, Lake Oswego, Oregon, USA) were employed.

Regions of interest (ROIs) were positioned on individual cone pedicles and, in case of the CSLM measurements, also on cone IS and somata. Background fluorescence was subtracted and the ratio ($R=F_A/F_D$) between the fluorescence signal of the donor (F_D) ECFP and that of the acceptor (F_A) Citrine was calculated. An increase in R (or $\Delta R/R = (R_{drug} - R_{control}) / R_{control}$) represents an increase in intracellular $[Ca^{2+}]$. We refrained from calibration of the ratiometric measurements (to yield absolute $[Ca^{2+}]$) because for the purpose of the present study, relative $[Ca^{2+}]$ that could be compared

between different conditions was sufficient. Therefore, we give the fluorescence ratio R as a measure of $[Ca^{2+}]$.

To quantify light-evoked Ca^{2+} changes recorded using the two-photon microscopy, the response traces were fitted with sigmoid curves (see Fig. 19B1) and the following parameters were extracted: pre-response baseline ratio (R_{base}), peak amplitude (ΔR), area (R_A), rise time (t_{rise}, time between 20% and 80% of ΔR) and decay time (t_{decay}, time between 80% and 20% of ΔR). R_{base} was obtained by averaging fluorescence ratio in the pre-response phase and ΔR was calculated by subtracting R_{base} from the peak amplitude. R_A was determined by the surface area of light response trace under the curve, despite differences in Ca^{2+} dynamic profiles, measurements of the area revealed relative quantity of transported Ca^{2+} induced by light stimuli. Note that “rise” refers to the initial drop in $[Ca^{2+}]$ at light-onset, whereas “decay” refers to the increase in $[Ca^{2+}]$ at light-offset. The effects of the drugs onto the different response parameters were statistically evaluated using the Wilcoxon’s rank sum test.

6. Results:

6.1. Three constructs were created for driving TN-XL expression specifically in mouse photoreceptors:

To target a calcium biosensor to mouse cone photoreceptors, we designed a construct that drives the expression of the TN-XL calcium biosensor under the control of the human red opsin promoter HR2.1 (Wang et al., 1992; Li et al., 2008).

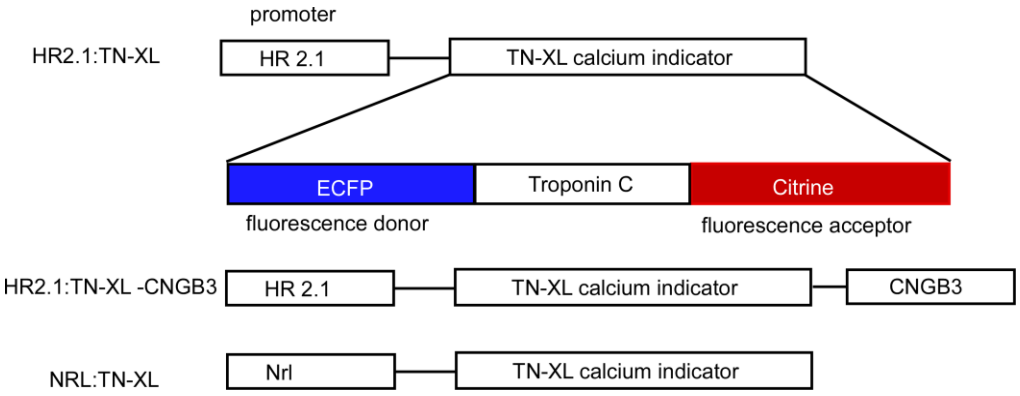

Fig 12: Schematic presentation of three designed constructs.
Calcium biosensor TN-XL is under the control of HR 2.1 or Nrl promoter. TN-XL is a ratiometric Ca^{2+} indicator and composed of ECFP as fluorescence donor and Citrine as fluorescence acceptor; mutated Troponin C from chicken skeletal muscle serves as Ca^{2+} binding moiety. Additionally, in the HR2.1:TN-XL–CNGB3 construct, the CNGB3 gene was attached to the 3' end.

Two more constructs (Fig. 12) were designed using the same procedure. First, the HR2.1:TN-XL-CNGB3 construct was designed to allow probing very local Ca^{2+} dynamics (Ca^{2+} microdomain) close to CNG channels directly in the cone OS. The term Ca^{2+} microdomain generally refers to an increase in cytosolic Ca^{2+} that remains in vicinity of the mouth of Ca^{2+} channels (for review see (Rizzuto and Pozzan, 2006)). The human CNGB3 gene was added to the downstream end of the HR2.1:TN-XL construct (Fig. 12). The strategy behind this construct design is that exogenous CNGB3 bound to TN-XL will be transported to OSs associated with endogenous CNGA3 (Ding et al., 2009). The exogenous CNGB3 subunit and the endogenous CNGA3 subunit will form functional CNG channels in the OS, so that TN-XL is localized to the mouth of the CNG channels and detects the local Ca^{2+} dynamics. Second, the Nrl:TN-XL construct was designed for targeting TN-XL expression in rod photoreceptors using the Nrl promoter (Akimoto et al., 2006). Nrl is a motif-leucine

zipper transcription factor that is specifically expressed in rod photoreceptors and pinealocytes. The Nrl promoter was shown to be able to drive reporter gene expression specifically in rods (Akimoto et al., 2006).

Transgenic mouse lines carrying the three constructs were generated by direct microinjection of the respective TN-XL constructs into the pronuclei of fertilized ova (Gordon and Ruddle, 1981), because stable expression of TN-XL in cones enables the evaluation of cone Ca^{2+} dynamics in an *in vivo*-like situation.

6.2. TN-XL expression is only found in HR2.1:TN-XL mouse retinas:

Received founder mice were screened by PCR for the integration of transgenes in the mouse genome and by fluorescence microscopy for their expression (see Table 1). For the HR2.1:TN-XL construct, a total of 97 mice were born from foster mothers which had been implanted with microinjected oocytes. Integration of HR2.1:TN-XL in the genome was confirmed for 10 of these mice by PCR analysis of DNA extracted from ear punches. Only 1 of the 10 founder mouse lines showed TN-XL expression in the retina with ~15 integrated transgene copies per haploid genome (=copy number) estimated using q-PCR. This copy number turned out to be stably inherited in the F1 generation, suggesting that the transgene copies had inserted into the genome at a single location.

For the HR2.1:TN-XL–CNGB3 and the Nrl:TN-XL constructs, 6 of 32 and 5 of 28 founder mice, respectively, were confirmed to carry the transgenes. However, inspection of their isolated retinas with fluorescence microcopy showed that none of these founder mice expresses TN-XL.

Taken together, only 1 HR2.1:TN-XL founder mouse did indeed express TN-XL in the retina, while none of the founder mice for the other two constructs displayed any retinal TN-XL expression.

The HR2.1:TN-XL founder mouse was used to establish a purebred line HR2.1:TN-XL carrying the integrated transgene insertion in both homologous chromosomes by cross-breeding transgene-positive mice. The purebred transgenic mouse line stably transmits the transgene at a copy number of about 10-15 per haploid genome, as measured by q-PCR-based analysis.

Table 1: Screening of transgenic mouse lines.

Mouse line	promoter	founder mice (n)	PCR	approx. copy numbers (q-PCR)	TN-XL expression (by fluorescence microscopy)
HR2.1:TN-XL	HR2.1	97	10 +	1, 1, 1, 1, 1, 2, 2, 4, 14, 15	1 + (copy number ~15)
HR2.1:TN-XL – CNGB3	HR2.1	32	6 +	1, 1, 3, 3, 29, 25	-
Nrl:TN-XL	Nrl	28	5 +	1, 1, 4, 4, 5	-

For each of the three constructs, number of founder mice, number of founder mouse lines carrying the transgene (tested by PCR), approximate copy numbers (by q-PCR) and number of lines confirmed to express TN-XL by fluorescence microscopy are listed.

6.3. TN-XL is expressed in both cone types in the HR2.1:TN-XL mouse line:

To characterize the expression pattern of TN-XL within cones and the distribution of TN-XL-positive cones across the retina, vertical sections and whole mounts of HR2.1:TN-XL retina (purebred line) were double-labeled with antibodies against GFP (to amplify TN-XL fluorescence) and against M- or S-opsin (Fig. 13). We found that in these animals TN-XL is present throughout the cone with the exception of the OS (Fig. 13 A-C). In M-cones identified by M-opsin labeling, TN-XL expression is restricted to IS, soma and terminal, whereas staining of M-opsin was confined to the OS (Figure 13 A-C). Despite the absence of an overlap in staining of TN-XL and M-opsin, it is evident that both antibodies labeled different parts of the same cells (inset in Figure 13C).

Mice possess a dorso-ventral opsin co-expression gradient, with M-cones dominating the dorsal and M/S double-expressing cones dominating the ventral retina (Szel et al., 1992), as found in a few other mammalian species (reviewed by (Lukats et al., 2005)). That this gradient is also present in the transgenic line was shown by S-opsin labeling of whole mounted retina (Fig. 13D). Despite the opsin co-expression gradient, cones that exclusively express S-opsin (“true” S-cones) are evenly distributed across the whole mouse retina (Haverkamp et al., 2005). Hence, to test if TN-XL is also expressed by “true” S-cones we stained a dorsal vertical section, where opsin co-expression is low (Fig. 13E,G with Fig. 13F,H). We found that infrequent S-opsin expressing cones in dorsal retina, which presumably represent the “true” S-cones - were TN-XL positive (Fig. 13G, inset), suggesting that the HR2.1

promoter drives TN-XL expression in both mouse cone types, consistent with earlier observations (Wang et al., 1992). As in the M-cones, TN-XL is present throughout the S-cone with the exception of the OS.

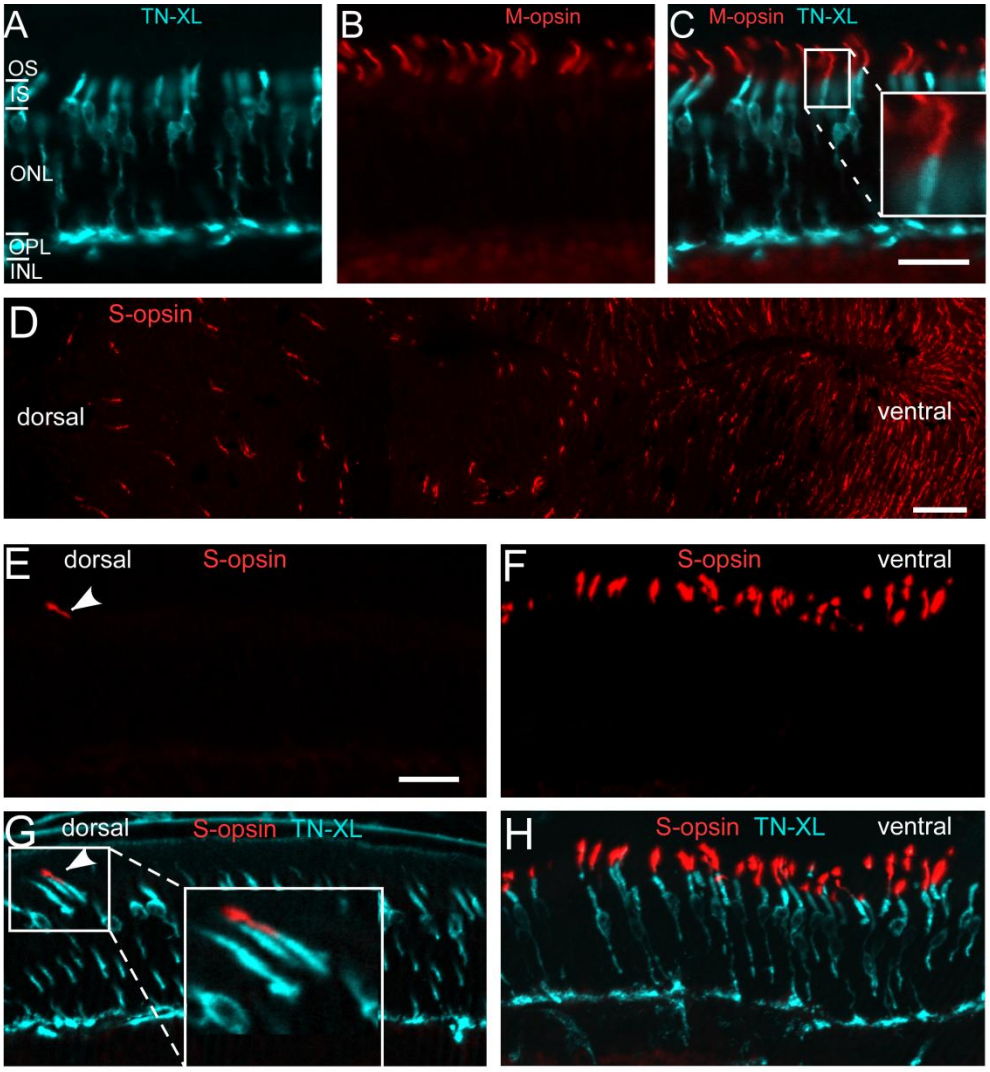

Fig. 13: TN-XL expression in cone photoreceptors of the HR2.1:TN-XL mouse line.
(**A-C**): Vertical sections stained with antibodies against GFP (labels TN-XL; blue) and M-opsin (red), showing the presence of the biosensor throughout the cone with the exception of OS. Magnified inset in (**C**) illustrates that TN-XL and opsin labeling does not overlap but is localized in same cone. (outer segment, OS; inner segment, IS; outer nuclear layer, ONL; outer plexiform layer, OPL; inner nuclear layer, INL).
(**D**): Retinal whole mount stained with antibody against S-opsin, confirming the presence of the dorsal-ventral opsin co-expression gradient described in mouse (Szel et al., 1992).
(**E-H**): Vertical sections taken from the dorsal (**E,G**) and the ventral (**F,H**) retina and stained for S-opsin. Example for S-opsin expressing, TN-XL-positive cone in the dorsal retina (**G**, see also magnification in inset). Scale bars: 20 µm (**A-C** and **E-H**), 50 µm in (**D**).

6.4. Cone function is unaffected by TN-XL expression:

Upon the generation of transgenic mice, it may happen that the random insertion of the transgene(s) disturbs endogenous gene functions. Additionally, in the HR2.1:TN-XL mouse line, TN-XL contains Troponin C as its Ca^{2+}-binding moiety (Mank et al., 2006), which might alter the intrinsic cone Ca^{2+} buffering capacity and thereby affect Ca^{2+} signal spread and neurotransmitter release to postsynaptic neurons. Therefore, we tested if photoreceptor function in the HR2.1:TN-XL line was normal by recording scotopic and photopic ERGs from one month old transgenic and wild-type mice. To assess cone function and synaptic transmission, we analyzed the photopic single flash b-wave, which is evoked by downstream ON-cone bipolar cells. The b-wave recorded from HR2.1:TN-XL mice was not significantly different from wild-type animals (P=0.13 to 0.67 for -0.5 to 1.5 cd·s/m^2), indicating normal ON-cone bipolar cell function (Fig. 14A-C). To assess OFF-cone bipolar cell function, we applied a flicker stimulus protocol at a fixed intensity of 0.5 log cd·s/m^2 which is defined as the *International Society for Clinical Electrophysiology of Vision* standard flash (ISCEV SF, (Marmor et al., 2004b)). Again, we found no significant difference between transgenic and wild-type mice in the flicker responses that reflect OFF-cone bipolar cell activity (Fig. 14D,E). This suggests that cone function as well as transmission from cones to bipolar cells is not substantially altered by the expression of TN-XL. Moreover, under scotopic conditions, the function of rods (indicated by the a-wave) and rod bipolar cells (indicated by the b-wave) is not significantly different between transgenic and wild-type mice (Fig. 14F-H). In conclusion, our ERG data indicate that neither the transgene insertion nor the expression levels of TN-XL in cones interfere with normal photoreceptor function in HR2.1:TN-XL mice.

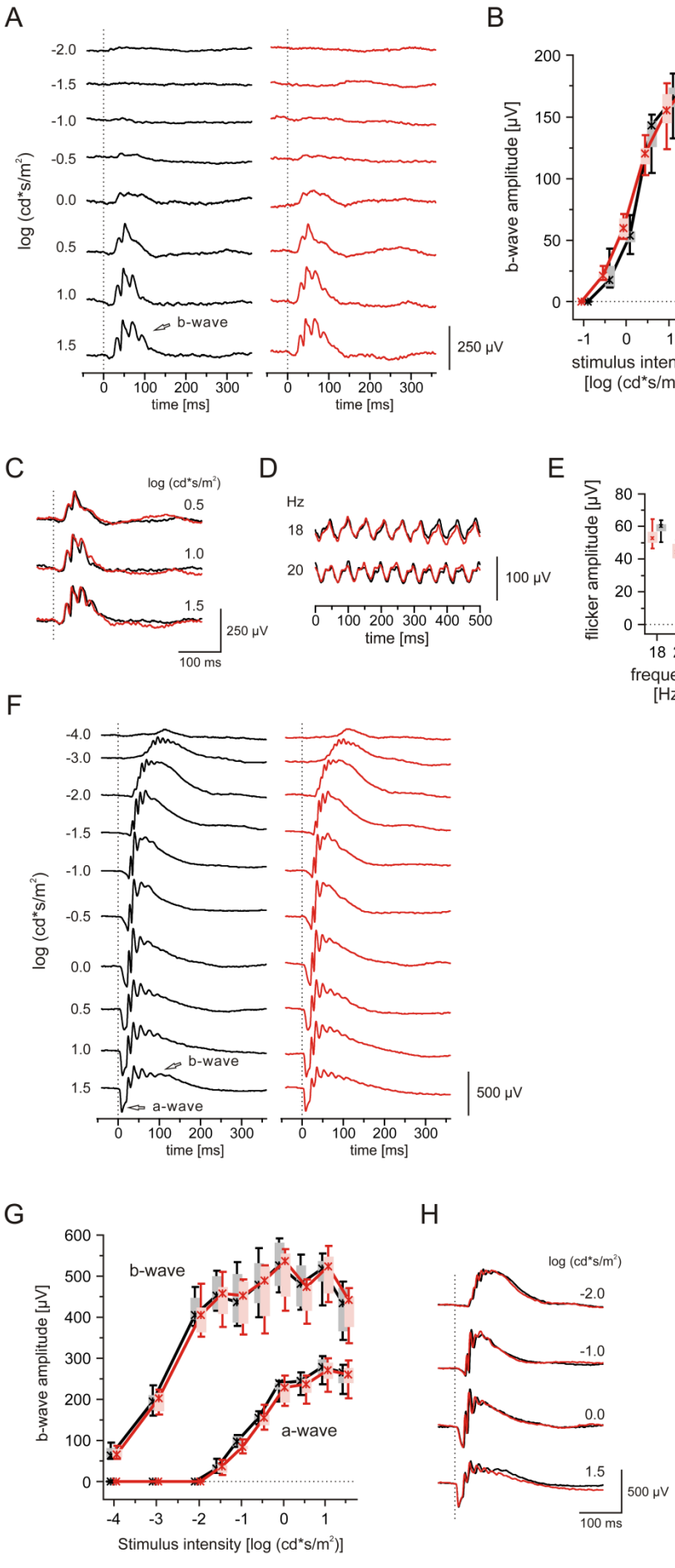
A
B
C
D
E
F
G
H
log (cd*s/m²)
-2.0
-1.5
-1.0
-0.5
0.0
0.5
1.0
1.5
b-wave
250 µV
time [ms]
b-wave amplitude [µV]
stimulus intensity
[log (cd*s/m²)]
Hz
18
20
100 µV
flicker amplitude [µV]
frequency
[Hz]
-4.0
-3.0
a-wave
500 µV
Stimulus intensity [log (cd*s/m²)]
100 ms

Fig. 14: Electroretinogram (ERG) analysis of HR2.1:TN-XL mice vs. wild-type mice.
(**A**): Representative photopic single flash ERGs in 1-month-old HR2.1:TN-XL (red) and wt (black) mice under a static background light (30 cd/m^2). The b-wave is indicated by an open arrow.
(**B**): Box-and-whisker plot showing photopic single flash b-wave amplitudes in wt (black) and HR2.1:TN-XL (red) mice. Boxes indicate the 25% and 75% quantile range, whiskers indicate the 5% and 95% quantiles, and the asterisks indicate the median of the data. The amplitude differences were not statistically significant at any intensity (*P*=0.13 - 0.67 for -0.5 to 1.5 cd·s/m^2).
(**C**): Overlay of the response traces of wt (black) and HR2.1:TN-XL (red) mice from **(A)**.
(**D**): Representative flicker ERG response traces at 18 and 20 Hz under dark-adapted condition in wt (black) and HR2.1:TN-XL (red).
(**E**): Box-and-whisker plot showing flicker response amplitudes of wt (black) and HR2.1:TN-XL (red) mice. (*P*=0.31 for 18 Hz and *P*=0.39 for 20Hz).
(**F**): Representative scotopic single flash ERGs in wt (black) and HR2.1:TN-XL (red) mice. The a-wave and the b-wave are indicated by open arrows.
(**G**): Box-and-whisker plot of scotopic single-flash a-wave and b-wave amplitudes in wt (black) and HR2.1:TN-XL (red) mice. The amplitude differences were not statistically significant at any intensity (*P*=0.093 - 1.00 for -1.5 to 1.5 cd·s/m^2-for the a-wave and *P*=0.39 - 0.94 for -4 to 1.5 cd·s/m^2-for the b-wave).
(**H**): Overlay of the response traces of wt (black) and HR2.1:TN-XL (red) mice from **(F)**.

6.5. Changes in calcium concentration are largely restricted to cone synaptic terminals:

To show that TN-XL allows monitoring of changes in cone cytosolic [Ca^{2+}] and to investigate the subcellular distribution of these changes, we performed Ca^{2+} imaging on light adapted retinal slices while puffing different pharmacological agents onto the tissue (Fig. 15-16).

In the light-adapted retina, the membrane potential of cones is hyperpolarized, such that the VGCCs are closed and the resting [Ca^{2+}] is low in cone terminals (Choi et al., 2005; Krizaj, 2005). Depolarization of cones with high extracellular KCl (Fig. 15) evoked large increases in fluorescence ratio – and therefore in [Ca^{2+}] – in cone terminals, reflecting Ca^{2+} influx through VGCCs – likely the L-type channels (Taylor and Morgans, 1998; Morgans et al., 2005). This increase was expressed as the normalized change in ratio, $\Delta R/R = (R_{drug} - R_{control}) / R_{control}$), and was found to be $\Delta R/R = 0.94 \pm 0.29$ (n=45 of 48 cone terminals from 4 experiments). Repeated puffs of KCl evoked a consistent Ca^{2+} increase in terminals with an approximate duration of 15 seconds. In contrast to the large responses observed in cone terminals, KCl-

evoked Ca^{2+} responses, when detected in IS and soma, were small (ΔR/R = 0.11 ± 0.10, n=48 in 4 experiments), indicating that Ca^{2+} regulation is compartmentalized in cones. Whether the occasionally observed small [Ca^{2+}] changes in IS and soma reflect Ca^{2+} diffusion from the terminal remains to be investigated.

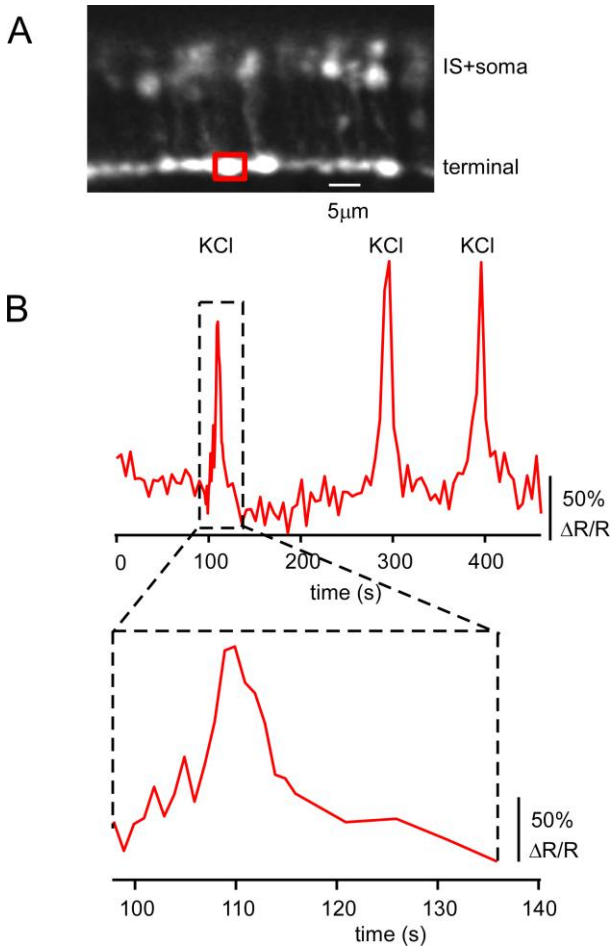

Fig. 15: Depolarization-evoked calcium increase in cone terminal indicated by TN-XL.
(**A**): Retinal slice from the HR2.1:TN-XL mouse imaged by a confocal microscope.
(**B**): Ca^{2+} signals (as fractional change of fluorescence ratio, ΔR/R; from ROI in **A**) measured in terminals in response to puffs of 100 mM KCl. Bottom: First depolarization evoked Ca^{2+} signal magnified along the x-axis.

Next, we tested if the biosensor would allow detection of drug evoked Ca^{2+} fluctuations via different pathways. In these experiments, we first confirmed the viability and responsiveness of the cones using KCl puffs (Fig. 16). Then we tested different drugs. Caffeine, a ryanodine receptor agonist, was applied to release Ca^{2+} from the ER (Blinks et al., 1972). Caffeine puffs increased [Ca^{2+}] in cone terminals (ΔR/R = 0.77 ± 0.35, observed in 38 of 40 cone terminals in 3 experiments) but not in the soma nor the IS (ΔR/R = 0.08 ± 0.08, n=40 in 3 experiments), suggesting that ER-mediated Ca^{2+}-induced Ca^{2+} release (CICR) is involved in Ca^{2+} regulation mainly

in cone terminals. This is different from what has been previously observed in rod photoreceptors, which displayed somatic [Ca^{2+}] changes in response to both KCl puffs and drugs that trigger CICR (Babai et al., 2010).

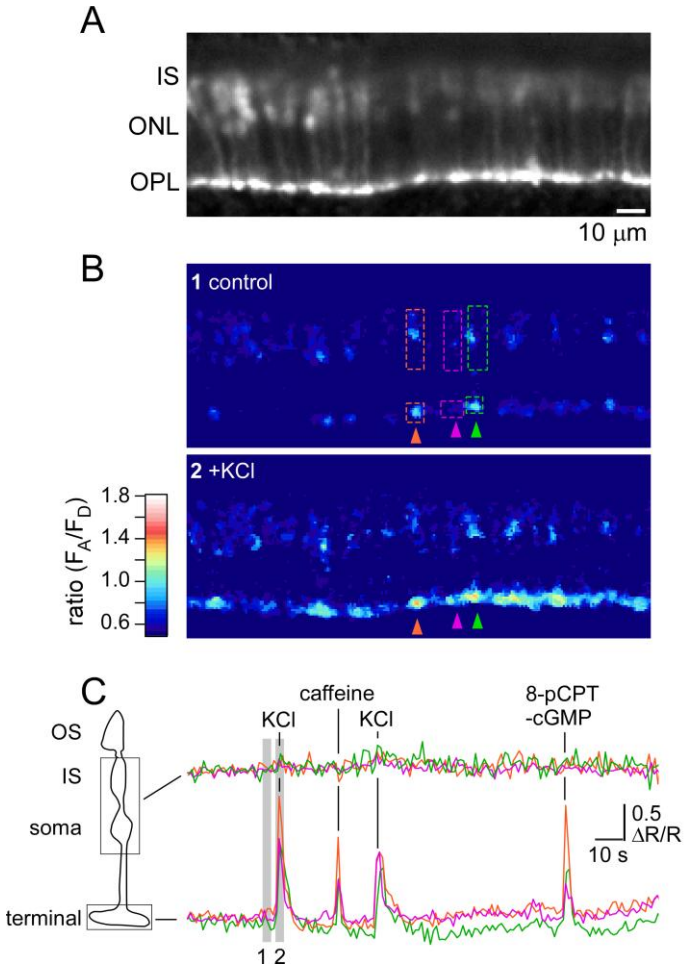

Fig. 16: Spatial distribution of pharmacologically evoked calcium changes in cones.

(**A**): Slice from HR2.1:TN-XL mouse imaged by a confocal microscope while puffing drugs. (inner segment, IS; outer nuclear layer, ONL; outer plexiform layer, OPL).

(**B**): Three TN-XL-positive cones with regions of interest (ROI) located on inner segments (IS) and soma as well as on the respective terminals before (top) and during a puff of 100 mM KCl (bottom) are shown (pseudo-colored images represent ratios $R=F_A/F_D$, reflecting the intracellular [Ca^{2+}] level, and are averages of 5 frames).

(**C**): Ca^{2+} signals (as fractional change of fluorescence ratio, ΔR/R; from ROIs in **B**) measured in IS+soma (upper trace) and terminals (lower trace) in response to puffs of 100 mM KCl (1 s), 50 mM caffeine and 500 µm 8-pPCPT-cGMP (both 5 s). Gray bars indicate the time window when frames for images in (**B**) were taken.

As TN-XL is not expressed in the cone OS, the transgenic line does not allow monitoring Ca^{2+} dynamics in this compartment directly. To show that OS was intact in TN-XL-expressing cones the cGMP analog 8-pCPT-cGMP was puffed onto

photoreceptors on the slices. This caused CNG channels to open and thereby depolarized the cones, leading to Ca^{2+} influx through VGCCs in the terminals (ΔR/R = 0.73 ± 0.32, observed in 31 of 38 cone terminals in 3 experiments). No 8-pCPT-cGMP-evoked rise in [Ca^{2+}] was detected in soma or IS (ΔR/R = 0.07 ± 0.07, n=38 in 3 experiments), consistent with the KCl-evoked depolarization results. The data indicate that CNG channel-mediated Ca^{2+} influx into OS (Wei et al., 1998) has no detectable direct effect, e.g. by diffusion, on the rise in [Ca^{2+}] recorded in the terminals.

In conclusion, for all tested drugs that induced cone [Ca^{2+}] changes, these changes were largely restricted to the cone terminals, with no or only small responses in soma or IS, pointing at a high degree of compartmentalization of Ca^{2+} regulation in mammalian cones. In addition, these results confirm that the TN-XL biosensor allows detection of drug-evoked changes in cone [Ca^{2+}] via different pathways.

6.6. HR2.1:TN-XL allows recording of light-evoked calcium responses in cone terminals:

To evaluate cone Ca^{2+} dynamics under physiological conditions, light-evoked Ca^{2+} responses in cone terminals of HR2.1:TN-XL mice were recorded. To this end, retinal slices from dark-adapted animals were imaged using two-photon microscopy (Denk et al., 1990). Laser scanning was restricted to a narrow region covering cone terminals in the OPL (see Fig. 11). The perpendicular orientation of the laser beam to the slice surface prevented direct laser illumination of the cones' light-sensitive OS. This was crucial to avoid bleaching of photopigments by the excitation laser, because even ~100 µm away from the focal plane, two-photon excitation of photopigments is the largest contributor to the light responses evoked by the pulsed infrared scanning laser beam (here ~860 nm) (Denk et al., 1990; Euler et al., 2009).

Light-evoked hyperpolarization closes L-type VGCCs in photoreceptor terminals, resulting in a decrease of presynaptic [Ca^{2+}] (Choi et al., 2005). Therefore, also a decrease in fluorescence ratio R was expected in response to light stimulation. This was confirmed using a light-on flash stimulus (see the first light stimulation protocol in 5.8): light flashes reduced R and therefore terminal [Ca^{2+}] repeatedly (Fig. 17, n=10 stimuli). It should be mentioned that even in the described recording configuration, laser scanning decreased both resting [Ca^{2+}] and cone light responses (Fig. 17B). Whether the decrease in baseline [Ca^{2+}] was due to scattered laser light or the evoked TN-XL fluorescence or a combination of both was not further explored. In any

case, the scanned cones adapted to this “background illumination” within 30-60 seconds (Fig. 17). Consequently, the scanning laser was started for more than 30 seconds before the actual light stimuli were presented (see also 5.8). Under these conditions, light responses could be measured from individual cone terminals at single trial level to both increases as well as decreases (“dark flashes”) in stimulus intensity (Fig. 18, conditions a, b).

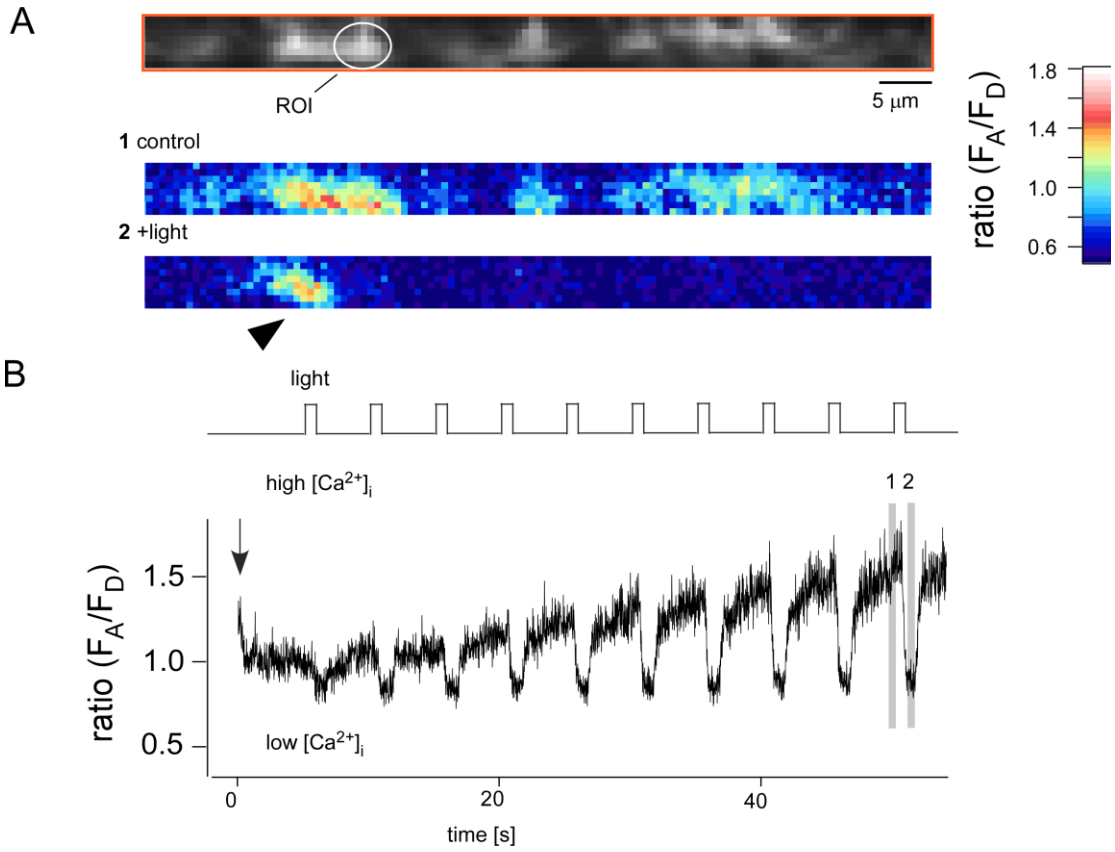

Fig. 17: Light-evoked calcium responses recorded from cone terminals.

(**A**): The imaged area covered the OPL, as indicated by the orange box. Ratio images (1 control and 2 +light, averages of n=20 frames) reflect [Ca^{2+}] before (1) and during a flash of light (2). Note single non-responsive cone terminal (arrowhead in **A**).

(**B**): Light-evoked Ca^{2+} responses (black trace, as ratio $R=F_A/F_D$) reflect [Ca^{2+}] before (1) and during a flash of light (2). Multiple light responses (**B**, as ratio $R=F_A/F_D$) recorded from a ROI placed on an exemplary cone terminal (circle in **A**). Laser scanning was started (arrow) briefly before the light stimulation (1 second bright flashes, $13 \cdot 10^3$ $P^*s^{-1}cone^{-1}$ for both types of cones). Gray bars indicated time windows when frames for images (in **A**) were taken.

Sometimes we observed that the retinal slices contained cones with TN-XL fluorescence that did not respond to light stimuli (see an example in Fig. 17A, arrowhead). Seemingly, the fraction of light responding cones depends on the quality of the retina slices. This is very likely related to damage of cone OS during the slicing

process. In support of this explanation is the finding that almost all cone terminals were responsive when using depolarizing KCl puffs (Fig. 15 and 16).

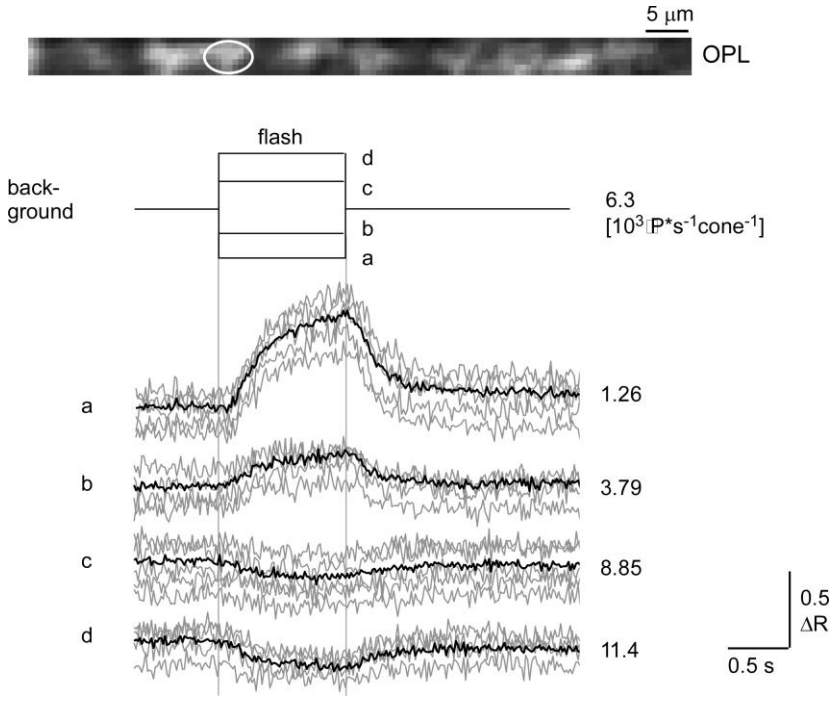

Fig. 18: Light-evoked calcium responses to both incremental and decremental steps of light flashes.
Ca^{2+} responses, as measured by the change in ratio (ΔR), could be evoked by darker-than-background (conditions a, b) and brighter-than-background flashes (conditions c, d) of different intensities in a single cone terminal (background and flash isomerization rates next to traces; averages of n=10 trials in black, single-trials in gray).

In summary, our light response data indicate that TN-XL allows measuring cone Ca^{2+} dynamics under largely physiological conditions and within the physiological [Ca^{2+}] range.

6.7. Light-evoked calcium responses are quantified for further analysis:

Light response traces of single cones to repeated light stimuli were averaged (Fig. 19 A; 7 cells and 10 stimuli). For quantification the averaged light-evoked Ca^{2+} response traces were fitted to extract 5 parameters (see Methods 5.10 for details and Fig. 19B1) that described pre-response baseline [Ca^{2+}] (R_{base}), response size (peak amplitude, ΔR; area under the curve, R_A) and time course (rise time, t_{rise}; decay time, t_{decay}). Note that t_{rise} refers to the beginning of the Ca^{2+} response that is the decrease

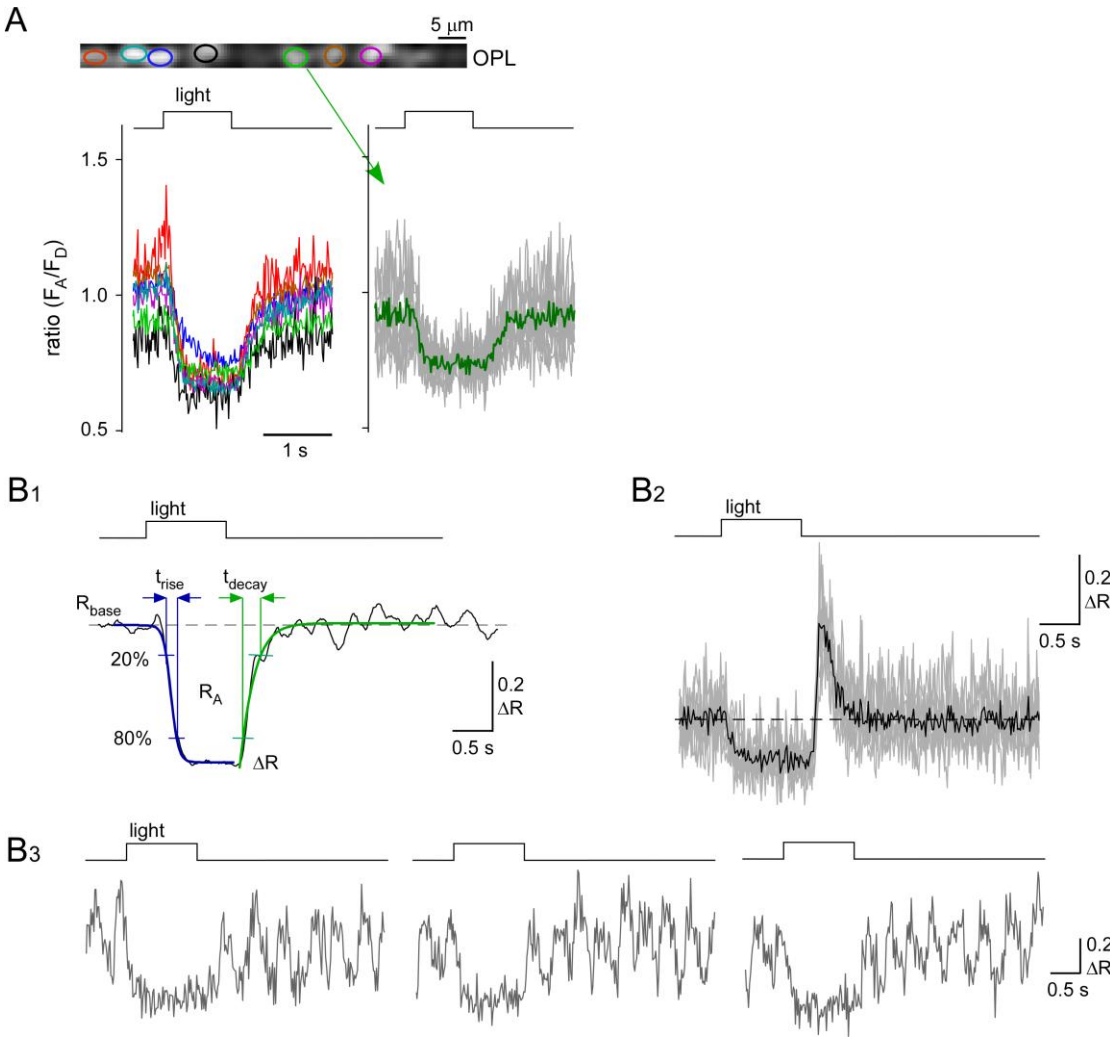

Fig. 19: Averaged light responses and quantification of light response traces.

(**A**): Light-evoked Ca^{2+} responses from 7 cone terminals, as marked by color-coded ROIs. Left: Averaged traces of 7 ROIs from n=10 trials; right: single-trial traces (gray) with average overlaid (green) for one of the ROIs (arrow).

(**B**): For quantification 5 parameters were determined from the responses (black, B1): baseline ratio (R_{base}), reflecting resting [Ca^{2+}]; peak amplitude (ΔR) and area under the curve (R_A) as measures for response size; rise (t_{rise}) and decay time (t_{decay}), characterizing the time course, were determined from two sigmoid functions fitted to rise (blue) and decay (green) of the response (for details see Methods). Examples for two less frequent response profiles: an overshoot at light-off (not quantified) was observed in some cones (B2, n=9 trials overlaid in grey); some responses displayed spike-like activity (B3; 3 exemplary single-trials). Only responses like those shown in B1 and B2 were included in the statistical analysis.

in [Ca^{2+}], whereas t_{decay} refers to the Ca^{2+} response end, when [Ca^{2+}] is rising back to baseline.

Besides what is referred to as the “standard” response, which was seen in the majority of cones (Fig. 19 B1), two other response “types” were observed; 22 of 216

(~10%) of the analyzed cones displayed an “overshoot” component at light-offset (Fig. 19 B2), which may correspond to the current “undershoot” observed in electrical recordings of single cones (Baylor et al., 1987). Because this type of response was observed infrequently, we did not further quantify the overshoot component. Another set of light-responsive cones (25 of 216, ~12%) displayed spontaneous spiking-like activity (Fig. 19 B3). We assume that this was likely due to slicing-related tissue damage, since it typically occurred in multiple cones of the same slice. On the other hand, the cones with such spontaneous activity were still responsive to light (Fig. 19 B3; 3 single light response curves presented as examples). Since it was doubtful whether or not these cones were healthy and also because fitting the responses was unreliable, we decided to exclude cones with spontaneous activity from the statistical analysis. Also, pharmacology experiments on light-evoked Ca^{2+} responses (see section 5.9.2) were only carried out, when the cones lacked spontaneous activity in the control phase.

While baseline Ca^{2+} levels (R_{base}= 0.93 ± 0.14, n = 58) were rather constant, their response sizes (ΔR= -0.20 ± 0.13, R_A= -0.23 ± 0.14) varied among analyzed cones. Interestingly, the response rise at light-onset (t_{rise}= 219 ± 131 ms) was significantly shorter than the response decay at light-offset (t_{decay}= 550 ± 504 ms), suggesting that the extrusion of Ca^{2+} from cone terminals may happen faster than Ca^{2+} influx through VGCCs.

6.8. Functional imaging of light-evoked calcium responses allows detailed analysis of phototransduction:

To evaluate the sensitivity of the measured Ca^{2+} signal in TN-XL-expressing cone terminals, light stimulation was combined with pharmacological manipulation of the phototransduction cascade. In these experiments, we used the cGMP analog 8-pCPT-cGMP (50 µM) to activate CNG channels and zaprinast (200 µM) to inhibit PDE6 activity.

Since 8-pCPT-cGMP is ~80 times more potent for CNG channels than cGMP (Wei et al., 1998) and resistant to hydrolysis by PDE6 (Hurwitz et al., 1985; Thompson, 1991), it “clamps” the channels in the open state, leading to a tonic depolarization of cones and thereby a strong Ca^{2+} influx at their terminals. As expected, 8-pCPT-cGMP increased R_{base} (Fig. 20A,B) suggesting that 8-pCPT-cGMP introduces Ca^{2+} and Na^{+} influx through CNG channels in OS resulting in depolarization of the membrane potential thereby increasing [Ca^{2+}] in the terminal.

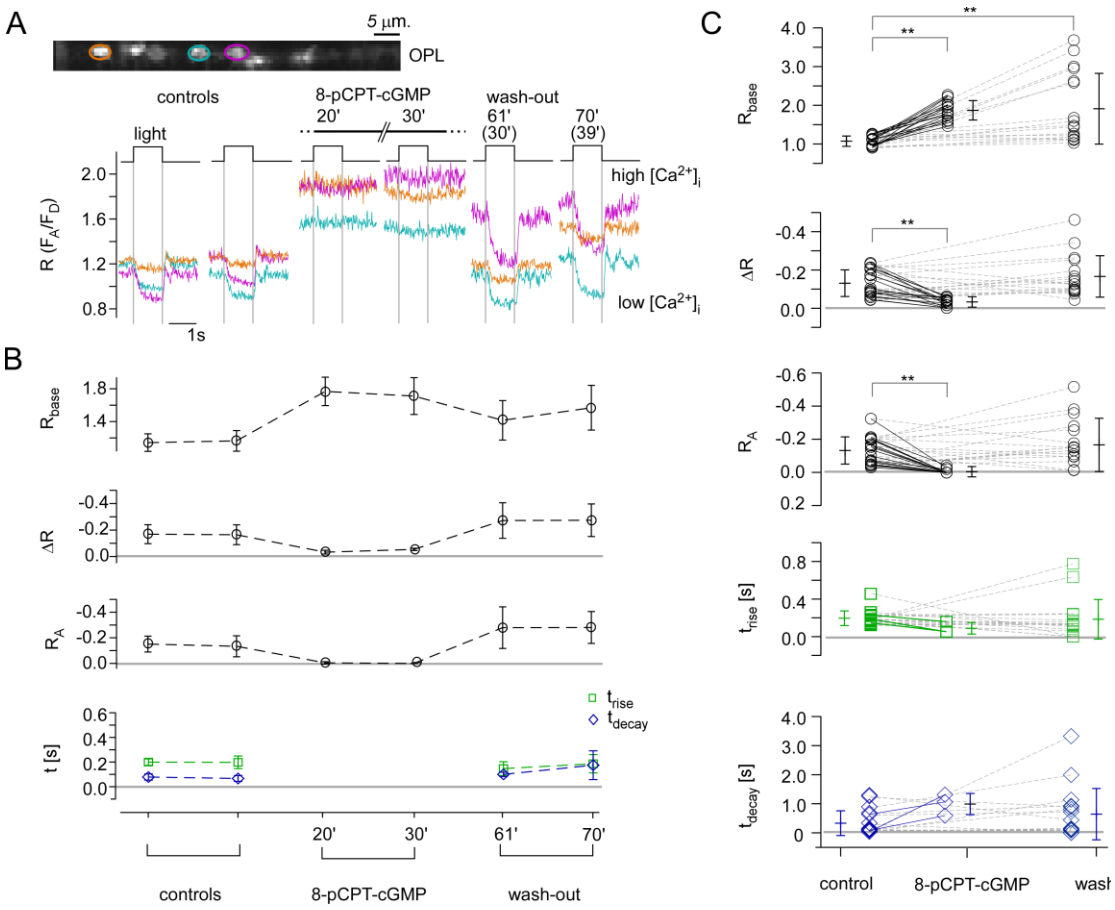

Fig. 20: Effect of 8-pCPT-cGMP on the light-evoked calcium response in cone terminals.

(**A**): Light-evoked Ca^{2+} responses in three representative cone terminals (marked by color-coded ROIs; outer plexiform layer, OPL) before, during and after drug application of 8-pCPT-cGMP (50 µM, bath application). Time points given from application start (in brackets: from beginning of wash-out).

(**B**): Quantification of the responses of all 7 cone terminals recorded in the experiment shown in (**A**).

(**C**): Summary of the 8-pCPT-cGMP effect on light-evoked Ca^{2+} responses for n=17 terminals (from 4 retinas), with each symbol representing a cone (averages ± S.D. are given next to each symbol column). For the timing parameters (t_{rise}, t_{decay}), values are only plotted for cones (n=3) in which the response was not completely suppressed by 8-pCPT-cGMP. (Wilcoxon signed test for paired samples, ** = p<0.01, * =p<0.05, if not indicated: non-significant).

During application of 8-pCPT-cGMP, light-evoked Ca^{2+} changes were abolished in almost all cones (mean ΔR and R_A were significantly reduced, Fig. 20C; for all statistics see Table 2). The wash-out was likely incomplete, since the light responses recovered but the resting Ca^{2+} level (R_{base}) remained higher than before the application (Fig. 20C). This is possibly due to the high affinity of 8-pCPT-cGMP to CNG channels. Its effect on the response time course could not be analyzed, because in most cases light responses completely vanished.

Table 2: Summary of pharmacological effects on light-evoked calcium responses in cone terminals.

	n	R_{base}	ΔR	R_A	t_{rise} (ms)	t_{decay} (ms)
8-pCPT-cGMP						
control	17	1.07 ± 0.13	-0.13 ± 0.07	-0.13 ± 0.08	195 ± 78	333 ± 432
drug	17	1.85 ± 0.25 (**)	-0.02 ± 0.02 (**)	-0.01 ± 0.001 (**)	89 ± 61[1)]	951 ± 365[1)]
wash-out	17	1.91 ± 0.91 (**)	-0.17 ± 0.11	-0.17 ± 0.16	184 ± 210	642 ± 882
zaprinast						
control	15	0.90 ± 0.13	-0.13 ± 0.06	-0.18 ± 0.10	228 ± 104	797 ± 369
drug	15	1.38 ± 0.33 (**)	-0.36 ± 0.28 (**)	-0.46 ± 0.31 (**)	375 ± 196 (*)	932 ± 490
wash-out	11	1.23 ± 0.10 (**)	-0.25 ± 0.06 (**)	-0.21 ± 0.08	132 ± 20 (*)	121 ± 156 (**)
SNAP						
control	19	0.97 ± 0.13	-0.31 ± 0.10	-0.32 ± 0.13	196 ± 88	180 ± 103
drug	19	0.80 ± 0.07 (**)	-0.15 ± 0.05 (**)	-0.15 ± 0.07 (**)	194 ± 57	180 ± 240
wash-out	19	0.81 ± 0.05 (**)	-0.18 ± 0.05 (**)	-0.16 ± 0.07 (**)	206 ± 133	111 ± 113 (**)
ODQ						
control	16	1.20 ± 0.22	-0.29 ± 0.14	-0.25 ± 0.10	159 ± 28	374 ± 325
drug	16	1.46 ± 0.25 (*)	-0.37 ± 0.09 (*)	-0.41 ± 0.13 (**)	184 ± 68	399 ± 380
wash-out	12	1.22 ± 0.12	-0.23 ± 0.09 (**)	-0.19 ± 0.08	182 ± 73	300 ± 539

Parameters are presented as mean ± standard deviation (S.D.). Significance levels are determined using the Wilcoxon signed test for paired samples (always vs. control condition, ** = p<0.01, * =p<0.05, if not indicated: non-significant; n is number of cells; [1)] n=3).

Another way of modulating the open probability of CNG channels is to inhibit PDE6, which leads to an accumulation and delayed degradation of cGMP in cones (Sahaboglu et al., 2010). To this end, the selective PDE5/6 inhibitor zaprinast (Zhang et al., 2005) was used. Zaprinast induced a strong increase in resting [Ca^{2+}] (R_{base}) as well as a prolonged response rise time (t_{rise}) and, at least in some cones, a large increase in response size (ΔR, R_A, Fig. 21A-C; for statistics see Table 2). In contrast to the results with the cGMP-analog, the light responses remained intact, indicating that PDE6 activity was only partially blocked by zaprinast, resulting in a “slowed down” phototransduction cascade. This is supported by the finding that zaprinast significantly slowed down the response rise (but not the decay), which can most likely be explained by the inhibited PDE6 not being able to reduce cGMP levels quickly enough, such that open CNG channels compete with Ca^{2+} extrusion mechanisms at the on-set of the light response. As with the cGMP-analog, wash-out appeared

incomplete, since neither resting [Ca^{2+}] nor peak response returned to their pre-application levels (Fig. 21C).

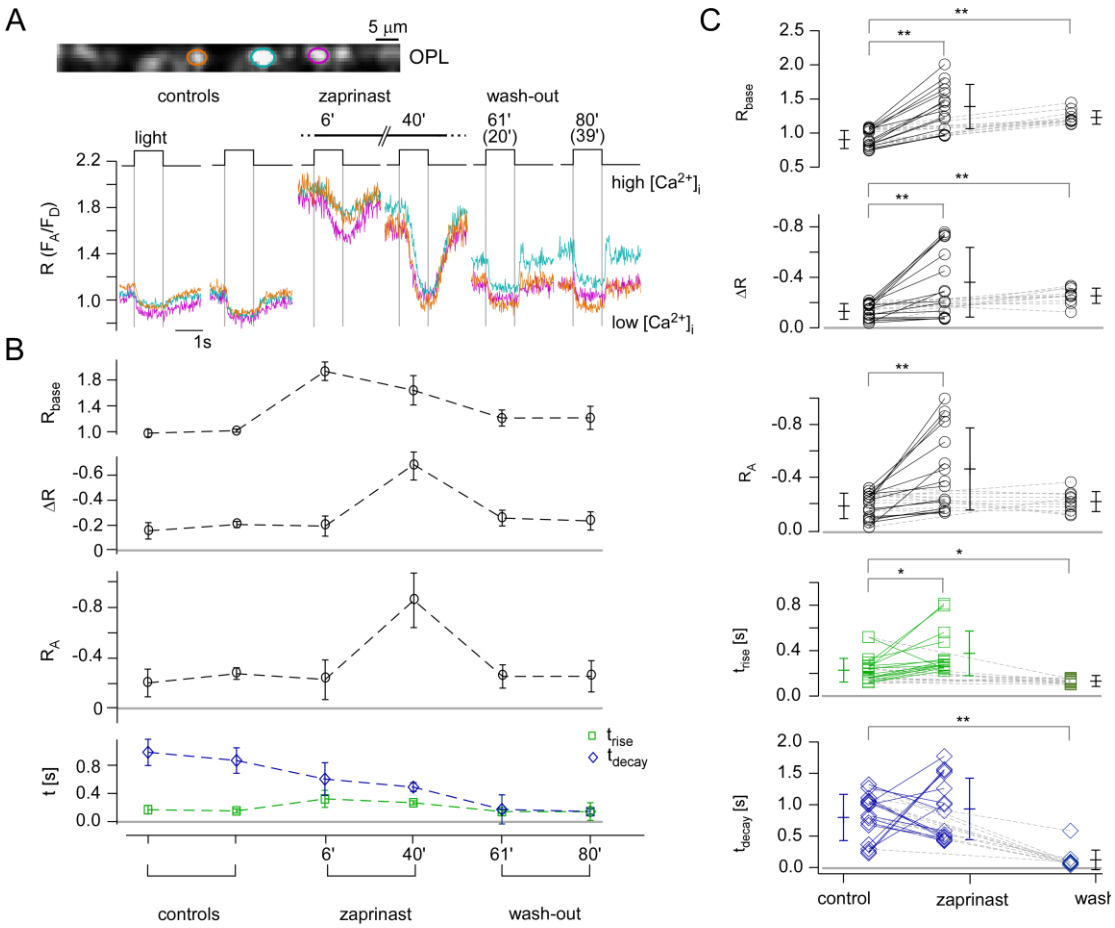

Fig. 21: Effect of zaprinast on the light-evoked calcium response in cone terminals.

(**A**): Light-evoked Ca^{2+} responses in three representative cone terminals (marked by color-coded ROIs; outer plexiform layer, OPL) before, during and after drug application of zaprinast, a PDE5/6 inhibitor (200 µM, bath application).

(**B**): Quantification of the responses in all 6 cone terminals recorded in the experiment shown in **(A).**

(**C**): Summary of the zaprinast effect on light-evoked Ca^{2+} responses for n=15 terminals (from 3 retinas). In wash-out values for each parameter are only plotted for n=11 cones that retained their light responsiveness.

Taken together, these results show that HR2.1:TN-XL mice allow the efficient examination of different functional aspects of phototransduction in cones by supporting the observation of light-driven Ca^{2+} dynamics in cone terminals.

6.9. Nitric oxide suppresses light-evoked calcium responses in cones:

With these tools in hand, we tested whether the long-standing hypothesis of a NO-mediated regulation of cone photoreceptor output is supported in mouse retina.

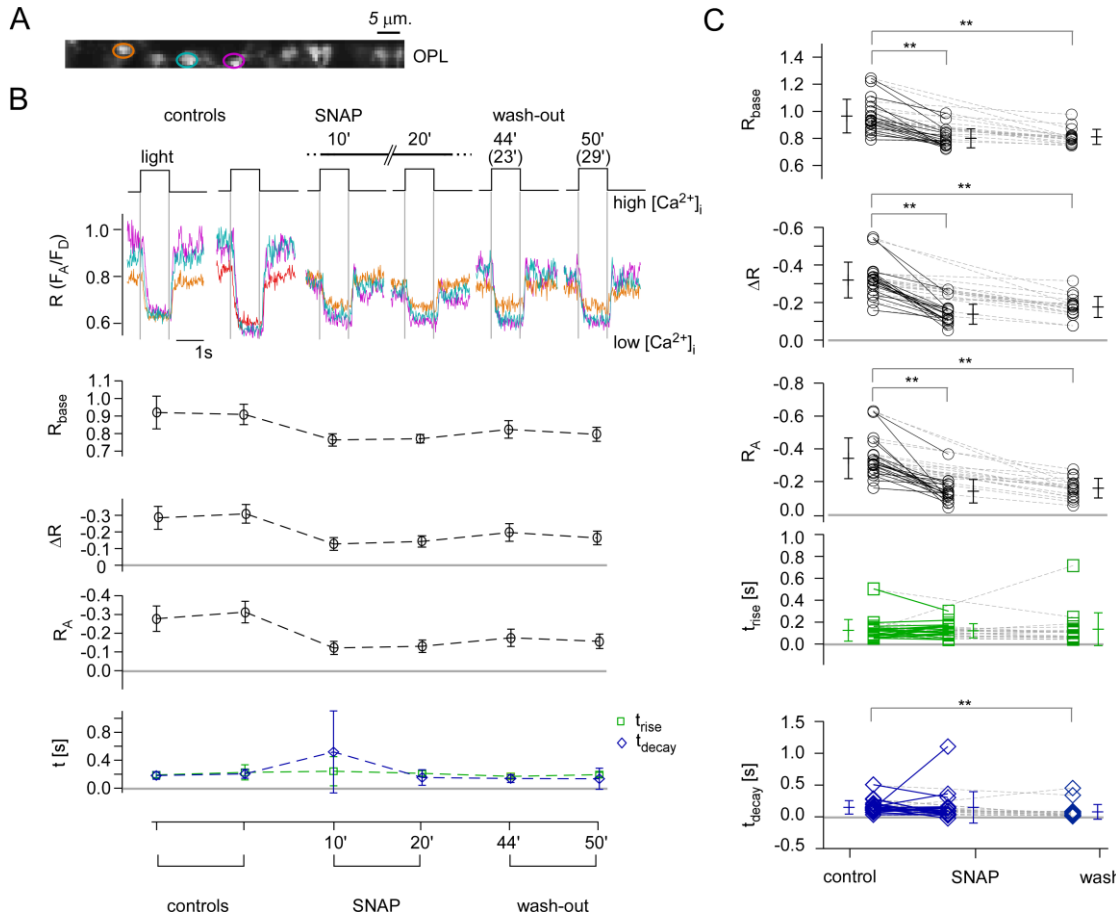

Fig. 22: Effect of nitric oxide on the light-evoked calcium response in cone terminals.

(**A**): Light-evoked Ca^{2+} responses in three representative cone terminals (marked by color-coded ROIs; outer plexiform layer, OPL) before, during and after wash-out of SNAP, a NO donor (200 µM, bath application).

(**B**): Quantification of the responses of all 6 cone terminals recorded in the experiment shown in (**A**).

(**C**): Summary of SNAP's effect on light-evoked Ca^{2+} responses for n=19 terminals (from 3 retinas). See Fig.20 for further experimental details.

Diffusing nitric oxide (NO) as a retrograde messenger has been proposed to modulate synaptic transmission in the brain (Odell et al., 1991; Schuman and Madison, 1994), but see (Schmidt, 2004). It was also proposed to regulate photoreceptor synaptic output via a sGC-mediated signaling pathway (NO-sGC pathway, see Fig. 9) in amphibian retina (Kurenny et al., 1994; Rieke and Schwartz,

1994; Savchenko et al., 1997). While NO has been shown to modulate phototransduction in mammalian cones (Sato and Ohtsuka, 2010; Vielma et al., 2010), at present it is unclear whether or not this NO effect is based on this NO-sGC pathway. We therefore examined whether the HR2.1:TN-XL mouse supports the detection of NO-mediated signaling in cones.

To address this question, we measured light-evoked Ca^{2+} responses in HR2.1:TN-XL mouse cones and applied NO pathway-related pharmacology. First we applied the NO donor SNAP (Fig. 22) at a concentration (200 µM) that was inspired by recent ERG recordings of NO effects in mammalian photoreceptors (Sato and Ohtsuka, 2010). In the presence of SNAP, resting [Ca^{2+}] (R_{base}) and light responses size (ΔR and R_A) decreased (Fig. 22A,B). These changes were statistically significant (Fig. 22C, for statistics see Table 2) and not reversible, even after a prolonged wash-out period. Neither t_{rise} nor t_{decay} was significantly altered by the NO donor. The continuous decrease of t_{decay} over the course of the experiment appeared to follow a general trend (Fig. 22C in "wash-out" cf. also Fig. 21C) and may therefore not be drug-related (see also Discussion 7.3). To confirm that the observed effects were indeed NO-mediated, degassed SNAP solution (solution left in an open lab vial over night) was applied to retinal slices, with no significant effect on light responses (data not shown). To examine the possibility of endogenous NO-signaling, we used the NO scavenger cPTIO (100 µM). In 1 out of 4 experiments, bath-application of cPTIO increased both resting Ca^{2+} level and response size weakly, hinting at a possible involvement of endogenous NO signaling on Ca^{2+} dynamics. However, in the remaining 3 experiments no consistent/significant effects could be observed (data not shown).

6.10. NO modulates light-evoked calcium response in cones through a sGC-independent pathway:

To elucidate whether the observed NO effect on light response at cone terminals is mediated by the aforementioned NO-sGC pathway, we examined whether the required pathway components are present in the outer retina of the mouse.

Since NO is a small, membrane-permeable molecule with a short half-life (Knowles and Moncada, 1992; Feldman et al., 1993; Hakim et al., 1996), a NO mediated pathway requires the activity of NOS in either the cone terminal or in immediately adjacent cells (such as horizontal cells and bipolar cells). Using the diaphorase assay, we tested for endogenous NO production in mouse retina. Nitric oxide synthase

activity was readily detectable in amacrine cells and processes in the IPL, but absent from cells in the OPL (Fig. 23A-C). Combined with the inconsistent results of NO scavenger application, this lack of detectable NOS activity in OPL makes an involvement of NO in photoreceptor synapse signaling unlikely.

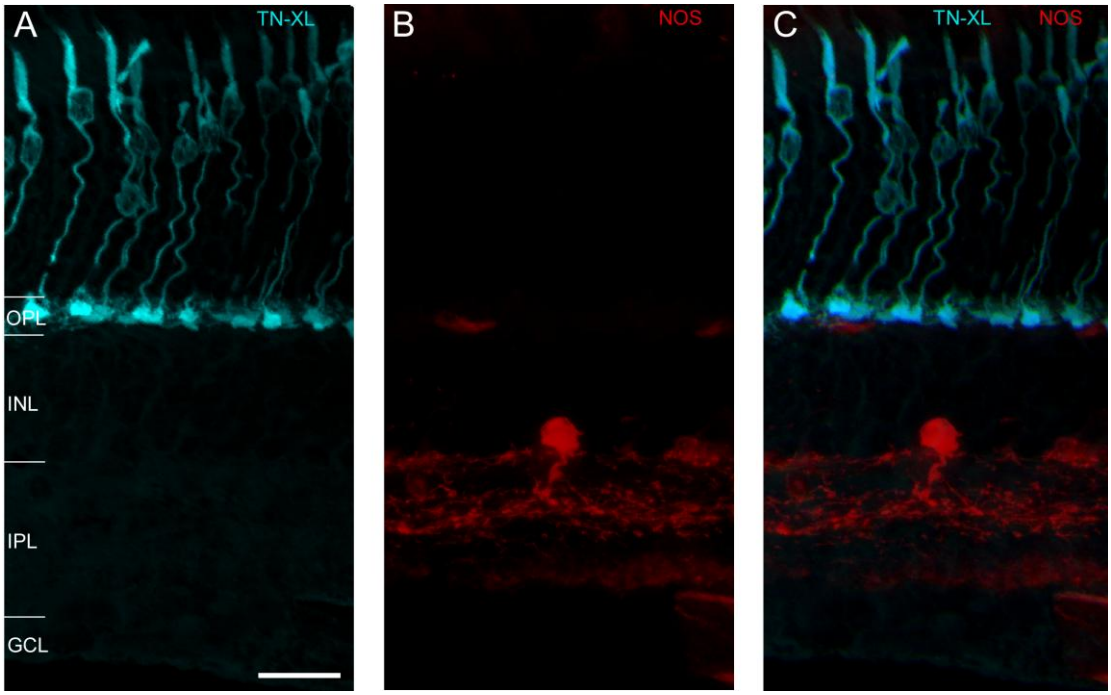

Fig. 23: NOS activity assay on vertical retinal section.
(**A-C**): Vertical section of HR2.1:TN-XL mouse retina stained with antibodies against GFP (**A**, blue) and processed to reveal nitric oxide synthase (NOS) activity using a NOS/diaphorase assay (**B**, red). (outer plexiform layer, OPL; inner nuclear layer, INL; inner plexiform layer, IPL; ganglion cell layer, GCL). Scale bars: 20 µm.

Nonetheless, our data show that (exogenous) NO can strongly modulate cone light responses (Fig. 22). SNAP decreased both resting [Ca^{2+}] as well as response amplitudes, suggesting a suppressive effect of NO on light responses in cones. Yet, these effects are not what would be expected from the “classical” NO-sGC pathway, in which a NO-induced sGC-generated increase in cGMP production should result in Ca^{2+} influx through CNG channels and hence an increased [Ca^{2+}]. To test if sGC played a role in modulating Ca^{2+} dynamics in cone terminal, sGC was blocked and its effect on light responses was measured. Surprisingly, bath application of the selective sGC blocker ODQ caused a small but significant and reversible increase in resting [Ca^{2+}] as well as response size (Fig. 24, for statistics see Table 2) - hinting at a possible role for sGC in shaping cone Ca^{2+} dynamics. However, immuno-histochemical staining showed that sGC expression was readily found in bipolar cells of HR2.1:TN-XL mouse retina but was not detected in cone terminals (Fig. 24A-C),

consistent with finding in rat retina (Ding and Weinberg, 2007). The lack of sGC expression in cone terminals suggests that the effects of ODQ may have been only indirect.

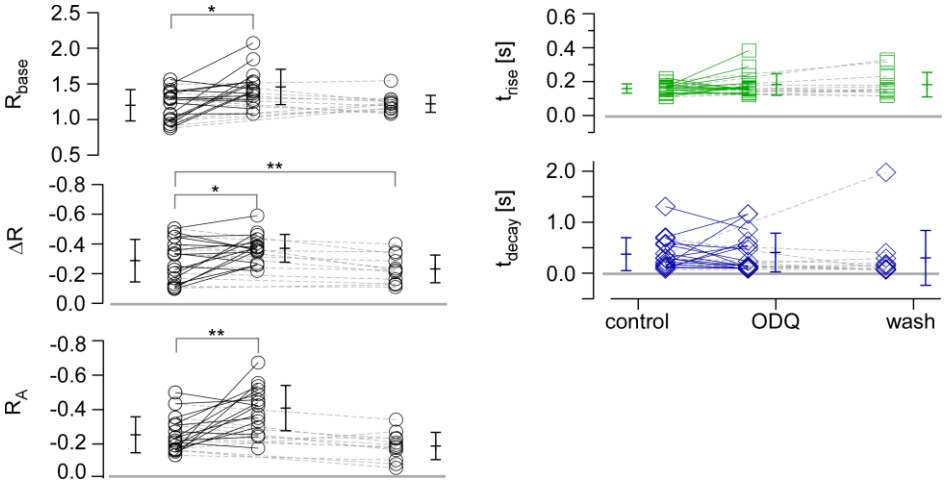

Fig. 24: Effect of inhibition of sGC on light-evoked calcium response.
Summary of the effect of ODQ, a selective sGC inhibitor, on light-evoked Ca^{2+} responses for n=16 terminals (from three retinas), with each symbol representing a cone (averages ± S.D. are illustrated next to each symbol column). For the wash-out, only data from n=12 cones is plotted; the remaining cells lost light excitability. (Wilcoxon signed test for paired samples, ** = p<0.01, * =p<0.05, if not indicated: non-significant).

In conclusion, while we demonstrate strong evidence for NO modulation of the Ca^{2+} dynamics in the mouse cone terminal, our data do not support the “classical” NO-sGC pathway, as it has been previously proposed for amphibian photoreceptors (Kurenny et al., 1994; Savchenko et al., 1997).

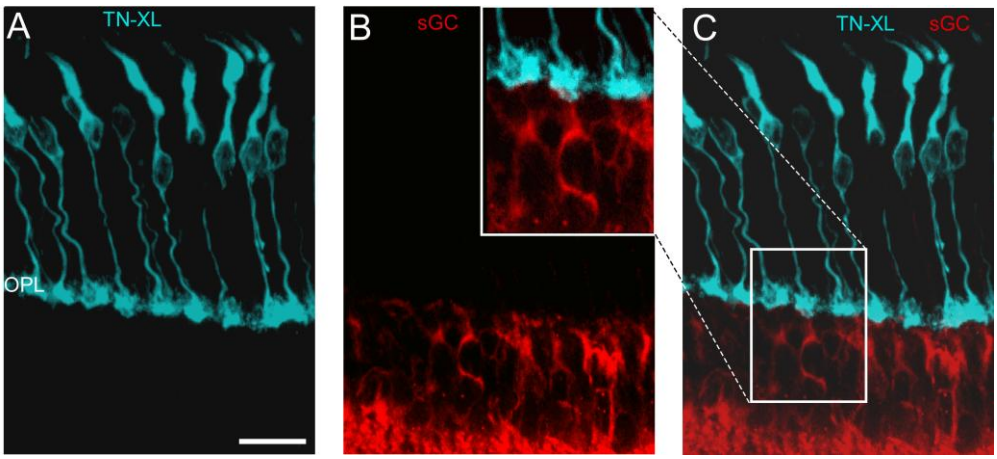

Fig. 25: sGC staining on vertical retinal section.
(**A-C**): Vertical section stained for TN-XL (**A**, blue) and sGC (**B**, red). Inset in (**B**) shows magnification of sGC and TN-XL labeling in the outer plexiform layer (OPL), from (**C**). (outer plexiform layer, OPL; soluble guanylyl cyclase, sGC). Scale bar: 20 µm.

7. Discussion:

Studying Ca^{2+} dynamics in cone photoreceptors has previously been hampered by the relatively low number of cone photoreceptors in the retina of model species such as mice and the lack of specific labeling techniques with Ca^{2+} indicators. The successful generation of the HR2.1:TN-XL mouse line for monitoring Ca^{2+} signals selectively in cones represents a major technical advance in this area. Another benefit of the HR2.1:TN-XL mouse is that many transgenic mouse models for human vision diseases are available (for review see (Won et al., 2011)) and by simply cross-breeding these models with the HR2.1:TN-XL, it will allow monitoring cone Ca^{2+} dynamics in the context of the respective diseases directly – for example, to study the mechanisms of inherited cone dystrophies and mutation-independent cone death followed by rod death.

In this study, it was demonstrated that in the transgenic mouse line 1) TN-XL-expressing cone photoreceptors have a normal morphology and that 2) the corresponding ERG components are indistinguishable from those recorded in wild-type littermates. It was further demonstrated that HR2.1:TN-XL allows measuring $[Ca^{2+}]$ changes in individual cones 3) at subcellular resolution, 4) in response to chemicals as well as light stimuli and 5) to probe the phototransduction cascade and its diverse regulatory mechanisms with pharmacology while monitoring cone output via changes in $[Ca^{2+}]$ at the cone terminal.

7.1. HR2.1:TN-XL, a transgenic mouse line to study calcium dynamics in cones:

The mouse is a very popular mammalian animal model, because, among other things, its genetics is very well understood, it can be easily genetically manipulated and it has a relatively short breeding cycle (van der Weyden et al., 2002; Graw, 2009). Transgenic mice carrying artificially modified DNA in their genomes serve as sophisticated “tools” and provide reproducible experimental systems for elucidating pathways of normal development and functions.

The success rate for generation of the transgenic mice for the HR2.1:TN-XL construct using direct microinjection was low; only 1 out of 10 founder mice carrying the integrated transgene expressed TN-XL in cones. This is likely due to the limitations of the direct microinjection technique used: the insertion site and its integrity, and the copy number of the transgene cannot be controlled for. There is a high probability that the introduced gene will not insert itself into an appropriate site in

the host genome that will permit its expression or that the introduced gene even inserts into a site that influences endogenous gene expression with lethal effects. The most likely explanation why in some cases the transgene was not expressed is transgene silencing (Milot et al., 1996; Clark et al., 1997; Pedram et al., 2006) by position effects in the local endogenous DNA environment.

In the resulting homozygote line (HR2.1:TN-XL), TN-XL is exclusively expressed in cones, consistent with earlier reports on the human red opsin promoter HR2.1 (Wang et al., 1992) we used here. TN-XL was absent from cone OS, which may, in fact, explain why the cells maintained apparently normal phototransduction. It is conceivable that this avoided potential interferences between photopigments and the TN-XL fluorescent proteins as well as Ca^{2+} buffering effects by the biosensor. The absence of TN-XL expression in cone OS may be due to a lack of recognition sites required for trafficking proteins from IS to OS (Williams, 2002; Insinna and Besharse, 2008; Kennedy and Malicki, 2009; Kizhatil et al., 2009), restricting the direct observation of Ca^{2+} dynamics to IS, soma and terminal. Nevertheless, changes of OS [Ca^{2+}] can at least partially be inferred from [Ca^{2+}] changes at the synaptic terminal, since these two compartments are linked via the cone's membrane potential and the VGCCs present in the terminal. The TN-XL biosensor possesses a relatively low Ca^{2+} affinity (Garaschuk et al., 2007; Hendel et al., 2008), which might limit its application to detecting large changes in [Ca^{2+}]. On the other hand, for the same reason it is also expected to have only little effect on intrinsic Ca^{2+} buffering capacity, and therefore little influence on normal cell physiology. In support of this is that no significant differences in ERG recordings were found between transgenic and wild-type mice, suggesting i.e. normal rod, cone and bipolar cell functions. Also the findings that light- and dark-evoked Ca^{2+} responses could be measured and cones remained responsive after adapting to different light levels indicate that cone function was largely normal. Therefore, our transgenic mouse line offers an excellent model to evaluate not only Ca^{2+} dynamics in cones, but also to gain insight in retinal signaling pathways from cones to postsynaptic neurons (see also 7.6)

7.2. Using HR2.1:TN-XL allows monitoring calcium dynamics in mouse cones in subcellular resolution:

With synthetic Ca^{2+} dyes it is possible to label photoreceptors for Ca^{2+} imaging experiments in mouse retinal slices, however the achieved signal is strongly dominated by the overwhelming number of rods (Mansergh et al., 2005; Babai et al., 2010), such that the cone signal is difficult to isolate. While enzymatically isolated

cones allow for higher spatial resolution, better control of the experimental conditions and easy access by electrodes (Szikra et al., 2009; Krizaj et al., 2011), this preparation is, of course, not suitable for measuring Ca^{2+} dynamics in cones under physiological conditions and interacting with their local microcircuit.

Except for the OS, the Ca^{2+} biosensor TN-XL was present throughout the cones, which allowed for resolving Ca^{2+} dynamics in the different cone compartments. Direct (KCl) and indirect (cGMP analogs) depolarization as well as activation of RyR-mediated CICR triggered large [Ca^{2+}] changes in the cone terminal but not in soma or IS. In fact, [Ca^{2+}] changes in latter compartments were rarely observed and rather resulted from prolonged Ca^{2+} influx in the terminal (and/or presumably the OS) and diffusion towards the soma/IS region. This is in contrast to findings in mouse rod photoreceptors, where depolarization evoked [Ca^{2+}] elevation and CICR were also observed in rod somata (Babai et al., 2010), and suggests differences in Ca^{2+} compartmentalization between rods and cones.

Photoreceptor terminals possess a specialized machinery for transmitter release called “synaptic ribbons” (Sterling and Matthews, 2005; tom Dieck and Brandstatter, 2006; Pan and Massey, 2007; Jackman et al., 2009) that are controlled by the very local Ca^{2+} dynamics. The Ca^{2+} imaging results obtained at cone terminal of the HR2.1:TN-XL mouse will provide the possibility for studying how neurotransmission is regulated at the cone ribbon synapse.

7.3. Light-evoked calcium responses can be recorded in mouse cone terminals of HR2.1:TN-XL mouse line:

Light-induced hyperpolarization (Baylor and Fuortes, 1970) and the resulting decrease of voltage-dependent Ca^{2+} currents (Corey et al., 1984) were described by electrical measurements. Optical recording of Ca^{2+} dynamics were performed also by using synthetic Ca^{2+} indicators (Ratto et al., 1988; Gray-Keller and Detwiler, 1994; McCarthy et al., 1996; Sampath et al., 1998; Matthews and Fain, 2001; Choi et al., 2005) which more focused on [Ca^{2+}] at steady status.

A recent study used an AAV-based system to introduce the Ca^{2+} biosensor GCaMP3 into different classes of retinal neurons, including cones (Borghuis et al., 2011), however, they did not report convincing cone light responses – whether this was due to technical issues or the expression level or type of biosensor is unclear. To the best of our knowledge, the HR2.1:TN-XL mouse line allows for the first time, to record

light-driven Ca^{2+} signals from mammalian cones with subcellular resolution and for time periods that allow chronic pharmacological manipulations.

Despite the orientation of the cones in the slice relative to the laser beam (see Results 6.6), laser scanning evoked effects were observed in the Ca^{2+} signals recorded from cone terminals directly after starting the scanning laser, resting [Ca^{2+}] were strongly depressed but then increased over a course of tens of seconds. At the same time, the sensitivity of cones to light stimuli increased until reaching a stable level. The practical consequence of this was the requirement to adapt the cones to the "background" illumination caused by the scanning laser. If this laser effect was due to scattered laser light or the evoked TN-XL fluorescence or a combination of both, it was not explored yet (for discussion see also (Denk and Detwiler, 1999; Euler et al., 2009)).

Over all, the response rise (=decrease in [Ca^{2+}]) at light-onset was about twice as fast as the response decay (=increase in [Ca^{2+}]) at light-offset. This may suggest that extrusion of Ca^{2+} from cone terminals was faster than Ca^{2+} influx through VGCCs, reflecting the fast clearance rate of the PMCA, which is energy dependent and was reported to be faster than passive Ca^{2+} influx through VGCCs along Ca^{2+} gradient (Caride et al., 2001; Johnson et al., 2007; Burette et al., 2009). Nevertheless, this temporal difference may also be at least partially due to the Ca^{2+} binding dynamics of TN-XL, which is unusual in that Ca^{2+} binding to TN-XL was reported to be two times slower than Ca^{2+} unbinding (Mank et al., 2006; Garaschuk et al., 2007; Hendel et al., 2008). Therefore, the biosensor kinetics is, in fact, expected to slow the observed response decay (=increase in [Ca^{2+}]), suggesting that the time difference between response rise and decay may actually be smaller.

In many cones the response decay time decreased over the course of a typical 1-hour experiment. Often, this was accompanied by the development of an overshoot at light-offset (Fig. 19 B2). Why this happened and whether or not this effect results from beginning of tissue degradation is unclear. Arguing against tissue degradation is the fact that the Ca^{2+} overshoot in mouse cones is reminiscent of the current undershoot reported for primate cones (Baylor et al., 1987). It has been proposed that this hyperpolarizing undershoot is related to the delayed activation of GC by GCAP2, which during light adaptation regulates GC activity to restore high resting [Ca^{2+}] (Mendez et al., 2001). If the overshoot is a relevant physiological regulation of Ca^{2+} dynamics during cone phototransduction, one is puzzled by the fact that it was only observed in ~10% of the cones. One possibility is that GCAP2 function decreases over time as a result of (degenerative) processes started in the tissue

after the slicing. However, this possibility remains to be explored. An alternative explanation for the “overshoot” is an increased voltage-dependent excitability of cones. In line with this is the observation that in some experiments cones showed strong spontaneous spike-like activity (Fig. 19 B3). The conditions that trigger this activity and whether or not it is physiologically relevant remain to be investigated.

Cone synaptic output is strongly controlled by feedback from horizontal cells (Byzov and Shura-Bura, 1986; Wu, 1992; Kamermans et al., 2001; Hirasawa and Kaneko, 2003; Barnes et al., 2005; Jackman et al., 2011). Therefore, it is likely that the light-evoked Ca^{2+} responses measured here also reflect some of this feedback. This may, however, vary from slice to slice, since at least some horizontal cells are damaged during the slicing procedure. While in this study the effects of horizontal cell feedback on the cone responses were not explored, some of the drug effects observed (see 7.4.) may be at least partially explained by horizontal cell feedback rather than direct action on cones.

7.4. Light-evoked calcium responses can be modulated pharmacologically:

We also demonstrated that the HR2.1:TN-XL mouse is suitable to evaluate the effects of pharmacological agents on intracellular processes in the cones – with the light-evoked Ca^{2+} response as the readout. PDE6 and CNG channels are known to regulate Ca^{2+} dynamics in cones. For instance, modulating the activity of CNG channels or PDE6 using highly specific drugs (inhibition of PDE6 by zaprinast; activation of CNG channels by cGMP analog 8-pCPT-cGMP) induced the expected changes in light response properties. In principle, this approach also allows screening for novel substances that affect cone Ca^{2+} dynamics. Such an approach could not only confirm the role of candidate factors for the Ca^{2+} regulation in cones but may also reveal their roles in phototransduction and light response.

7.5. Nitric oxide modulates light-evoked calcium responses in cone terminals:

For the mouse retina, it remains unclear whether or not NO exerts its effect in cones through the NO-sGC pathway, which was shown to modulate Ca^{2+} dynamics in amphibian photoreceptor terminals (Kurenny et al., 1994; Savchenko et al., 1997; Kourennyi et al., 2004). Since NO is a small and membrane-permeable molecule with a short half-life (Knowles and Moncada, 1992; Feldman et al., 1993; Hakim et al., 1996), this pathway requires the activity of NOS on either the synaptic side of the

cone terminal or in immediately adjacent cells. Our results did not show the presence of NOS in outer retina but in the IPL and in amacrine cells (see results 6.10 and Fig. 23), suggesting a role for NOS in visual processing in the inner retina, consistent with previous reports (Ahmad et al., 1994; Mills and Massey, 1995; Wang et al., 2003; Hoffpauir et al., 2006).

In addition to NOS, the expression of sGC and CNG channels in the presynapse (the cone terminal) is also needed by the hypothesized NO-sGC pathway. There are conflicting studies reporting the presence (rabbit: (Haberecht et al., 1998)) or absence (rat: (Ding and Weinberg, 2007)) of sGC in mammalian photoreceptor terminals, with the immunohistochemical sGC data in the present study supporting the latter. The absence of detectable sGC levels in cone terminals is in line with the physiological data: Although they confirm a strong effect of exogenous NO on mouse cone terminal [Ca^{2+}], instead of an increase as expected for NO-mediated sGC activation, a significant decrease in resting [Ca^{2+}] and light response amplitudes were observed. Also the finding that the sGC blocker ODQ increased resting [Ca^{2+}] – again opposite to what would be expected for the NO-sGC pathway – is difficult to explain by direct action of sGC in cones. As previously shown, sGC is present in some cone bipolar cells (Ding and Weinberg, 2007) (Fig. 25A-C), but it is unclear how modulation of sGC activity there would affect Ca^{2+} dynamics in cones. Inconsistent with a NO-sGC pathway in the OPL of the mammalian retina is also the fact that CNG channels could not be located in cone terminals (Matveev et al., 2008; Ding et al., 2009). However, it is possible that CNG channels are only very weakly expressed in terminals and therefore difficult to detect by immunohistochemical staining.

Nevertheless, our data clearly indicate that cone Ca^{2+} responses can be selectively decreased by exogenous NO. The results are in contrast to the data of previous ERG recordings in rats, where NO donors injected into the vitreous body were found to amplify the cone-specific ERG component (Sato and Ohtsuka, 2010; Vielma et al., 2010). This discrepancy may be explained by the different experimental conditions, and/or NO donors used, which may have led to different final NO concentrations in the tissue, although the final NO concentration in this project was expected to be in the range of the concentrations used in the ERG studies. Together with application of exogenous NO it was tested whether Ca^{2+} dynamics could be modulated by removing endogenous NO (NO scavenger cPTIO application, see 6.9). The conflicting results of the NO scavenger experiments may be due to difficulties of completely removing endogenous NO. In nervous system, the physiological concentration of NO is estimated to be in low nanomolar range (Garthwaite, 2008).

Thus, incomplete removal of NO by NO scavenger cPTIO may have led only to minor differences in NO concentration such that the resulting Ca^{2+} change was below our detection threshold.

Besides, there are a number of alternative potential explanations for the NO effects observed. As an oxidizing agent NO can also react with a variety of targets depending on its local concentrations and cell types. These NO effects include posttranslational protein nitration and S-nitrosylation that alter the activity of target proteins (Lipton et al., 1996; Broillet, 1999; Cassina et al., 2000; Doutheil et al., 2000; Amici et al., 2003), inhibition of cytochrome C oxidase in mitochondria (Brown and Cooper, 1994; Cleeter et al., 1994; Brown, 1999) and suppression of protein synthesis (Doutheil et al., 2000). For example, protein S-nitrosylation was suggested to underlie NO effects in photoreceptors (Vielma et al., 2010), however, whether S-nitrosylation is indeed a physiological mechanism to modulate protein activity is discussed controversially (reviewed by (Garthwaite, 2008)).

In conclusion, while it was found that NO modulates the Ca^{2+} dynamics in mouse cone terminals, it is unlikely that this effect employs the NO-sGC pathway. What pathway underlies the NO effects observed in cones and where NO might originate from remain to be seen. Nonetheless, on a more general level, the data illustrate the potential of the HR2.1:TN-XL mouse line in combination with two-photon imaging, light stimulation and pharmacology for functional studies of mammalian cone photoreceptors.

7.6. Further applications of the HR2.1:TN-XL mouse line:

The HR2.1:TN-XL mouse provides an excellent opportunity to study more “enigmatic” aspects of Ca^{2+} regulation in cones. For example, mice in which the cone-specific NCKX2 was knocked out failed to show any detectable dysfunction in cones (Li et al., 2006), possibly pointing at as of yet unidentified Ca^{2+} efflux pathways that compensate for the loss of NCKX2-mediate Ca^{2+} extrusion. Cross-breeding the NCKX2 knockout mouse line with the HR2.1:TN-XL mouse line will offer the possibility of monitoring Ca^{2+} dynamics in mouse cones in absence of NCKX2.

The transgenic mouse line may also be used to study synaptic interactions in the outer retina, in particular between cones and horizontal cells, where, for example, the cellular/synaptic mechanism(s) underlying negative (Byzov and Shura-Bura, 1986; Wu, 1992; Kamermans et al., 2001; Hirasawa and Kaneko, 2003; Barnes et al., 2005) or positive feedback (Jackman et al., 2011) are a matter of intense debate. Due to the low number and small size of mouse cones, it is quite a challenge to address

these questions in this increasingly prominent animal model for visual/retinal processing with electrical recordings. Thus, imaging light-driven Ca^{2+} responses in cone terminals while manipulating horizontal cells activity may prove an effective way to test different hypotheses on horizontal cell feedback mechanisms. Particularly exciting is also the possibility to image cone populations to gain high cell numbers and thus statistically more solid functional physiological data. Being able to acquire population data is also critical to systematically assess the functional properties of the different types of mouse cones, which include not only S- and M-cones but also opsin co-expressing (M/S-) cones, with M- and M/S-cones differentially distributed across the retina (Szel et al., 1992; Applebury et al., 2000; Haverkamp et al., 2005).

A particularly interesting application, however, is clearly the cross-breeding with cone degeneration models, such as the CNG channel subunit A3 knock-out mouse (*CNGA3*$^{-/-}$, (Michalakis et al., 2010)) or the *cpfl1* mouse (Chang et al., 2009). In the *CNGA3*$^{-/-}$ too low [Ca^{2+}] is thought to be connected to cone cell death, whereas in the *cpfl1* model cone degeneration has been proposed to be triggered by Ca^{2+} overload. In the latter model, the resulting elevation of [cGMP] due to the loss of cone-specific PDE6 function is thought to be the initial trigger for cone cell death (Trifunovic et al., 2010). Intracellular cGMP targets include CNG channels (Fox et al., 1999) and cGMP-activated PKG (Hofmann et al., 2006), both of which affect intracellular [Ca^{2+}] either directly (CNG channels are Ca^{2+}-permeable) or indirectly via modulation of CNG channel activity by PKG (Castro et al., 2010). One potential link between increased [Ca^{2+}] and degenerative processes in cones is the over-activation of Ca^{2+}-dependent calpain-type proteases (Paquet-Durand et al., 2006; Trifunovic et al., 2010). This is supported by the finding that in *rd1/CNG*$^{-/-}$ double-mutant animals, activity of calpains was strongly reduced and photoreceptor degeneration was slowed down significantly (Paquet-Durand et al., 2011). Cross-breeding of the HR2.1:TN-XL mouse line with the disease models mould allow us to gain direct insight in the Ca^{2+} dynamics in such degeneration processes.

In conclusion, the transgenic biosensor mouse line offers unprecedented possibilities to study cone Ca^{2+} dynamics in a wide range of conditions.

8. References:

Ahmad, I., Leinders-Zufall, T., Kocsis, J.D., Shepherd, G.M., Zufall, F., and Barnstable, C.J. (1994). Retinal ganglion cells express a cGMP-gated cation conductance activatable by nitric oxide donors. Neuron *12*, 155-165.

Akimoto, M., Cheng, H., Zhu, D., Brzezinski, J.A., Khanna, R., Filippova, E., Oh, E.C., Jing, Y., Linares, J.L., Brooks, M.*, et al.* (2006). Targeting of GFP to newborn rods by Nrl promoter and temporal expression profiling of flow-sorted photoreceptors. Proc Natl Acad Sci U S A *103*, 3890-3895.

Amici, M., Lupidi, G., Angeletti, M., Fioretti, E., and Eleuteri, A.M. (2003). Peroxynitrite-induced oxidation and its effects on isolated proteasomal systems. Free Radic Biol Med *34*, 987-996.

Applebury, M.L., Antoch, M.P., Baxter, L.C., Chun, L.L., Falk, J.D., Farhangfar, F., Kage, K., Krzystolik, M.G., Lyass, L.A., and Robbins, J.T. (2000). The murine cone photoreceptor: a single cone type expresses both S and M opsins with retinal spatial patterning. Neuron *27*, 513-523.

Arshavsky, V.Y., Lamb, T.D., and Pugh, E.N., Jr. (2002). G proteins and phototransduction. Annu Rev Physiol *64*, 153-187.

Babai, N., Morgans, C.W., and Thoreson, W.B. (2010). Calcium-induced calcium release contributes to synaptic release from mouse rod photoreceptors. Neuroscience *165*, 1447-1456.

Baccus, S.A., and Meister, M. (2004). Retina versus cortex; contrast adaptation in parallel visual pathways. Neuron *42*, 5-7.

Barnes, S., Vessey, J.P., Stratis, A.K., Daniels, B.A., Da Silva, N., Jonz, M.G., Lalonde, M.R., and Baldridge, W.H. (2005). Proton-mediated feedback inhibition of presynaptic calcium channels at the cone photoreceptor synapse. Journal of Neuroscience *25*, 4108-4117.

Baylor, D.A., and Fuortes, M.G. (1970). Electrical responses of single cones in the retina of the turtle. J Physiol *207*, 77-92.

Baylor, D.A., Nunn, B.J., and Schnapf, J.L. (1987). Spectral sensitivity of cones of the monkey Macaca fascicularis. J Physiol *390*, 145-160.

Berliocchi, L., Bano, D., and Nicotera, P. (2005). Ca2+ signals and death programmes in neurons. Philos T R Soc B *360*, 2255-2258.

Berridge, M.J. (2009). Inositol trisphosphate and calcium signalling mechanisms. Biochim Biophys Acta *1793*, 933-940.

Berridge, M.J., Bootman, M.D., and Roderick, H.L. (2003). Calcium signalling: dynamics, homeostasis and remodelling. Nat Rev Mol Cell Biol *4*, 517-529.

Berridge, M.J., Lipp, P., and Bootman, M.D. (2000). The versatility and universality of calcium signalling. Nat Rev Mol Cell Biol *1*, 11-21.

Blinks, J.R., Olson, C.B., Jewell, B.R., and Braveny, P. (1972). Influence of caffeine and other methylxanthines on mechanical properties of isolated mammalian heart muscle. Evidence for a dual mechanism of action. Circ Res *30*, 367-392.

Blom, J.J., Blute, T.A., and Eldred, W.D. (2009). Functional localization of the nitric oxide/cGMP pathway in the salamander retina. Vis Neurosci *26*, 275-286.

Borghuis, B.G., Tian, L., Xu, Y., Nikonov, S.S., Vardi, N., Zemelman, B.V., and Looger, L.L. (2011). Imaging light responses of targeted neuron populations in the rodent retina. J Neurosci *31*, 2855-2867.

Bowes, C., Li, T., Danciger, M., Baxter, L.C., Applebury, M.L., and Farber, D.B. (1990). Retinal degeneration in the rd mouse is caused by a defect in the beta subunit of rod cGMP-phosphodiesterase. Nature *347*, 677-680.

Boycott, B., and Wassle, H. (1999). Parallel processing in the mammalian retina: the Proctor Lecture. Invest Ophthalmol Vis Sci *40*, 1313-1327.

Boycott, B.B., and Hopkins, J.M. (1981). Microglia in the retina of monkey and other mammals: its distinction from other types of glia and horizontal cells. Neuroscience *6*, 679-688.

Breuninger, T., Puller, C., Haverkamp, S., and Euler, T. (2011). Chromatic bipolar cell pathways in the mouse retina. J Neurosci *31*, 6504-6517.

Broillet, M.C. (1999). S-nitrosylation of proteins. Cell Mol Life Sci *55*, 1036-1042.

Brown, G.C. (1999). Nitric oxide and mitochondrial respiration. Biochim Biophys Acta *1411*, 351-369.

Brown, G.C., and Cooper, C.E. (1994). Nanomolar concentrations of nitric oxide reversibly inhibit synaptosomal respiration by competing with oxygen at cytochrome oxidase. FEBS Lett *356*, 295-298.

Brown, S.P., and Masland, R.H. (2001). Spatial scale and cellular substrate of contrast adaptation by retinal ganglion cells. Nat Neurosci *4*, 44-51.

Burette, A.C., Strehler, E.E., and Weinberg, R.J. (2009). "Fast" plasma membrane calcium pump PMCA2a concentrates in GABAergic terminals in the adult rat brain. J Comp Neurol *512*, 500-513.

Burns, M.E., and Baylor, D.A. (2001). Activation, deactivation, and adaptation in vertebrate photoreceptor cells. Annu Rev Neurosci *24*, 779-805.

Byzov, A.L., and Shura-Bura, T.M. (1986). Electrical feedback mechanism in the processing of signals in the outer plexiform layer of the retina. Vision Res *26*, 33-44.

Cadetti, L., Bryson, E.J., Ciccone, C.A., Rabl, K., and Thoreson, W.B. (2006). Calcium-induced calcium release in rod photoreceptor terminals boosts synaptic transmission during maintained depolarization. Eur J Neurosci *23*, 2983-2990.

Calabrese, V., Mancuso, C., Calvani, M., Rizzarelli, E., Butterfield, D.A., and Stella, A.M. (2007). Nitric oxide in the central nervous system: neuroprotection versus neurotoxicity. Nat Rev Neurosci *8*, 766-775.

Carafoli, E., Santella, L., Branca, D., and Brini, M. (2001). Generation, control, and processing of cellular calcium signals. Crit Rev Biochem Mol Biol *36*, 107-260.

Caride, A.J., Filoteo, A.G., Penheiter, A.R., Paszty, K., Enyedi, A., and Penniston, J.T. (2001). Delayed activation of the plasma membrane calcium pump by a sudden increase in Ca2+: fast pumps reside in fast cells. Cell Calcium *30*, 49-57.

Carretta, A., and Cavaggioni, A. (1976). On the metabolism of the rod outer segments. J Physiol *257*, 687-697.

Cassina, A.M., Hodara, R., Souza, J.M., Thomson, L., Castro, L., Ischiropoulos, H., Freeman, B.A., and Radi, R. (2000). Cytochrome c nitration by peroxynitrite. J Biol Chem *275*, 21409-21415.

Castro, L.R., Schittl, J., and Fischmeister, R. (2010). Feedback control through cGMP-dependent protein kinase contributes to differential regulation and compartmentation of cGMP in rat cardiac myocytes. Circ Res *107*, 1232-1240.

Cepko, C. (1993). Lineage versus environment in the embryonic retina. Trends Neurosci *16*, 96-97; author reply 98.

Chang, B., Grau, T., Dangel, S., Hurd, R., Jurklies, B., Sener, E.C., Andreasson, S., Dollfus, H., Baumann, B., Bolz, S*., et al.* (2009). A homologous genetic basis of the murine cpfl1 mutant and human achromatopsia linked to mutations in the PDE6C gene. Proc Natl Acad Sci U S A *106*, 19581-19586.

Chang, G.Q., Hao, Y., and Wong, F. (1993). Apoptosis: final common pathway of photoreceptor death in rd, rds, and rhodopsin mutant mice. Neuron *11*, 595-605.

Cheng, H.P., Wei, S., Wei, L.P., and Verkhratsky, A. (2006). Calcium signaling in physiology and pathophysiology. Acta Pharmacol Sin *27*, 767-772.

Choi, D.W. (1992). Excitotoxic Cell-Death. J Neurobiol *23*, 1261-1276.

Choi, S.Y., Borghuis, B.G., Rea, R., Levitan, E.S., Sterling, P., and Kramer, R.H. (2005). Encoding light intensity by the cone photoreceptor synapse. Neuron *48*, 555-562.

Clark, A.J., Harold, G., and Yull, F.E. (1997). Mammalian cDNA and prokaryotic reporter sequences silence adjacent transgenes in transgenic mice. Nucleic Acids Res *25*, 1009-1014.

Cleeter, M.W., Cooper, J.M., Darley-Usmar, V.M., Moncada, S., and Schapira, A.H. (1994). Reversible inhibition of cytochrome c oxidase, the terminal enzyme of the mitochondrial respiratory chain, by nitric oxide. Implications for neurodegenerative diseases. FEBS Lett *345*, 50-54.

Copenhagen, D.R., Ashmore, J.F., and Schnapf, J.K. (1983). Kinetics of synaptic transmission from photoreceptors to horizontal and bipolar cells in turtle retina. Vision Res *23*, 363-369.

Corey, D.P., Dubinsky, J.M., and Schwartz, E.A. (1984). The calcium current in inner segments of rods from the salamander (Ambystoma tigrinum) retina. J Physiol *354*, 557-575.

Cossart, R., Aronov, D., and Yuste, R. (2003). Attractor dynamics of network UP states in the neocortex. Nature *423*, 283-288.

Dacey, D.M., and Packer, O.S. (2003). Colour coding in the primate retina: diverse cell types and cone-specific circuitry. Curr Opin Neurobiol *13*, 421-427.

Denk, W., and Detwiler, P.B. (1999). Optical recording of light-evoked calcium signals in the functionally intact retina. Proc Natl Acad Sci U S A *96*, 7035-7040.

Denk, W., Strickler, J.H., and Webb, W.W. (1990). Two-photon laser scanning fluorescence microscopy. Science *248*, 73-76.

Denninger, J.W., and Marletta, M.A. (1999). Guanylate cyclase and the .NO/cGMP signaling pathway. Biochim Biophys Acta *1411*, 334-350.

Devries, S.H., and Schwartz, E.A. (1992). Hemi-Gap-Junction Channels in Solitary Horizontal Cells of the Catfish Retina. J Physiol-London *445*, 201-230.

Ding, J.D., and Weinberg, R.J. (2007). Distribution of soluble guanylyl cyclase in rat retina. J Comp Neurol *502*, 734-745.

Ding, X.Q., Harry, C.S., Umino, Y., Matveev, A.V., Fliesler, S.J., and Barlow, R.B. (2009). Impaired cone function and cone degeneration resulting from CNGB3 deficiency: down-regulation of CNGA3 biosynthesis as a potential mechanism. Hum Mol Genet *18*, 4770-4780.

Djamgoz, M.B., Sekaran, S., Angotzi, A.R., Haamedi, S., Vallerga, S., Hirano, J., and Yamada, M. (2000). Light-adaptive role of nitric oxide in the outer retina of lower vertebrates: a brief review. Philos Trans R Soc Lond B Biol Sci *355*, 1199-1203.

Doutheil, J., Althausen, S., Treiman, M., and Paschen, W. (2000). Effect of nitric oxide on endoplasmic reticulum calcium homeostasis, protein synthesis and energy metabolism. Cell Calcium *27*, 107-115.

Eimerl, S., and Schramm, M. (1994). The Quantity of Calcium That Appears to Induce Neuronal Death. J Neurochem *62*, 1223-1226.

Endo, M., Tanaka, M., and Ogawa, Y. (1970). Calcium induced release of calcium from the sarcoplasmic reticulum of skinned skeletal muscle fibres. Nature *228*, 34-36.

Euler, T., Detwiler, P.B., and Denk, W. (2002). Directionally selective calcium signals in dendrites of starburst amacrine cells. Nature *418*, 845-852.

Euler, T., Hausselt, S.E., Margolis, D.J., Breuninger, T., Castell, X., Detwiler, P.B., and Denk, W. (2009). Eyecup scope-optical recordings of light stimulus-evoked fluorescence signals in the retina. Pflug Arch Eur J Phy *457*, 1393-1414.

Fabiato, A. (1983). Calcium-induced release of calcium from the cardiac sarcoplasmic reticulum. Am J Physiol *245*, C1-14.

Fabiato, A., and Fabiato, F. (1975). Contractions induced by a calcium-triggered release of calcium from the sarcoplasmic reticulum of single skinned cardiac cells. J Physiol *249*, 469-495.

Fain, G.L., Matthews, H.R., Cornwall, M.C., and Koutalos, Y. (2001). Adaptation in vertebrate photoreceptors. Physiol Rev *81*, 117-151.

Feldman, P.L., Griffith, O.W., and Stuehr, D.J. (1993). The Surprising Life of Nitric-Oxide. Chem Eng News *71*, 26-38.

Fox, D.A., Poblenz, A.T., and He, L. (1999). Calcium overload triggers rod photoreceptor apoptotic cell death in chemical-induced and inherited retinal degenerations. Ann N Y Acad Sci *893*, 282-285.

Fried, S.I., Munch, T.A., and Werblin, F.S. (2002). Mechanisms and circuitry underlying directional selectivity in the retina. Nature *420*, 411-414.

Fu, Y., and Yau, K.W. (2007). Phototransduction in mouse rods and cones. Pflugers Arch *454*, 805-819.

Garaschuk, O., Griesbeck, O., and Konnerth, A. (2007). Troponin C-based biosensors: a new family of genetically encoded indicators for in vivo calcium imaging in the nervous system. Cell Calcium *42*, 351-361.

Garthwaite, J. (2008). Concepts of neural nitric oxide-mediated transmission. Eur J Neurosci *27*, 2783-2802.

Ghozland, S., Aguado, F., Espinosa-Parrilla, J.F., Soriano, E., and Maldonado, R. (2002). Spontaneous network activity of cerebellar granule neurons: impairment by in vivo chronic cannabinoid administration. Eur J Neurosci *16*, 641-651.

Gobel, W., and Helmchen, F. (2007). In vivo calcium imaging of neural network function. Physiology (Bethesda) *22*, 358-365.

Goldstein, I.M., Ostwald, P., and Roth, S. (1996). Nitric oxide: a review of its role in retinal function and disease. Vision Res *36*, 2979-2994.

Gordon, J.W., and Ruddle, F.H. (1981). Integration and stable germ line transmission of genes injected into mouse pronuclei. Science *214*, 1244-1246.

Gotoh, T., and Mori, M. (2006). Nitric oxide and endoplasmic reticulum stress. Arterioscler Thromb Vasc Biol *26*, 1439-1446.

Gotzes, S., de Vente, J., and Muller, F. (1998). Nitric oxide modulates cGMP levels in neurons of the inner and outer retina in opposite ways. Vis Neurosci *15*, 945-955.

Graw, J. (2009). Mouse models of cataract. J Genet *88*, 469-486.

Gray-Keller, M.P., and Detwiler, P.B. (1994). The calcium feedback signal in the phototransduction cascade of vertebrate rods. Neuron *13*, 849-861.

Guix, F.X., Uribesalgo, I., Coma, M., and Munoz, F.J. (2005). The physiology and pathophysiology of nitric oxide in the brain. Prog Neurobiol *76*, 126-152.

Gunter, T.E., Buntinas, L., Sparagna, G., Eliseev, R., and Gunter, K. (2000). Mitochondrial calcium transport: mechanisms and functions. Cell Calcium *28*, 285-296.

Haberecht, M.F., Schmidt, H.H., Mills, S.L., Massey, S.C., Nakane, M., and Redburn-Johnson, D.A. (1998). Localization of nitric oxide synthase, NADPH diaphorase and soluble guanylyl cyclase in adult rabbit retina. Vis Neurosci *15*, 881-890.

Hakim, T.S., Sugimori, K., Camporesi, E.M., and Anderson, G. (1996). Half-life of nitric oxide in aqueous solutions with and without haemoglobin. Physiol Meas *17*, 267-277.

Haverkamp, S., Wassle, H., Duebel, J., Kuner, T., Augustine, G.J., Feng, G., and Euler, T. (2005). The primordial, blue-cone color system of the mouse retina. J Neurosci *25*, 5438-5445.

Hendel, T., Mank, M., Schnell, B., Griesbeck, O., Borst, A., and Reiff, D.F. (2008). Fluorescence changes of genetic calcium indicators and OGB-1 correlated with neural activity and calcium in vivo and in vitro. J Neurosci *28*, 7399-7411.

Hirasawa, H., and Kaneko, A. (2003). pH changes in the invaginating synaptic cleft mediate feedback from horizontal cells to cone photoreceptors by modulating Ca2+ channels. J Gen Physiol *122*, 657-671.

Hoffpauir, B., McMains, E., and Gleason, E. (2006). Nitric oxide transiently converts synaptic inhibition to excitation in retinal amacrine cells. J Neurophysiol *95*, 2866-2877.

Hofmann, F., Feil, R., Kleppisch, T., and Schlossmann, J. (2006). Function of cGMP-dependent protein kinases as revealed by gene deletion. Physiol Rev *86*, 1-23.

Hope, B.T., Michael, G.J., Knigge, K.M., and Vincent, S.R. (1991). Neuronal NADPH diaphorase is a nitric oxide synthase. Proc Natl Acad Sci U S A *88*, 2811-2814.

Hurwitz, R.L., Bunt-Milam, A.H., Chang, M.L., and Beavo, J.A. (1985). cGMP phosphodiesterase in rod and cone outer segments of the retina. J Biol Chem *260*, 568-573.

Insinna, C., and Besharse, J.C. (2008). Intraflagellar transport and the sensory outer segment of vertebrate photoreceptors. Dev Dyn *237*, 1982-1992.

Jackman, S.L., Babai, N., Chambers, J.J., Thoreson, W.B., and Kramer, R.H. (2011). A positive feedback synapse from retinal horizontal cells to cone photoreceptors. Plos Biol *9*, e1001057.

Jackman, S.L., Choi, S.Y., Thoreson, W.B., Rabl, K., Bartoletti, T.M., and Kramer, R.H. (2009). Role of the synaptic ribbon in transmitting the cone light response. Nat Neurosci *12*, 303-310.

Jacobs, G.H. (1993). The Distribution and Nature of Color-Vision among the Mammals. Biol Rev *68*, 413-471.

Jacobs, G.H., Neitz, J., and Deegan, J.F., 2nd (1991). Retinal receptors in rodents maximally sensitive to ultraviolet light. Nature *353*, 655-656.

Jeon, C.J., Strettoi, E., and Masland, R.H. (1998). The major cell populations of the mouse retina. J Neurosci *18*, 8936-8946.

Johnson, J.E., Jr., Perkins, G.A., Giddabasappa, A., Chaney, S., Xiao, W., White, A.D., Brown, J.M., Waggoner, J., Ellisman, M.H., and Fox, D.A. (2007). Spatiotemporal regulation of ATP and Ca2+ dynamics in vertebrate rod and cone ribbon synapses. Mol Vis *13*, 887-919.

Juedes, M.J., and Wogan, G.N. (1996). Peroxynitrite-induced mutation spectra of pSP189 following replication in bacteria and in human cells. Mutat Res-Fund Mol M *349*, 51-61.

Kamermans, M., Fahrenfort, I., Schultz, K., Janssen-Bienhold, U., Sjoerdsma, T., and Weiler, R. (2001). Hemichannel-mediated inhibition in the outer retina. Science *292*, 1178-1180.

Kaneko, A. (1979). Physiology of the retina. Annu Rev Neurosci *2*, 169-191.

Kaupp, U.B., and Seifert, R. (2002). Cyclic nucleotide-gated ion channels. Physiol Rev *82*, 769-824.

Kefalov, V., Fu, Y., Marsh-Armstrong, N., and Yau, K.W. (2003). Role of visual pigment properties in rod and cone phototransduction. Nature *425*, 526-531.

Kelly, M.E.M., and Barnes, S. (1997). Physiology and pathophysiology of nitric oxide in the retina. Neuroscientist *3*, 357-360.

Kennedy, B., and Malicki, J. (2009). What Drives Cell Morphogenesis: A Look Inside the Vertebrate Photoreceptor. Dev Dynam *238*, 2115-2138.

Kizhatil, K., Baker, S.A., Arshavsky, V.Y., and Bennett, V. (2009). Ankyrin-G promotes cyclic nucleotide-gated channel transport to rod photoreceptor sensory cilia. Science *323*, 1614-1617.

Knot, H.J., Laher, I., Sobie, E.A., Guatimosim, S., Gomez-Viquez, L., Hartmann, H., Song, L.S., Lederer, W.J., Graier, W.F., Malli, R.*, et al.* (2005). Twenty years of calcium imaging: cell physiology to dye for. Mol Interv *5*, 112-127.

Knowles, R.G., and Moncada, S. (1992). Nitric-Oxide as a Signal in Blood-Vessels. Trends Biochem Sci *17*, 399-402.

Koch, K.W. (1991). Purification and identification of photoreceptor guanylate cyclase. J Biol Chem *266*, 8634-8637.

Kolb, H. (2003). How the retina works - Much of the construction of an image takes place in the retina itself through the use of specialized neural circuits. Am Sci *91*, 28-35.

Korenbrot, J.I. (1995). Ca2+ flux in retinal rod and cone outer segments: differences in Ca2+ selectivity of the cGMP-gated ion channels and Ca2+ clearance rates. Cell Calcium *18*, 285-300.

Korenbrot, J.I., and Rebrik, T.I. (2002). Tuning outer segment Ca2+ homeostasis to phototransduction in rods and cones. Adv Exp Med Biol *514*, 179-203.

Kourennyi, D.E., Liu, X.D., Hart, J., Mahmud, F., Baldridge, W.H., and Barnes, S. (2004). Reciprocal modulation of calcium dynamics at rod and cone photoreceptor synapses by nitric oxide. J Neurophysiol *92*, 477-483.

Koutalos, Y., and Yau, K.W. (1996). Regulation of sensitivity in vertebrate rod photoreceptors by calcium. Trends Neurosci *19*, 73-81.

Kramer, R.H., Sheng, Z.J., Choi, S.Y., Dharia, A., Li, J., and Sterling, P. (2007). Synaptic Ca2+ in darkness is lower in rods than cones, causing slower tonic release of vesicles. Journal of Neuroscience *27*, 5033-5042.

Krizaj, D. (2005). Compartmentalization of calcium entry pathways in mouse rods. Eur J Neurosci *22*, 3292-3296.

Krizaj, D., Bao, J.X., Schmitz, Y., Witkovsky, P., and Copenhagen, D.R. (1999). Caffeine-sensitive calcium stores regulate synaptic transmission from retinal rod photoreceptors. J Neurosci *19*, 7249-7261.

Krizaj, D., and Copenhagen, D.R. (1998). Compartmentalization of calcium extrusion mechanisms in the outer and inner segments of photoreceptors. Neuron *21*, 249-256.

Krizaj, D., and Copenhagen, D.R. (2002). Calcium regulation in photoreceptors. Front Biosci *7*, d2023-2044.

Krizaj, D., Demarco, S.J., Johnson, J., Strehler, E.E., and Copenhagen, D.R. (2002). Cell-specific expression of plasma membrane calcium ATPase isoforms in retinal neurons. J Comp Neurol *451*, 1-21.

Krizaj, D., Mercer, A.J., Thoreson, W.B., and Barabas, P. (2011). Intracellular pH modulates inner segment calcium homeostasis in vertebrate photoreceptors. Am J Physiol Cell Physiol *300*, C187-197.

Kurenny, D.E., Moroz, L.L., Turner, R.W., Sharkey, K.A., and Barnes, S. (1994). Modulation of ion channels in rod photoreceptors by nitric oxide. Neuron *13*, 315-324.

Kwon, N.S., Stuehr, D.J., and Nathan, C.F. (1991). Inhibition of Tumor-Cell Ribonucleotide Reductase by Macrophage-Derived Nitric-Oxide. J Exp Med *174*, 761-767.

Lepoivre, M., Fieschi, F., Coves, J., Thelander, L., and Fontecave, M. (1991). Inactivation of Ribonucleotide Reductase by Nitric-Oxide. Biochem Biophys Res Commun *179*, 442-448.

Levy, H., Twig, G., and Perlman, I. (2004). Nitric oxide modulates the transfer function between cones and horizontal cells during changing conditions of ambient illumination. Eur J Neurosci *20*, 2963-2974.

Li, N., Zou, A.P., Ge, Z.D., Campbell, W.B., and Li, P.L. (2000). Effect of nitric oxide on calcium-induced calcium release in coronary arterial smooth muscle. Gen Pharmacol *35*, 37-45.

Li, Q., Timmers, A.M., Guy, J., Pang, J., and Hauswirth, W.W. (2008). Cone-specific expression using a human red opsin promoter in recombinant AAV. Vision Res *48*, 332-338.

Li, X.F., Kiedrowski, L., Tremblay, F., Fernandez, F.R., Perizzolo, M., Winkfein, R.J., Turner, R.W., Bains, J.S., Rancourt, D.E., and Lytton, J. (2006). Importance of K+-dependent Na+/Ca2+-exchanger 2, NCKX2, in motor learning and memory. J Biol Chem *281*, 6273-6282.

Lipton, S.A., Choi, Y.B., Sucher, N.J., Pan, Z.H., and Stamler, J.S. (1996). Redox state, NMDA receptors and NO-related species. Trends Pharmacol Sci *17*, 186-187;discussion 187-189.

Livak, K.J., and Schmittgen, T.D. (2001). Analysis of relative gene expression data using real-time quantitative PCR and the 2(T)(-Delta Delta C) method. Methods *25*, 402-408.

Livesey, F.J., and Cepko, C.L. (2001). Vertebrate neural cell-fate determination: lessons from the retina. Nat Rev Neurosci *2*, 109-118.

Lubos, E., Handy, D.E., and Loscalzo, J. (2008). Role of oxidative stress and nitric oxide in atherothrombosis. Front Biosci *13*, 5323-5344.

Lukats, A., Szabo, A., Rohlich, P., Vigh, B., and Szel, A. (2005). Photopigment coexpression in mammals: comparative and developmental aspects. Histol Histopathol *20*, 551-574.

Mank, M., and Griesbeck, O. (2008). Genetically encoded calcium indicators. Chem Rev *108*, 1550-1564.

Mank, M., Reiff, D.F., Heim, N., Friedrich, M.W., Borst, A., and Griesbeck, O. (2006). A FRET-based calcium biosensor with fast signal kinetics and high fluorescence change. Biophys J *90*, 1790-1796.

Mansergh, F., Orton, N.C., Vessey, J.P., Lalonde, M.R., Stell, W.K., Tremblay, F., Barnes, S., Rancourt, D.E., and Bech-Hansen, N.T. (2005). Mutation of the calcium channel gene Cacna1f disrupts calcium signaling, synaptic transmission and cellular organization in mouse retina. Hum Mol Genet *14*, 3035-3046.

Mao, B.Q., Hamzei-Sichani, F., Aronov, D., Froemke, R.C., and Yuste, R. (2001). Dynamics of spontaneous activity in neocortical slices. Neuron *32*, 883-898.

Marmor, M.F., Cabael, L., Shukla, S., Hwang, J.C., and Marcus, M. (2004a). Clinical S-cone ERG recording with a commercial hand-held full-field stimulator. Doc Ophthalmol *109*, 101-107.

Marmor, M.F., Holder, G.E., Seeliger, M.W., and Yamamoto, S. (2004b). Standard for clinical electroretinography (2004 update). Doc Ophthalmol *108*, 107-114.

Masland, R.H. (2001). The fundamental plan of the retina. Nat Neurosci *4*, 877-886.

Matthews, H.R., and Fain, G.L. (2001). A light-dependent increase in free Ca2+ concentration in the salamander rod outer segment. J Physiol *532*, 305-321.

Matulef, K., and Zagotta, W.N. (2003). Cyclic nucleotide-gated ion channels. Annu Rev Cell Dev Biol *19*, 23-44.

Matveev, A.V., Quiambao, A.B., Browning Fitzgerald, J., and Ding, X.Q. (2008). Native cone photoreceptor cyclic nucleotide-gated channel is a heterotetrameric complex comprising both CNGA3 and CNGB3: a study using the cone-dominant retina of Nrl-/- mice. J Neurochem *106*, 2042-2055.

McCarthy, S.T., Younger, J.P., and Owen, W.G. (1996). Dynamic, spatially nonuniform calcium regulation in frog rods exposed to light. J Neurophysiol *76*, 1991-2004.

McCombs, J.E., and Palmer, A.E. (2008). Measuring calcium dynamics in living cells with genetically encodable calcium indicators. Methods *46*, 152-159.

McMahon, D.G., and Ponomareva, L.V. (1996). Nitric oxide and cGMP modulate retinal glutamate receptors. J Neurophysiol *76*, 2307-2315.

Mendez, A., Burns, M.E., Sokal, I., Dizhoor, A.M., Baehr, W., Palczewski, K., Baylor, D.A., and Chen, J. (2001). Role of guanylate cyclase-activating proteins (GCAPs) in setting the flash sensitivity of rod photoreceptors. Proc Natl Acad Sci U S A *98*, 9948-9953.

Michalakis, S., Muhlfriedel, R., Tanimoto, N., Krishnamoorthy, V., Koch, S., Fischer, M.D., Becirovic, E., Bai, L., Huber, G., Beck, S.C*., et al.* (2010). Restoration of Cone Vision in the CNGA3(-/-) Mouse Model of Congenital Complete Lack of Cone Photoreceptor Function. Hum Gene Ther *21*, 1181-1181.

Mills, S.L., and Massey, S.C. (1995). Differential properties of two gap junctional pathways made by AII amacrine cells. Nature *377*, 734-737.

Milot, E., Strouboulis, J., Trimborn, T., Wijgerde, M., de Boer, E., Langeveld, A., Tan-Un, K., Vergeer, W., Yannoutsos, N., Grosveld, F., and Fraser, P. (1996). Heterochromatin effects on the frequency and duration of LCR-mediated gene transcription. Cell *87*, 105-114.

Morgans, C.W., Bayley, P.R., Oesch, N.W., Ren, G., Akileswaran, L., and Taylor, W.R. (2005). Photoreceptor calcium channels: insight from night blindness. Vis Neurosci *22*, 561-568.

Muller, F., and Kaupp, U.B. (1998). [Signal transduction in photoreceptor cells]. Naturwissenschaften *85*, 49-61.

Muller, F., and Koch, K.W. (1998). Calcium-binding proteins and nitric oxide in retinal function and disease. Acta Anat (Basel) *162*, 142-150.

Mustafi, D., Engel, A.H., and Palczewski, K. (2009). Structure of cone photoreceptors. Prog Retin Eye Res *28*, 289-302.

Nachman-Clewner, M., St Jules, R., and Townes-Anderson, E. (1999). L-type calcium channels in the photoreceptor ribbon synapse: localization and role in plasticity. J Comp Neurol *415*, 1-16.

Nguyen, T., Brunson, D., Crespi, C.L., Penman, B.W., Wishnok, J.S., and Tannenbaum, S.R. (1992). DNA Damage and Mutation in Human-Cells Exposed to Nitric-Oxide Invitro. Proc Natl Acad Sci U S A *89*, 3030-3034.

Nicotera, P., and Orrenius, S. (1998). The role of calcium in apoptosis. Cell Calcium *23*, 173-180.

Nikonov, S.S., Kholodenko, R., Lem, J., and Pugh, E.N., Jr. (2006). Physiological features of the S- and M-cone photoreceptors of wild-type mice from single-cell recordings. J Gen Physiol *127*, 359-374.

Odell, T.J., Hawkins, R.D., Kandel, E.R., and Arancio, O. (1991). Tests of the Roles of 2 Diffusible Substances in Long-Term Potentiation - Evidence for Nitric-Oxide as a Possible Early Retrograde Messenger. Proc Natl Acad Sci U S A *88*, 11285-11289.

Olshevskaya, E.V., Hughes, R.E., Hurley, J.B., and Dizhoor, A.M. (1997). Calcium binding, but not a calcium-myristoyl switch, controls the ability of guanylyl cyclase-activating protein GCAP-2 to regulate photoreceptor guanylyl cyclase. J Biol Chem *272*, 14327-14333.

Olveczky, B.P., Baccus, S.A., and Meister, M. (2003). Segregation of object and background motion in the retina. Nature *423*, 401-408.

Palmer, A.E., and Tsien, R.Y. (2006). Measuring calcium signaling using genetically targetable fluorescent indicators. Nat Protoc *1*, 1057-1065.

Pan, F., and Massey, S.C. (2007). Rod and cone input to horizontal cells in the rabbit retina. J Comp Neurol *500*, 815-831.

Panfoli, I., Morelli, A., and Pepe, I.M. (1994). Calcium pump in the disk membranes isolated from bovine retinal rod outer segments. J Photochem Photobiol B *24*, 187-194.

Paquet-Durand, F., Azadi, S., Hauck, S.M., Ueffing, M., van Veen, T., and Ekstrom, P. (2006). Calpain is activated in degenerating photoreceptors in the rd1 mouse. J Neurochem *96*, 802-814.

Paquet-Durand, F., Beck, S., Michalakis, S., Goldmann, T., Huber, G., Muhlfriedel, R., Trifunovic, D., Fischer, M.D., Fahl, E., Duetsch, G.*, et al.* (2011). A key role for cyclic nucleotide gated (CNG) channels in cGMP-related retinitis pigmentosa. Hum Mol Genet *20*, 941-947.

Paredes, R.M., Etzler, J.C., Watts, L.T., Zheng, W., and Lechleiter, J.D. (2008). Chemical calcium indicators. Methods *46*, 143-151.

Paschen, W., and Mengesdorf, T. (2005). Endoplasmic reticulum stress response and neurodegeneration. Cell Calcium *38*, 409-415.

Pedram, M., Sprung, C.N., Gao, Q., Lo, A.W., Reynolds, G.E., and Murnane, J.P. (2006). Telomere position effect and silencing of transgenes near telomeres in the mouse. Mol Cell Biol *26*, 1865-1878.

Prinsen, C.F., Szerencsei, R.T., and Schnetkamp, P.P. (2000). Molecular cloning and functional expression of the potassium-dependent sodium-calcium exchanger from human and chicken retinal cone photoreceptors. J Neurosci *20*, 1424-1434.

Puckett, K.L., Aronson, E.T., and Goldin, S.M. (1985). ATP-dependent calcium uptake activity associated with a disk membrane fraction isolated from bovine retinal rod outer segments. Biochemistry *24*, 390-400.

Pugh, E.N., Jr., and Lamb, T.D. (1993). Amplification and kinetics of the activation steps in phototransduction. Biochim Biophys Acta *1141*, 111-149.

Puzianowska-Kuznicka, M., and Kuznicki, J. (2009). The ER and ageing II: calcium homeostasis. Ageing Res Rev *8*, 160-172.

Ramón y Cajal, S., Glickstein, M., and Thorpe, S.A. (1972). The structure of the retina. Compiled and translated by Sylvia A. Thorpe and Mitchell Glickstein (Springfield, Ill.,: Thomas).

Ratto, G.M., Payne, R., Owen, W.G., and Tsien, R.Y. (1988). The concentration of cytosolic free calcium in vertebrate rod outer segments measured with fura-2. J Neurosci *8*, 3240-3246.

Rebrik, T.I., and Korenbrot, J.I. (2004). In intact mammalian photoreceptors, Ca2+-dependent modulation of cGMP-gated ion channels is detectable in cones but not in rods. J Gen Physiol *123*, 63-75.

Rieke, F., and Schwartz, E.A. (1994). A Cgmp-Gated Current Can Control Exocytosis at Cone Synapses. Neuron *13*, 863-873.

Rizzuto, R., and Pozzan, T. (2006). Microdomains of intracellular Ca2+: molecular determinants and functional consequences. Physiol Rev *86*, 369-408.

Rosselli, M., Keller, P.J., and Dubey, R.K. (1998). Role of nitric oxide in the biology, physiology and pathophysiology of reproduction. Hum Reprod Update *4*, 3-24.

Routledge, M.N., Mirsky, F.J., Wink, D.A., Keefer, L.K., and Dipple, A. (1994). Nitrite-Induced Mutations in a Forward Mutation Assay - Influence of Nitrite Concentration and Ph. Mutat Res-Genet Tox *322*, 341-346.

Sack, R.A., and Harris, C.M. (1977). Ca2+ dependent ATPase activity of bovine receptor cell outer segment. Nature *265*, 465-466.

Sahaboglu, A., Tanimoto, N., Kaur, J., Sancho-Pelluz, J., Huber, G., Fahl, E., Arango-Gonzalez, B., Zrenner, E., Ekstrom, P., Lowenheim, H.*, et al.* (2010). PARP1 gene knock-out increases resistance to retinal degeneration without affecting retinal function. PLoS One *5*, e15495.

Sampath, A.P., Matthews, H.R., Cornwall, M.C., and Fain, G.L. (1998). Bleached pigment produces a maintained decrease in outer segment Ca2+ in salamander rods. J Gen Physiol *111*, 53-64.

Sancho-Pelluz, J., Arango-Gonzalez, B., Kustermann, S., Romero, F.J., van Veen, T., Zrenner, E., Ekstrom, P., and Paquet-Durand, F. (2008). Photoreceptor cell death mechanisms in inherited retinal degeneration. Mol Neurobiol *38*, 253-269.

Sato, M., and Ohtsuka, T. (2010). Opposite effects of nitric oxide on rod and cone photoreceptors of rat retina in situ. Neurosci Lett *473*, 62-66.

Savchenko, A., Barnes, S., and Kramer, R.H. (1997). Cyclic-nucleotide-gated channels mediate synaptic feedback by nitric oxide. Nature *390*, 694-698.

Schmidt, J.T. (2004). Activity-driven sharpening of the retinotectal projection: the search for retrograde synaptic signaling pathways. J Neurobiol *59*, 114-133.

Schmidt, K.F., Noll, G.N., and Yamamoto, Y. (1992). Sodium nitroprusside alters dark voltage and light responses in isolated retinal rods during whole-cell recording. Vis Neurosci *9*, 205-209.

Schmittgen, T.D., and Livak, K.J. (2008). Analyzing real-time PCR data by the comparative C(T) method. Nat Protoc *3*, 1101-1108.

Schnapf, J.L., and Copenhagen, D.R. (1982). Differences in the kinetics of rod and cone synaptic transmission. Nature *296*, 862-864.

Schnetkamp, P.P. (2004). The SLC24 Na+/Ca2+-K+ exchanger family: vision and beyond. Pflugers Arch *447*, 683-688.

Schuman, E.M., and Madison, D.V. (1994). Nitric oxide and synaptic function. Annu Rev Neurosci *17*, 153-183.

Seeliger, M.W., Grimm, C., Stahlberg, F., Friedburg, C., Jaissle, G., Zrenner, E., Guo, H., Reme, C.E., Humphries, P., Hofmann, F.*, et al.* (2001). New views on RPE65 deficiency: the rod system is the source of vision in a mouse model of Leber congenital amaurosis. Nat Genet *29*, 70-74.

Sheng, Z.J., Choi, S.Y., Dharia, A., Li, J., Sterling, P., and Kramer, R.H. (2007). Synaptic Ca2+ in darkness is lower in rods than cones, causing slower tonic release of vesicles. Journal of Neuroscience *27*, 5033-5042.

Shiells, R., and Falk, G. (1992). Retinal on-bipolar cells contain a nitric oxide-sensitive guanylate cyclase. Neuroreport *3*, 845-848.

Shoshan-Barmatz, V., Zakar, M., Shmuelivich, F., Nahon, E., and Vardi, N. (2007). Retina expresses a novel variant of the ryanodine receptor. Eur J Neurosci *26*, 3113-3125.

Snellman, J., and Nawy, S. (2004). cGMP-dependent kinase regulates response sensitivity of the mouse on bipolar cell. J Neurosci *24*, 6621-6628.

Stenkamp, R.E., Filipek, S., Driessen, C.A., Teller, D.C., and Palczewski, K. (2002). Crystal structure of rhodopsin: a template for cone visual pigments and other G protein-coupled receptors. Biochim Biophys Acta *1565*, 168-182.

Sterling, P., and Matthews, G. (2005). Structure and function of ribbon synapses. Trends Neurosci *28*, 20-29.

Stockman, A., and Sharpe, L.T. (2000). The spectral sensitivities of the middle- and long-wavelength-sensitive cones derived from measurements in observers of known genotype. Vision Res *40*, 1711-1737.

Subbaraya, I., Ruiz, C.C., Helekar, B.S., Zhao, X., Gorczyca, W.A., Pettenati, M.J., Rao, P.N., Palczewski, K., and Baehr, W. (1994). Molecular characterization of human and mouse photoreceptor guanylate cyclase-activating protein (GCAP) and chromosomal localization of the human gene. J Biol Chem *269*, 31080-31089.

Suryanarayanan, A., and Slaughter, M.M. (2006). Synaptic transmission mediated by internal calcium stores in rod photoreceptors. J Neurosci *26*, 1759-1766.

Szabadkai, G., and Duchen, M.R. (2008). Mitochondria: the hub of cellular Ca2+ signaling. Physiology (Bethesda) *23*, 84-94.

Szel, A., Rohlich, P., Caffe, A.R., Juliusson, B., Aguirre, G., and Van Veen, T. (1992). Unique topographic separation of two spectral classes of cones in the mouse retina. J Comp Neurol *325*, 327-342.

Szikra, T., Barabas, P., Bartoletti, T.M., Huang, W., Akopian, A., Thoreson, W.B., and Krizaj, D. (2009). Calcium homeostasis and cone signaling are regulated by interactions between calcium stores and plasma membrane ion channels. PLoS One *4*, e6723.

Szikra, T., and Krizaj, D. (2006). The dynamic range and domain-specific signals of intracellular calcium in photoreceptors. Neuroscience *141*, 143-155.

Tachibanaki, S., Tsushima, S., and Kawamura, S. (2001). Low amplification and fast visual pigment phosphorylation as mechanisms characterizing cone photoresponses. Proc Natl Acad Sci U S A *98*, 14044-14049.

Takahashi, A., Camacho, P., Lechleiter, J.D., and Herman, B. (1999). Measurement of intracellular calcium. Physiol Rev *79*, 1089-1125.

Tanimoto, N., Muehlfriedel, R.L., Fischer, M.D., Fahl, E., Humphries, P., Biel, M., and Seeliger, M.W. (2009). Vision tests in the mouse: Functional phenotyping with electroretinography. Front Biosci *14*, 2730-2737.

Taylor, W.R., He, S., Levick, W.R., and Vaney, D.I. (2000). Dendritic computation of direction selectivity by retinal ganglion cells. Science *289*, 2347-2350.

Taylor, W.R., and Morgans, C. (1998). Localization and properties of voltage-gated calcium channels in cone photoreceptors of Tupaia belangeri. Vis Neurosci *15*, 541-552.

Thompson, W.J. (1991). Cyclic nucleotide phosphodiesterases: pharmacology, biochemistry and function. Pharmacol Ther *51*, 13-33.

Thoreson, W.B. (2007). Kinetics of synaptic transmission at ribbon synapses of rods and cones. Mol Neurobiol *36*, 205-223.

Toescu, E.C. (2004). Hypoxia sensing and pathways of cytosolic Ca2+ increases. Cell Calcium *36*, 187-199.

Toescu, E.C., and Verkhratsky, A. (2003). Neuronal ageing from an intraneuronal perspective: roles of endoplasmic reticulum and mitochondria. Cell Calcium *34*, 311-323.

tom Dieck, S., and Brandstatter, J.H. (2006). Ribbon synapses of the retina. Cell Tissue Res *326*, 339-346.

Trifunovic, D., Dengler, K., Michalakis, S., Zrenner, E., Wissinger, B., and Paquet-Durand, F. (2010). cGMP-dependent cone photoreceptor degeneration in the cpfl1 mouse retina. J Comp Neurol *518*, 3604-3617.

Tsien, R.Y. (1989). Fluorescent probes of cell signaling. Annu Rev Neurosci *12*, 227-253.

Tsien, R.Y. (1992). Intracellular signal transduction in four dimensions: from molecular design to physiology. Am J Physiol *263*, C723-728.

van der Weyden, L., Adams, D.J., and Bradley, A. (2002). Tools for targeted manipulation of the mouse genome. Physiol Genomics *11*, 133-164.

Venkataraman, V., Duda, T., Vardi, N., Koch, K.W., and Sharma, R.K. (2003). Calcium-modulated guanylate cyclase transduction machinery in the photoreceptor--bipolar synaptic region. Biochemistry *42*, 5640-5648.

Verkhratsky, A. (2005). Physiology and pathophysiology of the calcium store in the endoplasmic reticulum of neurons. Physiol Rev *85*, 201-279.

Verkhratsky, A., and Toescu, E.C. (2003). Endoplasmic reticulum Ca2+ homeostasis and neuronal death. J Cell Mol Med *7*, 351-361.

Vielma, A., Delgado, L., Elgueta, C., Osorio, R., Palacios, A.G., and Schmachtenberg, O. (2010). Nitric oxide amplifies the rat electroretinogram. Exp Eye Res *91*, 700-709.

Voitenko, N.V., Kostyuk, E.P., Kruglikov, I.A., and Kostyuk, P.G. (1999). Changes in calcium signalling in dorsal horn neurons in rats with streptozotocin-induced diabetes. Neuroscience *94*, 887-890.

Wang, G.Y., Liets, L.C., and Chalupa, L.M. (2003). Nitric oxide differentially modulates ON and OFF responses of retinal ganglion cells. J Neurophysiol *90*, 1304-1313.

Wang, T.L., Sterling, P., and Vardi, N. (1999). Localization of type I inositol 1,4,5-triphosphate receptor in the outer segments of mammalian cones. J Neurosci *19*, 4221-4228.

Wang, Y., Macke, J.P., Merbs, S.L., Zack, D.J., Klaunberg, B., Bennett, J., Gearhart, J., and Nathans, J. (1992). A locus control region adjacent to the human red and green visual pigment genes. Neuron *9*, 429-440.

Wassle, H. (2004). Parallel processing in the mammalian retina. Nat Rev Neurosci *5*, 747-757.

Wei, J.Y., Cohen, E.D., Genieser, H.G., and Barnstable, C.J. (1998). Substituted cGMP analogs can act as selective agonists of the rod photoreceptor cGMP-gated cation channel. J Mol Neurosci *10*, 53-64.

Werblin, F.S. (1978). Transmission along and between rods in the tiger salamander retina. J Physiol *280*, 449-470.

Williams, D.S. (2002). Transport to the photoreceptor outer segment by myosin VIIa and kinesin II. Vision Res *42*, 455-462.

Won, J., Shi, L.Y., Hicks, W., Wang, J., Hurd, R., Naggert, J.K., Chang, B., and Nishina, P.M. (2011). Mouse model resources for vision research. J Ophthalmol *2011*, 391384.

Wu, S.M. (1992). Feedback connections and operation of the outer plexiform layer of the retina. Curr Opin Neurobiol *2*, 462-468.

Wykes, V., and Garthwaite, J. (2004). Membrane-association and the sensitivity of guanylyl cyclase-coupled receptors to nitric oxide. Br J Pharmacol *141*, 1087-1090.

Zhang, X., Feng, Q., and Cote, R.H. (2005). Efficacy and selectivity of phosphodiesterase-targeted drugs in inhibiting photoreceptor phosphodiesterase (PDE6) in retinal photoreceptors. Invest Ophthalmol Vis Sci *46*, 3060-3066.

Zylinska, L., and Soszynski, M. (2000). Plasma membrane Ca2+-ATPase in excitable and nonexcitable cells. Acta Biochim Pol *47*, 529-539.

9. Education Background:

Eberhard-Karls-University of Tübingen, Germany
Center for Integrative Neuroscience/Institute for Ophthalmic Research,
Faculty of mathematics and natural sciences
June 2008 - present: PhD student

Carl von Ossietzky University of Oldenburg, Germany
Faculty of mathematics and natural sciences,
September 2002 - November 2007,
Graduated in November 2007 with a Diplom of Biology
Diplom Thesis: “Identification of a potential interaction partner of recoverin in the Outer Plexiform Layer (OPL-layer) of mammalian retina”

Dalian University, **China**
Medical College,
September, 1995 – July, 2000,
Graduated in July 2000 with a Bachelor of Science in Medical Inspection